Reduction of Selected Road Noise Phenomena by Modifying Suspension Kinematics Using Metamodels in the Digital Vehicle Development Phase

Zur Erlangung des akademischen Grades eines

Doktors der Ingenieurwissenschaften
(Dr.-Ing.)

von der KIT-Fakultät für Maschinenbau
des Karlsruher Instituts für Technologie (KIT)

genehmigte

Dissertation

von

M. Sc.

Timo von Wysocki

Tag der mündlichen Prüfung:	12.07.2024
Erster Gutachter:	Prof. Dr. rer. nat. Frank Gauterin
Zweiter Gutachter:	Prof. Dr.-Ing. Thomas Schirle

Abstract

Road noise reduction inside passenger cars has become more important in recent years. Electrification reduces engine noise masking, making road noise phenomena more prominent and dominant. Additionally, customers expect more and more comfort especially due to the spread of automated driving functions.

In suspension development, road noise is reduced by modification of component design. The suspension kinematics is usually out of scope for the reduction of specific road noise phenomena.

This research investigates the possibility to modify specific road noise phenomena by suspension kinematics optimization. The investigation targets the early suspension development phase, requiring a fast digital evaluation of the correlations between kinematics changes and road noise phenomena under consideration of suspension boundary conditions. A morphing approach modifies full vehicle Finite Element (FE) simulation models, in order to create a large simulation data set. This data set enables a data driven approach of creating metamodels for the acoustical suspension kinematics optimization.

For a five link rear suspension, small changes to the location of five kinematic hard points between wheel carrier and suspension links are under investigation. A data set consisting of 500 suspension kinematics variations is represented by Artificial Neural Network (ANN) metamodels, enabling both numerical and qualitative optimization of the suspension kinematics. In multiple simulation examples, a typical target conflict in Noise, Vibration, and Harshness (NVH) between different road noise phenomena is addressed and a combination of road noise phenomena optimization and suspension parameter preservation is performed. Finally, a cavity noise optimization using graphical metamodel

representations as design rules is performed in cooperation between different suspension development domains like packaging or durability. The obtained optimized suspension kinematics is validated in hardware on a complete vehicle, which proved the optimization approach to be effective and efficient.

The approach enables a cost- and weight-neutral NVH optimization in an early development stage, which allows later NVH measures to start on a more robust product maturity. This helps reducing range and CO_2 emission impact of NVH measures, in particular for electric vehicles.

Kurzfassung

Rollgeräuschreduktion in PKW wird in den letzten Jahren immer wichtiger. Die zunehmende Elektrifizierung reduziert bisher existierende Maskierungseffekte, was zu einem markanteren und dominierenderen Rollgeräusch führt. Zusätzlich erwarten Kund:innen mehr und mehr Komfort, besonders hervorgerufen durch die zunehmende Verbreitung automatisierter Fahrfunktionen.

In der Fahrwerksentwicklung wird Rollgeräusch üblicherweise durch die Modifikation von Bauteileigenschaften und -gestalt beeinflusst. Die Achskinematik wird üblicherweise nicht für die Reduktion bestimmter Rollgeräuschphänomene eingesetzt.

Die vorliegende Forschungsarbeit untersucht die Möglichkeit, bestimmte Rollgeräuschphänomene gezielt durch Achskinematikoptimierung zu beeinflussen. Die Untersuchung zielt auf die frühen Achsentwicklungsphasen ab, in denen eine schnelle digitale Erfassung der Zusammenhänge zwischen Kinematikänderungen und Rollgeräuschoptimierung erforderlich ist. Dabei finden die Randbedingungen der Achsentwicklung Berücksichtigung. Ein Morphingansatz modifiziert Gesamtfahrzeug-Finite-Elemente-Simulationsmodelle um einen Simulationsdatensatz zu erzeugen. Dieser Datensatz ermöglicht die Nutzung eines datengetriebenen Ansatzes, bei dem Optimierungsmetamodelle der akustischen Optimierung der Achskinematik dienen.

Für eine Fünflenkerhinterachse werden kleine Änderungen der Position der fünf Verbindungspunkte zwischen Radträger und Fahrwerkslenkern untersucht. Ein Datensatz aus 500 Achskinematikvariationen wird durch Metamodelle in Form von Künstlichen Neuronalen Netzen (KNN) abgebildet, was sowohl

die numerische, als auch qualitative Optimierung der Achskinematik ermöglicht. In mehreren Simulationsbeispielen wird ein NVH[a]-typischer Zielkonflikt zwischen verschiedenen Rollgeräuschphänomenen betrachtet sowie eine Kombination aus Rollgeräuschoptimierung und Erhaltung der Achseigenschaften durchgeführt. Zuletzt wird eine Optimierung des Reifen-Kavitätsgeräusches unter Nutzung grafischer Metamodelle als Designregeln mit Beteiligung verschiedener Achsentwicklungsbereiche, wie z. B. Bauraum oder Betriebsfestigkeit, durchgeführt. Die entwickelte optimierte Achskinematik wird in Hardware an einem Gesamtfahrzeug validiert, was den Optimierungsansatz als effektiv und effizient bestätigt.

Der Ansatz ermöglicht eine kosten- und gewichtsneutrale NVH-Optimierung in einer frühen Entwicklungsphase, was die späteren NVH-Maßnahmen auf einer robusteren Auslegung aufbauen lässt. Insbesondere für Elektrofahrzeuge hilft dies dabei, die Einflüsse von NVH-Maßnahmen auf Reichweite und CO_2-Ausstoß zu reduzieren.

[a] Noise, Vibration, and Harshness (NVH): Geräusch, Vibration und Rauigkeit

Danksagung

Die vorliegende Arbeit entstand während meiner Doktorandenzeit in der Rollgeräuschsimulation bei Mercedes-Benz. Ich möchte mich an dieser Stelle herzlich bei allen bedanken, die mich auf diesem Weg begleitet haben.

Mein Dank gilt Prof. Dr. rer. nat. Frank Gauterin für die Betreuung dieser Arbeit. In diversen Meilensteinen und Institutstreffen habe ich den Austausch und die Unterstützung stets sehr geschätzt. Vielen Dank für die Möglichkeit, die Forschungsarbeit auf der DAGA einem großen Publikum zu präsentieren.

Prof. Dr.-Ing. Thomas Schirle möchte ich für die Übernahme des Korreferats danken. Vielen Dank für die inspirierenden Diskussionen bei geplanten und ungeplanten Gelegenheiten.

Meinen ganz besonderen Dank möchte ich Achim Winandi aussprechen. Ohne Deine Unterstützung während meiner Masterarbeit wäre ich nicht bei Mercedes-Benz gelandet. Vielen Dank für den kontinuierlichen Austausch, das immer offene Ohr und Deine Zeit über all die Jahre. Du hast mich und meine Promotionszeit sehr geprägt.

Danken möchte ich auch Stefanie Grollius für den Anschub meines Promotionsprojektes und Ernst Prescha für die Betreuung während meiner Doktorandenzeit und das Erinnern an Raketenstarts. Vielen Dank für den Zuspruch und dein Vertrauen in meine Arbeit über all die Jahre. Du hast damit mehr bewirkt, als Du denkst.

Den NVH-Fahrwerkern Thomas, Payam und Klaus-Peter, Chetan und Steven möchte ich für die Aufnahme ins Team und die Diskussionen in diversen Fahrwerkrunden danken. Stellvertretend für alle weiteren Kolleg:innen danke

ich Christian, Stefan, Eric, und Oskar für die Unterstützung und viele anregende Diskussionen.

Stéphanie Anthoine danke ich für die Freiräume in der ersten Phase des Promotionsprojektes. Ohne diese wäre das Projekt nicht so schnell und erfolgreich gewachsen. Christian Olfens danke ich für die Unterstützung in der zweiten Phase des Promotionsprojektes. Deine Unterstützung bei der Verbreitung und Umsetzung des Projektes hat mich fachlich und persönlich stark geprägt. Vielen Dank Dir und allen Teamkolleg:innen für die Aufnahme und Integration ins neue Team während der Pandemie!

Wibke Lommatzsch danke ich für die Management-Unterstützung des Promotionsprojektes und die persönliche Unterstützung und Weiterentwicklung über die Jahre. Hans Storck und Oliver Storz möchte ich für die Möglichkeit zur Fortführung des Projektes sowie das seither in mich gesetzte Vertrauen danken.

Ganz besonderen Dank möchte ich den Versuchskollegen Ingo Busch und Ralf Lehmann aussprechen, ohne die die Validierungsmessungen nicht stattgefunden hätten. Den Kollegen der Achsentwicklung Dirk Herkenrath, Philipp Sickinger und Christian Mosler möchte ich für die Möglichkeit zur Validierung und Fortführung des Projektes danken. Vielen Dank für die Offenheit gegenüber meiner Forschungsarbeit und die Möglichkeit zur Hospitanz. Markus Riedel möchte ich für die Initiierung der Validierungsmessungen danken. Sascha Gemeinhardt möchte ich für die Unterstützung bei der Fortführung des Projektes, die Offenheit und den Austausch danken.

Vielen Dank Eva Schwarz! Vielen Dank für Deine Unterstützung am Ende meiner Doktorandenzeit sowie die gemeinsame Weiterführung des Projektes und die Motivation im Schlussspurt. Ohne dich wäre aus dem Projekt nicht das geworden, was es heute ist.

Ich möchte allen Student:innen danken, die mich über die Jahre begleitet haben. Ich danke Euch für Eure hervorragende Arbeit, Euer Interesse und Einsatz sowie viele inspirierende Diskussionen. Den Doktoranden der Forschungsgruppe Geräusch und Schwingungen danke ich dafür, dass ich mich am Institut immer wohlfühlen durfte. Den Doks von Mercedes-Benz, ganz besonders Dimi

Tsokaktsidis und Michael Leupolz danke ich für viel Spaß am gemeinsamen Promovieren und die gegenseitige Unterstützung.

Tobi, Michi, Manu, und Elias, ich danke Euch für die Treue über all die Jahre und ganz besonders die digitale Gesellschaft in der Pandemie.

Zu guter Letzt möchte ich meiner Familie und ganz besonders meinen Eltern für die Unterstützung und den Rückhalt über all die Jahre danken. Jetzt ist es geschafft.

Timo von Wysocki

Contents

Appendix

1 Introduction

Improving the driving comfort has been an important task in automotive engineering since the beginning of the automobile. Starting with ride comfort, Noise, Vibration, and Harshness (NVH) comfort joined the development requirements with better vehicle build quality [Sch18].

The importance of noise comfort inside the vehicle is becoming one of the most discussed features of new cars. For electric vehicles in particular, the customer focus shifts from exterior to interior, including interior noise comfort [Gäb18, Köl19, You19, Köl20].

For luxurious cars, interior silence is demanded by the customer [Sch12, Mei15, Let19]. This is achieved by reducing engine noise, wind noise, and road noise, which is the noise created in the contact patch between tires and road. Where engine noise—even for an electric engine—may sound nice or emotional, road noise is always disturbing and non-emotional for the passengers [Man18]. Since the combustion engine noise is missing for electric vehicles, the reduction of previously existing, but masked, road noise phenomena becomes a major task for automobile manufacturers [Kos14, Ram17, Uhl21a, Sei21]. This requires new approaches to reduce road noise and a fast and holistic integration into the vehicle development process [Ram17].

Comfort development, especially road noise development, should start as early as possible in the vehicle development process [Ram17]. This early development is usually referred to as frontloading [Ede15, Har19, Lei19] in the digital phase [Mar11]. The digital road noise development focuses on the transfer path from the excitation in the contact patch between tire and road to the passenger's ears. There is a structure-borne noise transfer path, dominating the lower road noise frequency ranges and an airborne noise transfer path for

higher frequency ranges. The structure-borne noise transfer path through the suspension is one of the main optimization systems and creates a foundation for a low road noise level inside the passenger cabin.

The transfer path through the suspension depends on the mass, stiffnesses, and damping properties of the suspension components and their interactions under vibration excitation [Sch12]. First investigations additionally hint at influences of the suspension kinematics on the vibration transfer in the tactile frequency range [Vos08, Sch12, Hab13, Wol14, Dro15, Uhl21b, Uhl20a] and the road noise frequency range [Har06, Kos14].

As the suspension kinematics is under development earlier than the remaining properties of the suspension, a systematic integration of NVH requirements would enable road noise reduction in an earlier development phase, making the development process more holistic.

This creates the research hypothesis for the present work: *Small changes in suspension kinematics enable the optimization of specific road noise phenomena in an early development phase.*

2 Investigation Background

Recent megatrends in the automotive industry encourage the investigation of suspension kinematics influences on road noise phenomena. This chapter introduces the megatrends electrification and automation. Their impact on road noise and suspension development is discussed and the basics, relevant for the presented investigation, are introduced.

2.1 Future of Individual Mobility

The development of electrification and automation currently impacts all development domains in automotive industry, including NVH and suspension development. Electrification removes acoustic masking, changes package concepts, and raises vehicle weights. Automation shifts passenger focus to driving comfort and enables innovative suspension concepts. The effects resulting from these two trends are of specific importance for the presented investigation.

2.1.1 Electrification

Electric vehicles increase their market shares in all major global markets. This trend even resisted the global economic crises of the last months and years [Sch21c, Con21]. Both regulatory pressure and changing consumer behavior push vehicle manufacturers, so-called Original Equipment Manufacturers (OEMs), to develop more electric vehicles [Con21]. Consequently, more OEMs declare the end of their Internal Combustion Engine (ICE) development in the coming years [Con21, Lan22].

For electric vehicles, both the exterior and interior noise levels change. On the exterior, noise is reduced drastically below 30 km h^{-1}, due to missing combustion engine and exhaust noise. Therefore, artificial noise generation is required to keep the vehicles safe for pedestrians [Zel18] and other vulnerable traffic participants.

Inside the vehicle, electrification changes the noise spectrum. Acoustical masking effects from the ICE are not present anymore, which reduces the overall Sound Pressure Level (SPL), but also increases the dominance of other noise sources [Hof15, Ram17, Gop20, Hua20, Sei21, Hua21]. Electric engine noise is hardly present at low power demands and wind noise only occurs at higher driving speeds [Gäb18, Zel18, Kra19]. Therefore, especially in urban and overland traffic, road noise dominates the interior noise [Gäb18, Man18, Kra19, Hua20, Sei21, Uhl21b]. With further urbanization, heavier traffic density, and reduced speed limits, the road noise dominance might further increase. In these driving conditions, Plugin Hybrid Electric Vehicles (PHEVs) are able to drive fully electric, too, so the dominance of road noise also applies to those vehicles [Jun20a].

2.1.2 Automation

Another megatrend in automotive industry is vehicle automation. The Society of Automotive Engineers (SAE) defined different levels of driving automation systems, indicated by a number from 0 to 5. From Level 3 and upwards, at least for a short time, the vehicle takes complete control, removing the interaction between driver and vehicle. [SAE J3016_202104]

In 2021 Mercedes-Benz received the world's first legal approval for conditional automated driving [Mer22a]. The SAE Level 3 *Drive Pilot* allows the driver to engage in other activities on specific roads up to 60 km h^{-1} [Mer22b]. In 2023, Germany allowed Level 3 up to 130 km h^{-1} [Köl23]. In addition, first test cases for Level 4 automated driving with people movers emerge [Sch20a, Lyo21].

The possibility to focus on activities other than driving changes passengers' expectations of the vehicle. The most notable change is the rising demand

for more comfort in both the lower frequency ride comfort and the higher frequency NVH comfort [Kra00, Ara15a, Sch17, Pfe18, Sch19b, Elb19, Rei19, Boh20]. When not operating the vehicle, the passengers expect the ride and NVH comfort of a modern high-speed train [Sch17] with reduced focus on driving dynamics [Sch17, Pfe18].

Starting with Level 3, automation requires a computer to take control over the vehicle. This reduces the requirement for subjective feedback to the driver regarding the instantaneous driving state [Sch17, Sch19b]. The first step towards computer takeover are Drive-by-Wire systems. Here, electronics replace the mechanical connections for throttle, steering, and braking. Electronic actuation of the throttle is considered state of the art for many years. Steer-by-Wire and Brake-by-Wire technology is currently under development and emerges into the market [Hei19, REE20, Par21, Sch21b], for example in rear suspension steering systems [Mer20b] or even in motorsports [Sch21a]. Steer-by-Wire not only decouples the driver from the steering in terms of NVH [Kra00], but also decouples the forces at the steering wheel from the forces in the steering system [Sch19b]. On the one hand, this enables suspension design without respect to the required feedback steering forces, as the actual forces are applied by the computer [Sch17, Sch19b, Hei19]. On the other hand, the package requirements for the steering system become available for new suspension concepts [Kra00, Mac21]. This enables completely different suspension tuning with changing trade-off between driving dynamics and driving comfort [Kra00, Sch17], or even completely new suspension concepts [Sch17, Nee19, Rau20, Tre20, Woo20].

People movers introduce wheel individual steering systems [Kei19, Pro19, Sch19a, Lam20, Woo20] in so-called motion boards. Motion boards are independently functional chassis systems containing the suspension systems, a usually electric powertrain, and energy storage [Rau20, Kei19, Lam20, Nee19, Gop20, REE20, REE21, Tre20, Mer18] and currently emerge into the market as first concepts and application tests [Mer18, 2ge19, Hei19, Kei19, Nee19, 2ge20, Bac20, Jun20b, Lam20, Lyo20, Rau20, REE20, Tem20, Tre20, Woo20, Lyo21, REE21, Sch21d]. Besides advanced steering applications like high maneuverability in urban environments [Kei19, Rau20, Tre20, Woo20], wheel

individual steering could add additional functionality, like for example toe angle adjustments while cornering and deflecting [Sch19b, Zop20].

The evolution of Steer-by-Wire is condensed into Drive-by-Wire. Additionally to the disconnected steering system, the braking system is also disconnected from direct driver input. Compared to Steer-by-Wire solutions, Drive-by-Wire is even more safety critical due to the potential loss of braking power. First Drive-by-Wire systems currently appear on the market [Hei19, Par21].

While all these changed requirements and desires could lead to whole new suspension concepts [Kra00, Pro19, Sch19b, Woo20, REE21], many recent people movers still use classical suspension concepts, like double wishbone suspensions [Bre11, Kei19]. This presents a new requirement in suspension development: altering existing suspension concepts to drastically changed boundary conditions in a fast and collaborative way.

2.2 Road Noise

The trend towards electrification and automation results in an increasing demand for comfort in upcoming vehicles. Comfort in vehicles has different aspects, including noise inside the passenger cabin, tactile vibrations, climate comfort, ergonomics, and many more [Let19]. Road noise, the noise originating from the contact patch between tire and road, is the focus of this work.

2.2.1 Road Noise in the Context of Vehicle Comfort

The vibrations that impact driving comfort, are usually separated by their frequency ranges. Phenomena up to 25 Hz contribute to ride comfort, including larger movements of the vehicle body while cornering or accelerating [Bot08, Wol14] and kinetosis [Boh20].

Higher frequency phenomena are clustered under the term Noise, Vibration, and Harshness (NVH). Noise (N) describes audible phenomena, vibration (V) describes tactile phenomena, and harshness (H) phenomena are both audible

and tactile. Harshness phenomena occur between 20 and 100 Hz, separating the solely tactile vibrations below and solely audible noise above. [Hei11, p. 421]

In this investigation, the focus lies on noise phenomena inside the vehicle. Interior noise mainly originates from three different sources: The engine, the airflow around the vehicle, and the contact patch between tire and road. These different noise sources dominate, depending on the vehicle type and the driving situation like speed or engine load. [Zel18, p. 268–270]

Road noise dominates the urban driving conditions at lower speeds from 30 to 100 $\mathrm{km\,h^{-1}}$, and little engine load [Gen10, Mei15, Gla17, Gäb18, Hua20]. The composition of the interior noise strongly depends on the type and luxuriousness of a vehicle. The speed at which wind noise dominates the interior noise varies strongly from car to car. Road noise dominates in the speed ranges where the first approved SAE Level 3 automations, mentioned in section 2.1.2, operate. This affirms the relevance of reducing road noise for future luxurious vehicles.

Not all interior noise is always considered disturbing. For example, engine noise can support a sporty vehicle character. Road noise can transmit information regarding the road condition to the driver [Gen10, p. 270], for example a road surface that is wet or covered with snow. Nevertheless, road noise does not evoke positive emotional response and needs to be reduced in the context of driving comfort [Man18].

2.2.2 Road Noise Origin

Road noise, emerging from the contact patch between tire and road, results from different interactions in the contact area. For example, road roughness induces forced displacements into the tire and excites vibrations [Kos14, Kra19]. Therefore, the roughness of the road is a crucial factor for the resulting vibrations without being influenced by the vehicle engineers [Gen10, Cao11, Gäb18, Zaf18]. As this work focuses on the transfer path for the induced vibrations, the details of the underlying emergence principles are not discussed here.

2.2.3 Road Noise Transfer Path

The vibrations emerging from the contact patch result in two different noise phenomena. The contact patch emits airborne noise to the environment of the vehicle, resulting in the vehicle pass-by noise. This exterior noise is able to reenter the vehicle as rolling noise, dominating above 400 Hz [Gen10, Uhl21a, Sei21], for example through the windows.

Additionally to the airborne noise, vibrations spread via structure-borne noise into the passenger cabin and induce road noise. The transfer path is illustrated in fig. 2.1. From the contact patch, structure-borne noise emerges into the tire. The vibrations traverse both directly and via the air inside the tire cavity to the rim. The rim induces the vibrations via the wheel hub into the suspension. A fictional point, the wheel center, represents the point for the force transfer between wheel and wheel hub. It is located in the intersection between the wheel-spin axis and the wheel plane [DIN ISO 8855:2013-11]. Through the suspension, the vibrations are induced into the vehicle body. The structure-borne noise in the vehicle body initiates surface vibrations in the passenger

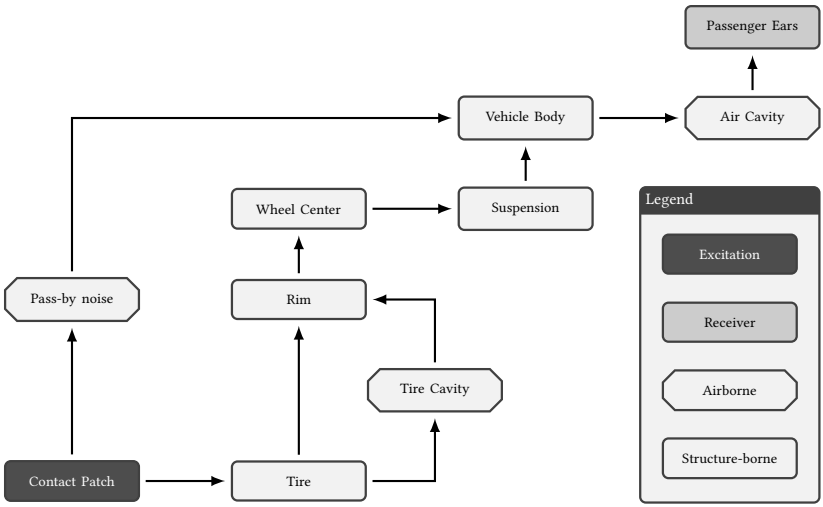

Figure 2.1: Transfer path for road induced vibrations emerging from the contact patch between road and tire to the passenger ears.

cabin, converting the structure-borne noise to airborne noise. This airborne noise is then audible for the passengers[a].

2.2.4 Road Noise Phenomena

Road noise entering the passenger cabin through the structure-borne suspension transfer path is considered in this investigation. This is the most relevant part of the noise generated in the contact patch and ranges from 20 Hz up to around 400 Hz [Gen10, Sch17, Gäb18, Zel18, Hua20, Sei21].

Similar to noise phenomena in general, road noise phenomena are separated by their frequency ranges as well. The exact frequency values differ in literature.

At the lowest audible frequencies, the phenomena start with booming noise between 20 and 70 Hz [Gen10, Her21, Uhl21a, Sei21]. Booming noise is often considered separately to road noise [Her21]. One of the most investigated phenomena is the droning noise in the frequency range from 50 to 110 Hz [Gen10]. Rumbling noise starts at 70 Hz and ranges up to 180 Hz and beyond [Gen10, Uhl21a, Sei21]. Contrary to the broader frequency ranges of these phenomena, tire cavity noise is located in a narrow frequency band located between 180 and 250 Hz, depending on the tire dimensions and driving speed [Gen10, Gro13, Gla17, Kra19, Sei21, Uhl21a]. Tire cavity noise is often clearly audible as a specific tone standing out of the other road noise phenomena. Beyond the cavity noise frequency range, there are higher frequency phenomena like singing or wet hissing [Gen10].

[a] The transfer path is further detailed in section 4.1. Figure A.1 on page 208 combines both illustrations into the full transfer path

2.3 Vehicle Suspension

The previous sections identified the structure-borne noise transfer path through the suspension as crucial for road noise transfer to the passenger ears. The suspension subsystem, its transfer path and development is discussed in this section.

2.3.1 Suspension Terms and Basics

In the last years, many technical revolutions changed vehicles drastically. Nevertheless, even the most fanciful studies still have four wheels and a chassis, connecting the vehicle to the ground [Kle18]. Depending on the definition, literature defines the chassis as the combination of systems like suspension, steering, stabilizer, subframe, tires, and wheels [Hei11]. In the present work, the term suspension is used as a general term for the system connecting the wheels to the vehicle body.

Passenger cars utilize different kinds of suspension systems. There are different suspension topologies such as McPherson, three to five link, or double wishbone suspensions, among many others [Hei11, Spi12, Lei19]. Even with the same topology, the suspensions can still differ in their configuration. For example, five link suspensions can be based on a push rod or a pull rod configuration. Within the same configuration, the design of the components or the location of the connection points still distinguishes suspensions from each other [Spi12]. This suggests that one single optimal suspension design does not exist [San10]. Depending on the vehicle segment, weight, front or rear suspension, and many other requirements, the best fitting suspension concept has to be selected and designed individually [Elb09].

The suspension under investigation here is a five link rear suspension. Therefore, the details presented in the next sections are based on this suspension topology.

A five link rear suspension consists of a wheel carrier[a], five suspension links or control arms, joints, mounts, and bushings, a spring and a damper element, a torsion bar, subframe, and additional components containing the brake system or sensors [Hei11]. Wheel carrier and subframe usually have complex geometric shapes, whereas the links and arms can have either simple rod shape or a complex shape. This mainly depends on the number of connection points to adjacent components, the applied load, their tasks, and package restrictions. The desired component shape varies the manufacturing process and material choice [Lei19, Ger19].

2.3.2 Suspension Tasks and Requirements

The suspension system performs one of the most important tasks of a vehicle: It connects the vehicle to the ground and provides driving dynamics, safety, stability, and comfort [Xue11, Hei11, Sch12, Lei19]. These tasks have to be fulfilled while complying to package, durability, weight, and cost restrictions [Sch12, Lei19].

The main task of the suspension links is to control the movement of the wheel carrier within the desired Degrees of Freedom (DOFs) [Hei11, Lei19]. An unsteered axle provides one DOF to the wheel carrier [Hei11, p. 288 & 393]. In a complex motion path, the wheel carrier can travel vertically. For steered axles, the wheel carrier steering rotation adds a second DOF to the movement capability [Hei11, p. 393].

The suspension links of a five link rear suspension can be divided into control links and support links. Control links control the wheel movement and only receive loads in the direction of the link. Support links have springs or dampers attached to them and carry the weight of the vehicle. Therefore, they are subjected to additional bending forces. [Hei11]

[a] The component attached to the wheel bearing is referred to as knuckle for a steered axis and wheel carrier otherwise [Hei11, p. 325]

The suspension system provides the driver with valuable feedback regarding the instantaneous driving state of the car. Forces at the steering wheel decode the state of the road or cornering behavior and are therefore crucial for the driver [Kra00]. Providing driving comfort is another important task, performed by the suspension system. It decouples the body for both ride comfort and NVH comfort.

2.3.3 Suspension Kinematics

The layout of the control and support links in the suspension system creates the suspension kinematics. It determines the movement possibilities or DOFs of the wheel carrier with respect to the vehicle body while steering and deflecting [San10, Lei19]. This includes both dynamic driving situations, but also weight dependent vehicle levels [Meß07]. The five link rear suspension under investigation provides only one DOF to the wheel carrier, as the suspension is not equipped with a rear wheel steering system.

Each suspension link is connected to the wheel carrier and the subframe, at least once. These connection points are referred to as *hard points* and represent the joint coordinate system origin [Hei11]. The connections are usually made out of elastomer joints, mounts and bushings providing required movement possibilities between the connected components [Hei11]. Additionally, the elastomer joints provide small longitudinal movement possibilities to the wheel, adding additional elasticity DOFs to the suspension [Hei11, p. 31]. As the elastomer elements provide flexibility in the movement of the wheel carrier, the suspension kinematics splits into the rigid suspension kinematics and the frequency dependent elastokinematics [Sel08, Hei11]. The rigid body suspension kinematics is independent from the used connection elements, as the connections are considered ideal frictionless and stiff joints constraining DOFs. The kinematic behavior of suspensions made out of higher numbers of individual suspension links, such as five link rear suspensions, is usually determined more by the rigid suspension kinematics than the elastokinematics [Nie12,

p. 80]. For the presented investigation, the rigid suspension kinematics is in focus and the simplified term *Suspension Kinematics* is used for rigid suspension kinematics, if not stated otherwise.

The suspension kinematics of a five link rear suspension is only determined by the kinematic hard point locations. Suspension parameters derived from these locations characterize the suspension kinematics and additionally provide first insights into the kinematic properties of the suspension. There are static suspension parameters, which describe the wheel alignment without any steering or deflection movement, and suspension parameter curves, describing the changes of the static parameters while steering and deflecting. A detailed explanation of the different suspension parameters is omitted here, with reference to Heißing et al. [Hei11], DIN ISO 8855:2013-11, and SAE J670_200801.

2.3.4 Suspension Development Process

Suspension development is one of the core competences of many OEMs. It contains the development of the previously discussed functionalities by different development domains such as ride and handling, safety, durability or NVH. The development is bound to restrictions and boundary conditions such as package, costs and functional target conflicts of different development domains.

The suspension development consists of different development phases. In the early concept phase, the suspension topology is determined. In the next steps, the development domains determine the suspension configuration and the detailed suspension design. Often, these development phases follow a V-Model procedure defined in VDI/VDE 2206:2021-11. In each phase, the vehicle requirements and boundary conditions are transferred to the component level specifications, resolved there and integrated again into the full vehicle [Sel22].

Starting the suspension development process, there are no hardware components or vehicles available [Wol14, Tre15, Ref15, Lei19]. Therefore, the majority of these development phases are performed digitally [Wol14, Lei19]. This work orients on the digital vehicle development process at Mercedes-Benz, named Digital Prototype (DPT) process. Among other development domains, the DPT

process includes NVH, ride and handling, durability, safety, and aerodynamics. Multiple DPT loops between defined milestones form the individual V-Model cycles. They contain the provisioning of geometric and functional data[a], as well as computation, assessment, and optimization for the different development domains. Wattenberg et al. describe the DPT process in detail. [Wat12]

The digital evaluation in each DPT loop relies on different calculation methods. Depending on the development domain, calculation is performed using analytical calculation, Multi Body Simulation (MBS), Finite Element Method (FEM) simulation, or a combination of all of them [Esk06, Nie12]. The rigid suspension kinematics evaluation for example relies on the analytical calculation [Zom70, Mat07, Bin14, Vem15, Abe17]. Ride and handling predominantly use MBS [Esk06, Nie12, Bin14, Wol14, Vem15, Sei16, Kha19, Uhl20a]. Durability, safety, and NVH also use MBS [Sel08, Elb09, Sch12, Sel22], but predominantly use FEM [Wil04, Hel12, Sel22].

The simulation models originate from different sources. The development of a new vehicle can begin based on the existing Computer Aided Design (CAD) models or simulation models of a predecessor vehicle or subsystem or from scratch [Sti10, Spi12, Gae14, Llo18].

The digital evaluation in the early development stages increases the product maturity early and reduces the number of required hardware prototypes and measurements helping to accelerate the product development process and reducing its costs [Tro02, Gen10, Mar11, Lei19]. In a development process, the options for modification become smaller and more costly with advancing development progress [Auw07, Gen10, Lei19]. Therefore, an effective and efficient digital vehicle development process requires highly flexible and fast modeling and evaluation processes [Elb09, Gen10, Hah17].

The suspension topology usually depends on the vehicle type and segment, front or rear suspension, and required steering possibilities. The vehicle concept determines package boundary conditions. This includes the location

[a] Functional data are component properties like for example elastomer bushing stiffnesses

of tank or battery, engines, or steering system, and the required space for passengers and luggage. [Bot08, Elb09, Sch19b, Tre20, Lv21]

After the suspension topology is set in one of the first development phases, the definition of the configuration and rigid suspension kinematics starts. The configuration and final design of the suspension is subject to many target conflicts between the different development domains. The dominating targets for the early kinematics development are suspension parameters, mostly required for the desired ride and handling properties [Vem15, p. 234]. Handling describes the vehicle movement response to driver input [Esk06, Bot08]. With the rigid suspension kinematics set, suspension concept changes are hardly possible and therefore serve as boundary conditions for upcoming development phases [Bot08, p. 6]. The further development of component shapes and elastomer elements then compromises the target conflicts and alters the elastokinematics. As a modification of the elastomer elements is possible without any package modifications, they are often used as a late stage tuning possibility for different requirements [Kos14, Fan15, Ram17]. Besides reducing noise transfer, the elastomer elements play an important role in the balancing of the vehicle handling.

Vehicle electrification imposed new boundary conditions for the suspension development. New package challenges and opportunities emerged with batteries obtaining space, where kinematic hard points used to be [Sel22], or suspension-integrated powertrains [Lei19, Sch19b]. Additional vehicle weight challenged durability requirements [Mar15] while lightweight design is required for CO_2 reduction [Mar15, Ger19, Zop20]. Suspension kinematics are subject to energy optimized design, reducing the required energy for the power steering [Röm22]. Additionally, there are approaches for energy harvesting in suspension components. Road irregularities induce displacement in the suspension dampers. Active dampers harvest and store this kinetic energy, reducing CO_2 emissions [Cao11, Hof16, Fro19].

Making the development more holistic by integrating the requirements and restrictions of multiple development domains requires new technological but also organizational adaptions [Sel08, Gra14, Jun21]. For example, generative engineering combines multiple development domains into one development

tool [Lei20]. Following digital design and simulation, using enormous computational power enables more advanced simulation and modeling or machine learning approaches.

Technological leaps and fast moving mobility trends require OEMs to accelerate the development process [Ram17, Erb19]. This includes moving investigations to earlier development phases, and modifying the development methodology itself [Jun21]. Simulation models require the possibility for fast updating and automation in order to quickly evaluate different variants without excessive manual interaction [Hei05, Cha06, Elb09, Zim13]. Parametric and automated modeling enables quickly changing either the CAD models or directly the derived simulation models [Hel12, Zim13]. This not only speeds up the design evaluation, but also enables new optimization possibilities, using Computer Aided Engineering (CAE) for design creation, instead of design verification [Nie12, Hel12]. These new development requirements and possibilities using enormous computing power and holistic requirement integration open up new possibilities for the suspension development. Braess states in 2019: "continue committing [...] to the chassis, because this will pay off in the long term" [Rei19].

2.4 Reducing Road Noise

Noise can be reduced either by reducing the excitation at the source or by improving the transfer path between source and receiver [Hua20, Sei21]. Omitting the excitation is impossible, as the contact between road and tire is indispensable and encapsulation is not possible [Gen10, p. 270]. Reducing the excitation can be achieved by influencing the roughness of the road [Kra19], which is out of scope for the vehicle engineers, though. Nevertheless, the tire and wheel part of the excitation is subject to constant optimization [Nie12, Zaf18, Jun20c]. For example, foam inlays dampen cavity noise effectively [Kra19], but increase costs and weight. The required CO_2 reduction and desired electric range extension makes heavy NVH solutions undesirable [Hof15, Sch20b]. This favors integrated optimizations, using existing components and concepts for additional NVH benefits.

Road noise reduction is mainly achieved by the modifications of the suspension subsystem transfer path. This part of the transfer path includes all suspension components and therefore differs for different suspension topologies and configurations [Zel18, p. 272–273]. Its optimization starts with concept and topology evaluation in the early DPT phases. Elastomer element optimization starts early, but is predominantly used in later development phases for fine tuning the structure-borne transfer path in accordance with other development domains. Body parameters like the stiffness of the attachment points between suspension and body and the transfer path through the vehicle body are also highly relevant and subject to optimization in the DPT loops, but not in focus here. In order to eliminate a large share of the body transfer path, NVH performance is often evaluated on subsystem level using transfer forces between suspension and body. This is done both in simulation and hardware testing [Sel08, Gag10, Bin14, Ref15, Ram17, Kim18, Sch17, Uhl20a, Uhl21b, Sei21, Sel22]. This increases the development speed, as both in the digital and the hardware phases, the suspension is available much earlier, compared to the full vehicle [Ram17].

The path of the structure-borne vibrations through the suspension predominantly depends on the mass and its distribution, stiffness, and damping properties of the suspension components [Tro04, Sch12]. Some component properties change, depending on the direction of the transferred forces in the wheel hub, the amplitudes, and the frequency [Tro04, Sel08, Gen10, Bin14], making the transfer path complex to evaluate. If excitation frequencies match an eigenfrequency in the suspension, resonance phenomena occur [Sch12, p. 22]. The suspension eigenmodes shift from modes with deformation predominantly in the elastomer elements at lower frequencies to eigenmodes with component deformations at higher frequencies [Sch12, Hua20]. The general stiffness of the suspension transfer path can be interpreted as a series connection of springs with the suspension components and elastomer elements forming the individual springs. The overall stiffness can stay constant, when reducing elastomer element stiffnesses and increasing all the other stiffnesses. This increases vibration damping by increasing the displacement in the elastomer elements, without changing the overall transfer path stiffness [Gen10, Hei11].

Usually, elastomer components have different stiffnesses in different directions [Tro04, Hei11, Nie12]. Additionally, the stiffness values depend on frequency and amplitude and differ from production variance, ageing, and temperature [Sel01, Gru03, Sel08, Hei11, Zhu12, Hab14, Uhl21a]. In simulation, these nonlinearities are usually handled by linearization for the load case under investigation [Uhl21a]. The parametrization for this linearization is usually determined by hardware measurements in operating conditions, determined by nonlinear Finite Element (FE) simulation [Kid99].

Generally, the main target for road noise reduction is the modal decoupling of all suspension components. Additionally, eigenmodes must not match with dominating excitation frequencies or sensitive frequencies in the transfer path [Sel08, Ram17, Har19, Sel22]. Often, the first eigenfrequency of a component is specified as an NVH requirement [Hei11, p. 462].

The modal decoupling in the early development stages mainly focuses on the suspension component shapes, stiffnesses, and weights [Zan13, Zaf18]. In the later stages, mass dampers help reducing noise transfer in specific frequency ranges but add additional costs and weight. Elastomer elements serve as a late tuning possibility, as modifications of the rubber shape and compound can be implemented without any package modifications [Hof15, Ram17].

Typically, there are elastomer elements between suspension links and both wheel carrier and subframe. Additional elastomer elements, so-called *subframe mounts*, decouple the subframe from the vehicle body [Zel18]. Whereas the elastomer elements connecting the suspension links are in conflict between driving dynamics and road noise, the subframe mounts are in conflict between driving dynamics and both road noise and engine or gearbox noise [Gru03]. The requirement for engine noise decoupling, especially for electric vehicles, often reduces the effectiveness of the subframe mounts for the road noise reduction [Gru03]. The target conflict between soft elastomer elements for driving comfort and stiff elastomer elements for driving dynamics is omnipresent in literature [Kar84, Kid99, Meß07, Bot08, Che09, Elb09, Gen10, Hei11, Xue11, Kim11, Rös12, Aly12, Kos14, Rah14, Wol14, Ara15a, Sei16, Hu17, Gäb18, Sch18, Uhl20a, Uhl21b, Jun21, Büt21, Kal21].

All previously mentioned approaches for road noise reduction modify the passive suspension system transfer path. Additionally, semi-active or active systems may be used for road noise reduction. Semi-active or adaptive suspensions are capable of stiffening or softening the suspension by switching properties like damping coefficients [Xue11, Sch12]. Active suspension systems introduce actors into the suspension, capable of applying forces to the suspension [Xue11, Gäb18]. While most of the currently developed active suspension systems aim at the target conflict between ride and handling [Bot08, Xue11, Hab13, Cyt18, Elb19, Yu21b], there are also approaches for the reduction of road noise using active or semi-active systems, for example controlled subframe mounts [Gäb18].

Instead of modifying the structure-borne transfer path, Active Noise Canceling (ANC) uses destructive interference to compensate noise in the passenger cabin. This is mainly used for narrow band engine noise phenomena [Jun20c], but there are also approaches for Active Road Noise Cancellation (ARNC) [Zaf18, Mer21b].

Even though active systems are capable of improving or even resolving the target conflict between driving comfort and other development domains, they do not make the passive suspension properties redundant. Whereas all vehicles use a suspension system to decouple the wheel from the body, active systems are still not widely spread in all vehicle segments [Cao11, Hei11, Xue11, Ara15b, Sch19b, Fro19]. Even though these systems are able to reduce road noise, they usually come with additional costs, weight, energy consumption, and complexity [Aly12, Ara15b, Kha19, Sch19b]. In general, active systems perform best, if applied into a well-engineered passive suspension system [Hab13].

2.5 Simulating Road Noise

The discussed measures in road noise reduction are performed digitally in the early development phases. This enables frontloading, which both reduces costs and the time required to get to an increased product maturity and reduces the amount of required hardware testing [Gen10, Mar11, Ede15, Lei19, Sel22].

In digital road noise development, there are different approaches differing in the utilized simulation method. The methods mainly differ by their appropriate frequency range [Gen10]. Starting with MBS, the frequency range increases with FEM and Boundary Element Method (BEM) and ends with Statistical Energy Analysis (SEA) [Gen10]. Combinations, for example using flexible components in MBS or coupling BEM fluid with FEM structure is also possible [Gen10, Hei11, Nie12, Her21]. These approaches differ both in modeling effort and calculation times, making the least complex model providing sufficient results the most favorable one [Hel12, p. 31].

On the lower end of the NVH frequency range, MBS is positioned. MBS is mainly used for tactile vibration simulation, but also for very low frequency noise phenomena. MBS models usually consist of rigid components, simulating the movement of components against each other. For the simulation of noise phenomena, where components deform, the rigid component approach does not apply anymore [Sch12, Ref15, Hei11]. Therefore, modern MBS tools allow the integration of flexible components into the model [Hei11, Nie12]. The usage of flexible components in MBS makes the modeling effort towards FEM simulation fluent.

FEM simulation currently dominates interior road noise simulation with many application examples [Har06, Mat14]. FEM models require the shape of each component as a mesh representation, originating for example from a CAD model [Hei11, p. 461]. This restricts the application of FEM simulation to development phases, where the component design is available, at least as a first iteration.

The complexity of FEM models can be altered as well. On the one side, complexity can be reduced by the integration of simplified substitution models, like for example superelements. This additional effort enables the integration of for example predecessor body subsystems or generalized components [Har06, Sti10, Mor12, Gae14]. Noise simulation in FEM is usually restricted to closed cavities, which on the other side, allows a combination with BEM to enable simulation of open space noise radiation [Gen10, p. 506f.].

BEM describes a noise field on the boundary surface [Gen10, p. 506]. It is often used for the simulation of noise radiation into the open space or for material transmission simulation [Gen10, p. 506f.]. On the higher NVH frequency ranges up to 20 000 Hz SEA is often used for interior noise simulation.

2.6 Influence of Suspension Kinematics on Road Noise

The suspension kinematics is subject to development and optimization in the early digital development phases. The development of suspension parameters for handling [Cha06, Esk06, Vem15], package, safety, and durability is mainly driving the design of the suspension kinematics. These established design paradigms are not in focus here and the presented sources only serve as selected examples.

The suspension kinematics design adapts to new development technologies. Instead of designing and modifying the suspension kinematics by hand, optimization and simulation technology fastens and improves the development process [Nie12]. In handling evaluation, this includes systematical large scale data creation using simulative Design of Experiments (DoE) methods [Cha06, Esk06, Nie12, Kim16]. This data creation process favors handling simulation, as the calculations rely on fast evaluating analytical or MBS calculations [Cha06, Esk06, Nie12, Vem15]. The collected data is then transformed into metamodels—predominantly first to third order polynomials—describing the regression between design variables and handling parameters [Cha06, Esk06, Vem15]. The metamodels are then used to optimize the location of the kinematic hard points to favor the vehicle handling behavior [Cha06, Esk06, Nie12, Vem15].

Suspension kinematics is also under investigation by development domains that are not directly responsible for the suspension design. Schütte et al. use MBS simulation combined with analytical tire wear laws to reduce tire wear by optimizing the suspension kinematics [Sch21e, Sch22]. Li et al. use MBS to optimize hard point locations for reduced tire wear and improved vehicle

control [Li07]. Kim et al. investigate the influence of geometric tolerances on the wheel alignment [Kim16].

In the last years, approaches emerged improving driving comfort by modifying the suspension kinematics. Especially ride and tactile vibration comfort is in focus. In a first step, transferred forces between suspension and vehicle body are under investigation.

Kim investigates the influence of toe angle, camber angle, and bushing stiffness changes on transferred forces evaluating different hardware suspensions. The force transfer in the ride and road noise frequency ranges is reduced with minimal changes to driving dynamics characteristics. [Kim11]

Harzheim et al. use body Noise Transfer Functions (NTFs) combined with transferred forces to optimize suspension kinematics. The kinematics changes are represented in the suspension FEM models using rigid elements for most hard points and a morphing approach for one specific hard point. The modification of the hard points results in eight design variables. A single scalar value representing a weighted combination of the suspension transfer functions between wheel hub and body attachment points serves as an optimization criterion. The investigation is performed on a suspension FEM model. The simulation model is excited by measured forces of a predecessor vehicle on the wheel hub. The vehicle body is integrated as a reduced substitution model. The optimization is performed using a gradient-based FEM design optimization[a], a linear, and a Kriging metamodel. Finally, the robustness of the solution against variance in hard point location and road excitation is ensured using the metamodel. [Har06, Har19]

In multiple publications, Uhlar optimizes the transferred forces between suspension and body in order to reduce NVH phenomena up to 70 Hz. He uses full vehicle and suspension MBS models with flexible bodies and a road surface excited CDTire [Fra] model, representing a real test bench situation for booming noise up to 70 Hz. For simplification of the optimization problem, the transferred forces at the coupling points between suspension and body are

[a] *NX Nastran Solution (SOL) 200*

reduced into one force spectrum envelope curve. This envelope curve is then reduced into scalar maximum values for specific frequency bands. In a DoE, the stiffnesses of subframe bushes, engine mounts, and drive shaft are modified. The results of the DoE are correlations and design variable sets for reduced dynamic forces. The outlook hints further investigations of component masses and stiffnesses, tire pressures and dimensions, and suspension kinematics[a], enabled by fast calculating simulation models. In another publication, Uhlar presents a hybrid simulation model for road noise up to 250 Hz. Using a coupled MBS and FEM approach, the road noise is predicted in a full vehicle context. [Uhl20a, Uhl21b, Uhl21a]

Kosaka et al. perform numerical road noise optimization by suspension kinematics modifications. A simulation model including rigid suspension links, modal models for body, tire, and shock absorbers, and the possibility to modify 24 translational and rotational DOFs of selected suspension hard points is used for road noise evaluation. An analytical sensitivity analysis determines the most dominating hard point displacements for road noise modification. Using the sensitivity results and rigid parametric suspension links, road noise is reduced in a numerical optimization with the target to reduce the combined transferred power to the body. Kosaka et al. find that rigidly modelled suspension components are suitable for road noise prediction and that mass changes due to kinematics changes do not influence road noise. [Kos14]

In multiple publications, Schlecht et al. investigate the influence of the front suspension kinematics on brake judder and wheel imbalance induced vibrations. The investigation is performed both digitally using MBS simulation models with both rigid and flexible components and in hardware. Using hardware validation, Schlecht proves elastically modeled suspension components to predict steering wheel vibrations better compared to rigid components. Numerical optimization of 30 hard point DOFs without previous sensitivity analysis is used to reduce the selected tactile vibration phenomena. The investigation and optimization show the potential to reduce selected tactile vibrations modifying the suspension kinematics. The utilized effects are the reduction of

[a] The suspension kinematics are only mentioned in the german version of the article [Uhl20b]

the normal steering axis offset and both frequency shifts and shape changes of suspension eigenmodes. [Sch09, Sch10, Sch12]

Schlecht mentions similar theoretical and experimental investigations regarding suspension kinematics and steering wheel vibrations by Sedlan, Zomotor, and Grotewohl [Sed06, Zom70, Zom71, Gro74].

Haberzettl et al. optimize steering wheel rotary oscillations, so-called *steering rowing*, by modifying parameters such as damper properties, axle load, location of torsion bar hard points, and driving speed. One of the optimization constraints is the constancy of the suspension parameters. The investigation shows the possibility to improve rowing by changing the torsion bar kinematics both in MBS and hardware testing. [Hab13] In another publication, Haberzettl et al. use MBS to reduce vibrations by modifying the damper position. [Hab14]

In two similar publications, Wolf-Monheim et al. and Drotar et al. investigate tactile vibration comfort up to 100 Hz using MBS with flexible bodies. Variations of isolation and stiffness changes are investigated. In the outlooks, an expansion to suspension kinematics is suggested. [Wol14, Dro15] In a connected publication, Thomas et al. optimize suspension kinematics regarding bump steer and roll steer using numerical optimization [Tho21].

Automotive Testing Papenburg GmbH (ATG) develops a hardware tool called Universeller Komponenten- und Aggregateträger (UNIKAT) for suspension development. The variable suspension kinematics of a double wishbone suspension enables the experimental investigation of influences on driving dynamics and not further specified driving comfort. [Vos08]

Regarding the extraction of correlations between kinematic hard point locations and road noise, there are few investigations, discussed above. The correlation between characteristic suspension parameters such as, e. g., trail or caster angle and road noise is—as far as the author knows—out of scope in the latest state of the art.

Connected to the fundamental research project presented here, multiple prepublications examine selected problems leading to the methodology, presented

here. The detailed content of these publications is discussed in later, appropriate sections. In a first publication from 2020, the correlation between suspension kinematics changes and transferred forces at the suspension connection points to the body was investigated. The achieved modifications to dedicated frequency bands in the Frequency Response Functions (FRFs) by changing suspension kinematics were the first hint for further investigations towards SPL investigations in the full vehicle [Wys20a]. A second publication compared different methods for achieving suspension kinematics changes in FE models [Wys20b]. Additional publications evaluated Artificial Neural Networks (ANNs) for the prediction of FRFs modified by geometric component changes [Tso19, Wys21]. The complete workflow for the investigation on a full vehicle level was presented on a conference in 2022 [Wys22].

Additionally to optimizing the passive suspension kinematics in the development phase, there are approaches to introduce active systems changing the suspension kinematics. The project Series Active Variable Geometry Suspension (SAVGS) changes the location of kinematic hard points using an electromechanical actuator and an epicyclic gearbox. The system actively moves the location of the upper end of the conventional spring–damper unit of a double wishbone suspension. [Yu19] This active suspension kinematics modification aims at chassis attitude control, ride comfort, and road holding enhancement. [i. e. Ara15b, Ara15a, Ara17, Yu19, Yu21a] The active system SAVGS seems not to investigate road noise modifications. The kinematics changes modify the location of the kinematic hard points without changing any component shapes.

With Parallel Active Link Suspension (PALS), the same researchers investigate a different configuration of their active system. An active element applies a force onto the lower wishbone of a double wishbone suspension. The system is able to improve chassis attitude and vehicle vibrations. [Yu21b]

More basic kinematics changes were shown for example in the Mercedes-Benz F 400 concept car, which actively changes the camber for either improved driving dynamics or driving comfort [Mer21a]. Further examples of actively modifying the suspension kinematics exist, without focus on road noise reduction [Nem11, Ber14].

3 Research Scope

The previous chapter condensed the most important strategies and methods for road noise reduction. Usually NVH optimization takes place in a later development phase compared to the suspension kinematics definition. Road noise optimization using the suspension kinematics is hardly present except for the works of Harzheim et al. [Har10, Har19]. There is no systematical investigation known to the author, how to extract design rules for suspension kinematics for a beneficial road noise performance.

In the introduction, the research hypothesis[a] was introduced after which the suspension development could use suspension kinematics in order to improve interior road noise performance in the early development phase. This work aims at the examination of the research hypothesis validity. For this purpose, four research questions are formed, used for validating the initial research hypothesis. These questions form the gap in the state of the art, this work aims at resolving. They describe the scope of the work and form the boundaries for the investigation.

3.1 Research Questions

The research questions follow a typical suspension development process, presented in fig. 3.1. This enables suspension kinematics optimization regarding road noise reduction. Starting in the top left corner, the suspension kinematics is created, mainly regarding suspension parameters and package requirements.

[a] Small changes in suspension kinematics enable the optimization of specific road noise phenomena in an early development phase.

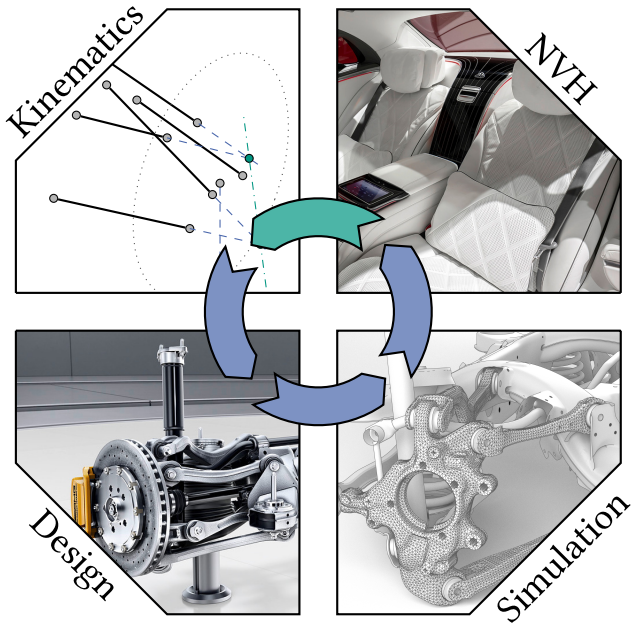

Figure 3.1: Development process for road noise development. Starting with the suspension kinematics, the component design is created, which is then used for FE simulation for NVH investigation. The connection between NVH and suspension kinematics development is the target of the present work. Image Sources: [Mer16, Mer20a].

Following the process counter clockwise, the suspension component design is set by creating CAD models. These models are then transformed into FE models, which are then used for NVH evaluation. This process is then repeated for each DPT loop implementing smaller changes each time. The target of this work is indicated by the topmost green arrow: The top right NVH optimization should be connected to the next kinematics iteration.

Usually, this circle is closed connecting the NVH optimization block with the component design block. This includes component and elastomer element stiffnesses. Besides shifting displacement to the elastomer elements and therefore amplifying the elastomer damping, this changes eigenfrequencies

in the suspension, altering the transfer path through the suspension. This is illustrated in fig. 3.2

The sketch represents a simplified suspension in the top view. Two links, represented by the two springs c_1 and c_2 connect a simplified wheel carrier to the vehicle body. The stiffnesses could represent the combined stiffnesses of links and elastomer elements. With the two springs, the wheel carrier can move in two DOFs: One translational DOF x and one rotational DOF φ. Both DOFs have their own eigenfrequencies, depending on the stiffness parameters c_1 and c_2. The rotational eigenfrequency also depends on the lever arms l_1 and l_2. This simplified model hints the possibilities for eigenfrequency modification by lever arm or kinematics modifications.

Of special interest is the fact that modifications of l_1 or l_2 only affect the rotational eigenfrequency[a], providing a dedicated tuning parameter for the rotational oscillation system. This effect is used for example in the bearing of electric traction machines in the subframe. Larger distances between elastomer elements change the forces and oscillation system [Ers17, p. 216]. Additionally, the modification of geometric parameters could enable the direction specific tuning of transfer paths containing rotational symmetric elastomer elements like for example the connection between track rod and wheel carrier. The indication of individual tweaking parameters poses the dominant research question, which, if this potential exists, would enable the closing of the development circle, indicated by the green arrow in fig. 3.1:

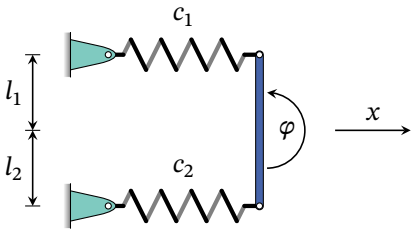

Figure 3.2: One mass oscillator with two DOFs.

[a] Assuming a rigid wheel carrier

Research Question 1. *Is it possible to modify dedicated road noise phenomena by changing the location of specific kinematic hard points?*

3.1.1 Modification of Dedicated Road Noise Phenomena

The investigation of the first research question requires some definitions and restrictions. The points under investigation are the locations of the connection points between suspension links, wheel carrier and subframe. These so-called kinematic hard points describe the coordinate of the geometric center of these connection points.

The modification of the kinematic hard points includes only small changes in the range of few millimeters. This excludes the investigation of topology changes or configuration changes with larger modifications like switching between push rod and pull rod, or shifting the track rod position between front and rear of the wheel carrier. These are not considered small changes. Small changes are of special interest, as after the definition of the general suspension topology and configuration, the individual development domains optimize the suspension kinematics using these small changes. If possible, NVH development could contribute to this optimization process.

Modifying kinematic hard points only shifts the location of these points including the required geometric changes in the suspension components. Additional geometric modifications or topology optimizations to the suspension components are not under investigation here.

A reduced version of the first research question was already investigated in an earlier publication [Wys20a]. A specific kinematics modification on a trapezoidal rear suspension showed a targeted modification of transferred forces through the suspension. Although only looking for a modification and not an optimization, this hinted the possibility of modifying FRFs by altering the suspension kinematics. As the NTFs through the vehicle body have sensitive and non-sensitive frequency ranges, shifting force transfer frequencies could reduce interior road noise. Here, the research question is under investigation on SPL and road noise phenomena level in chapter 5.

3.1.2 Adopting Simulation Models for Kinematics Changes

As the development of the suspension kinematics takes place in the early development phases, the investigation has to be based on digital simulation and investigation. The requirement of adopting these simulation models when investigating kinematics changes, poses the second research question:

Research Question 2. *How can modified suspension kinematics be easily and quickly applied to road noise simulation models, enabling a systematic investigation of the correlations between suspension kinematics and road noise phenomena?*

Chapter 4 presents the used methodology for the adoption of FE road noise simulation models. An automated morphing procedure, which alters a component's shape, is used for the creation of a large data set based on full vehicle simulation. One of the main targets is a dedicated kinematics morphing tool, which does not require intensive manual interaction. The morphing procedure should be based on the FE model and the suspension kinematics changes only, in order to enable a fast procedure in the development process.

3.1.3 Holistic Modification of the Interior Road Noise

If the fundamental investigation of the first research question hints the possibility for targeted road noise modifications, an integration into the development process needs to be established. An optimization focusing solely on the NVH performance is never holistic. Different development domains require certain specifications, which have to be considered while introducing NVH optimization. This is expressed in the research question:

Research Question 3. *How could a modified suspension kinematics be evaluated regarding different development domain requirements?*

These requirements could originate from ride, handling, durability, or package. This work introduces selected requirements in sections 4.4 and 5.5.3 and chapter 6.

3.1.4 Optimization of Interior Road Noise Phenomena

If the preceding research questions indicate the possibility for targeted NVH optimization by modifying the suspension kinematics, the optimization potential should be investigated. For such optimizations, it is necessary to implement a process, integrating the NVH optimization into the suspension development V-Model:

Research Question 4. *Do suspension kinematics optima exist for road noise and how can such optima be integrated into the development process?*

As suspension development is an iterative process, this poses certain additional requirements to the optimization methodology. Whereas the previous research question targeted the requirements of different development domains, this research question targets the optimization methodology itself. For a holistic and integrated optimization, the target is not to create one optimized suspension design, but to quickly generate kinematics variants, which can then be evaluated by all development domains. This is discussed in section 5.5.3 and chapter 6. The target is to obtain design rules and identify complex connections, which can then be resolved in the development process.

3.1.5 Assumptions, Simplifications, and Limitations

In order to define the scope of the investigation, certain assumptions, simplifications, and limitations need to be addressed. The fundamental research project addresses mainly NVH investigation of the road noise, transmitted via structure-borne noise into the passenger cabin in the frequency range up to 300 Hz. The integration into the vehicle development process is addressed for important development domains in the early development phases, but cannot include all existing requirements due to immense complexity.

As the investigation aims at the early development phase, no hardware is available yet. Therefore, the investigation is completely performed on a simulation level. The utilized development simulation models are considered as ground truth, in full awareness that a divergence between simulation and testing exists. This problem is independent from the optimization problem though, and applies for all NVH optimizations [Gen10, Sch12]. For the investigation, the identification of connections and trends between suspension kinematics and road noise is more important for the vehicle development than the accuracy of predicted SPL amplitudes. Even though the simulation results are considered as ground truth, the effectiveness of the optimizations should be tested in a hardware vehicle.

While vehicles of the same type differ in engine, optional equipments or tire sizes, the fundamental investigation has to reduce the variance complexity. For this reason, the simulation investigation is based on one selected vehicle. First insights regarding robustness on a vehicle platform are presented in section 8.2.3. Additionally to the restriction to one vehicle, the investigations are performed on one seating position only. Alternative metrics for further vehicle development are discussed in sections 5.2 and 8.2.3

Changing suspension kinematics requires many additional changes in the vehicle development. For example, modified suspension kinematics often induce elastomer stiffness changes. In order to investigate effects resulting solely from the kinematics changes, these additional modifications are omitted. This does not include component shape modifications, though. Modifying suspension kinematics requires modified suspension component shapes in order to create the new suspension kinematics. The resulting changes in component stiffness and weight are considered, as they are mandatory for hardware kinematics changes. In contrast to elastomer stiffness changes, a new suspension kinematics would be impossible to create without changing the suspension component shapes. The influence of these component shape modifications on the road noise is investigated in section 8.1.

The kinematics changes under investigation are limited to changes in the range of up to $\pm 10\,\mathrm{mm}$. Whereas in the earliest development, suspension kinematics change a lot, this aims at the development phase, where small and

final adaptions to the kinematics are being developed. In these development phases, kinematics changes of such scale have large impacts on the package and suspension parameters [Erb19]. Therefore, larger kinematics changes would be difficult to include into the vehicle, as they would set back the vehicle maturity.

As the suspension kinematics has to fulfill many requirements of different development domains, a road noise perfect suspension kinematics is highly unrealistic. Therefore, this work aims at creating suspension kinematics optimization suggestions, which allow other requirements to be fulfilled. The target is to carve out optimization potential, which can then be discussed and implemented by all development domains.

3.2 Methods Selection

The research questions

1 Is it possible to modify dedicated road noise phenomena by changing the location of specific kinematic hard points?

2 How can modified suspension kinematics be easily and quickly applied to road noise simulation models, enabling a systematic investigation of the correlations between suspension kinematics and road noise phenomena?

3 How could a modified suspension kinematics be evaluated regarding different development domain requirements?

4 Do suspension kinematics optima exist for road noise and how can such optima be integrated into the development process?

can be split into two categories. Question 1 and 4 evaluate the NVH optimization of the suspension kinematics. Question 2, 3, and 4 evaluate the methodology and tools, which are required to answer the NVH questions effectively and efficiently in a vehicle development process.

The developed methodology needs to focus on the integration of NVH optimizations into the development process, rather than creating one single optimized

suspension kinematics. Therefore, the target for the development process is to create design rules, which can then be utilized by all suspension development domains in order to create a suspension, which incorporates NVH demands.

Design rules connect design variables with the desired target values and describe their interaction. This can be done either qualitatively or quantitatively. A commonly used approach to aquire quantitative interactions are analytical solutions of physical models. For complex systems, these analytical solutions are often not available, requiring approximation models. The approximated mathematical connections between the design variables and target parameters are referred to as metamodels. Other names are global approximation models, response surface models, or surrogate models. [Mos08, Har19] Connecting metamodels with desired values or at least preferred directions for the metamodel target parameters creates design rules for the suspension development.

Using metamodels for optimization, especially qualitative optimization becomes more popular. One reason is the increased available processing power [Nol21], which is required to create large data sets containing results from time consuming complex simulation models [Mos08, Büt21]. Additional reasons are the universal application possibilities for the metamodels. The metamodels are not only usable by the creating design engineers, but they can also be made available to other development domains, which enables a better interdisciplinary understanding of the discipline specific connections [Büt21].

There are two ways of evaluating metamodels. Numeric evaluation leads to a result value for a set of desired design variables. Alternatively, the metamodels can be evaluated graphically, leading to qualitative hints for the development process by intuitively indicating sensitivities and visualizing correlations [Har19]. As the metamodels can direct a design process rather than providing one optimum design for each development domain, they could be considered as more important than creating one optimized design. A holistic numeric optimization would require all boundary conditions and requirements to be included into the optimization target, which is hardly possible [Vem15]. Directing the design process mainly requires identifications of tendencies and optimization directions, rather than perfect prediction quality of the metamodel [Mos08, Har10].

Figure 3.3 presents the desired process of metamodel creation for the investigation of suspension kinematics influences on the interior road noise[a]. Starting on the top and left of the diagram, the process starts by creating a DoE for the desired design variables. A DoE systematically varies the design variables, which are the kinematic hard point coordinates representing the suspension kinematics. Each variation of the design variables is referred to as a *sample*. The DoE creation is presented in section 5.1. Research Question 2[b] evaluates the requirement for a fast and easy DoE creation process.

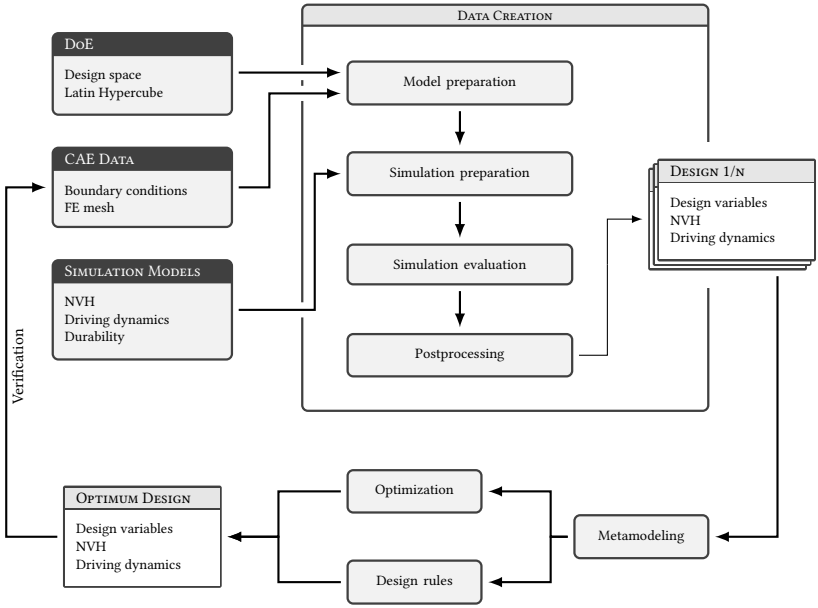

Figure 3.3: Investigation procedure for the creation of design rules or numeric optimization. Translated and extended from an earlier publication [Wys22].

[a] A similar visualization of the process was published on a conference in 2022 [Wys22].

[b] How can modified suspension kinematics be easily and quickly applied to road noise simulation models, enabling a systematic investigation of the correlations between suspension kinematics and road noise phenomena?

Together with CAE data like FE meshes or suspension kinematics tables and simulation models for road noise or driving dynamics, this forms the input for one large data creation block. In this data creation block, simulation data is gathered for the samples, specified in the DoE input. The tools and processes required inside this block are described in chapter 4.

The gathered data forms the basis for the metamodeling in the next step. These metamodels then serve for numerical optimization or the qualitative and cooperative search for compromises with other development domains using them as design rules. The metamodels can also help finding analytical explanations for observed system behavior.

As the prediction quality of the metamodels might not be perfect, a verification loop into the simulation environments is always required [Har19]. This ensures that predicted behavior actually can be observed in the simulation models. As this can be considered as verification, this does not replace hardware validation, which is desired at least once in the development of the methodology. Hardware validation cannot be part of the development process, as hardware—especially the one suiting NVH requirements—is not available in the suspension kinematics defining development phase [Gen10, Sch12, Ref15, Hah17, Ram17].

Both the realization of the methodology and the kinematics investigation follows a process inspired by the V-Model, defined in VDI/VDE 2206:2021-11. The V-Model is part of the holistic product life cycle, defining the tasks within product development. The left thigh of the V-shape represents the decomposition, which subdivides the system into separate tasks. On the bottom of the V-shape the implementation of the system elements takes place. The right thigh represents the step-by-step integration of the system elements into the overall system. From the right thigh to the left thigh, a continuous verification and validation takes place. [VDI/VDE 2206:2021-11]

Figure 3.4 presents the V-Model for the realization of the kinematics investigation. The decomposition and the implementation are further discussed in chapter 4. The integration of the methodology into the optimization for NVH purposes is discussed in chapters 5 and 6 and was additionally published

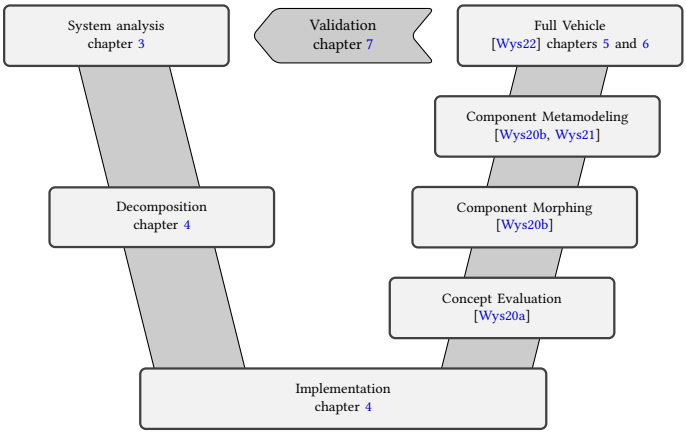

Figure 3.4: V-Model used for the investigation.

earlier [Wys20a, Wys20b, Wys21, Wys22]. The publications walk up the right thigh of the V starting with a first proof of concept [Wys20a], continuing with elaboration of the morphing and basic metamodeling on component level [Wys20b] and further metamodeling on component level [Wys21] up to full vehicle investigation [Wys22]. The last publication already mentioned the validation process, which is presented in detail in chapter 7.

The integration of the full optimization process into the vehicle development process forms an additional V-Model, described in section 8.2.2.

3.3 Selection of the Simulation Method

Figure 3.3 presented the required input data for the investigation. This section identifies the required simulation models. In a first step, the suitable development phase needs to be identified from the suspension development process, introduced in section 2.3.4. The earliest development stages define the suspension topology with large modifications in the suspension kinematics. The suspension configuration phase is the main phase, when suspension kinematics are modified and finally set. In this phase, an optimization of the suspension kinematics should be situated.

Given the first component designs for the suspension, the FE model creation starts, which is the enabler for first NVH investigations regarding interior road noise. As both a modifiable suspension kinematics, and a simulation model for road noise evaluation are required for the investigated kinematics optimization, this development phase is ideally suited. It enables the kinematics modification investigation on a development proven simulation model, including potential consequences from required component shape modifications.

The window for optimization is narrow, though. The later in the development process, the less margin exists for kinematics modification. This is due to fixed evaluations of package, durability, or handling requirements. Additionally, first manufacturing tools might be specified, prohibiting any alteration of the suspension kinematics.

For road noise evaluation, the standard road noise simulation model at Mercedes-Benz is used, indicated by NVH in the *simulation model* box in fig. 3.3. This simulation model is FEM-based and includes the full vehicle including excitation, tire, suspension, body, and air cavity inside the passenger cabin. Using FE simulation models with flexible suspension components enables the evaluation of both the changing lever arms and component stiffnesses due to kinematics changes. The *CAE Data* box in fig. 3.3 includes mainly the suspension kinematics and FE meshes of the involved components. The details of the *simulation model* and *CAE Data* and are discussed in chapter 4.

Suspension parameters are one of the main indicators used in early suspension kinematics determination. Therefore, these suspension parameters are included in the evaluation of NVH optimized suspension kinematics. In the *CAE Data* box, this requires only the suspension kinematics in the form of coordinates for each kinematic hard point location. The details of the calculation are discussed in section 4.4. It is to note that the consideration of suspension parameters as additional boundary conditions for the suspension kinematics optimization is only seen as an example. Additionally, more complex load cases could be integrated after a positive fundamental investigation.

4 Simulation Model

For road noise investigations in the early development phase, no hardware is available. Therefore, the investigation and optimization is based on simulation models. This section presents the vehicle under investigation and its simulation models for transfer functions, SPLs, and suspension parameters. These simulation models are the basis for the implementation of a suspension kinematics modification process, required in Research Question 2[a].

4.1 System under Investigation

The system under investigation is the five link rear suspension of a Mercedes-Benz *W206*[b]. As the kinematics investigation performs fundamental research, it is important to work on a final suspension version, which could also be made available for hardware validation without prototyping a complete suspension subassembly. If the methodology is successfully applied here, an investigation in the early development phase of a new platform is possible.

A vehicle with five link suspension is selected, as the five link suspension provides the most DOFs in the suspension link positioning. This enables the possibility to precisely compensate undesired kinematic effects caused by the acoustic kinematics optimization. The selected suspension in fig. 4.1 consists of the wheel carrier with brake system and wheel hub, the five links track rod, spring link, camber arm, pulling strut, and pushing strut, torsion bar, torsion

[a] How can modified suspension kinematics be easily and quickly applied to road noise simulation models, enabling a systematic investigation of the correlations between suspension kinematics and road noise phenomena?

[b] 2021 model of the *C-Class* sedan *C200*

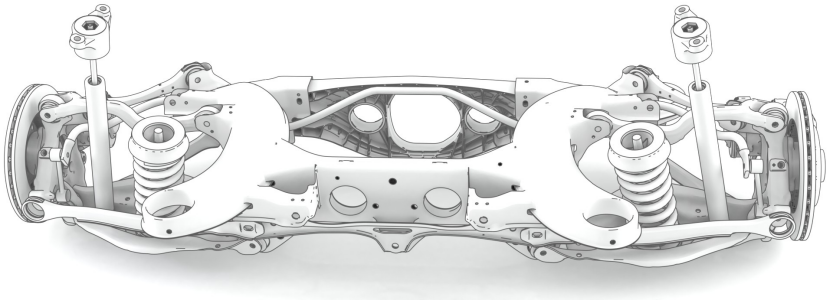

Figure 4.1: Five link rear suspension under investigation.

bar linkage, subframe, steel spring, damper, and additional attached parts such as sensors or protection covers. The wheel carrier, links, and subframe are connected via elastomer bushings. The suspension is connected to the body via subframe mounts and spring and damper top mounts.

The transfer path for structure-borne noise in the hearing frequency range from the wheel center to the vehicle body is presented in fig. 4.2. It details the *suspension* part of the full vehicle transfer path presented in fig. 2.1 on page 8[a].

The structure-borne noise transfers into the wheel carrier via the wheel hub. From there, the suspension links and torsion bar transfer the vibrations to the subframe and through the subframe mounts further to the vehicle body. The additional transfer path between subframe and vehicle body via the powertrain is neglectable for road noise evaluation. Spring and damper provide a direct path from the spring link into the vehicle body. From the vehicle body, the structure-borne noise transfers into the air cavity inside the passenger cabin and becomes airborne noise, which is then perceived as road noise by the passengers. Additional transfer paths like direct transfer from the wheel center through the powertrain, transfer via cables and tubes, or airborne noise transfer around the vehicle are omitted here. Each connection point between the components in Figure 4.2 is usually provided with an elastomer connection element. This further increases the complexity of the transfer path system.

[a] Figure A.1 on page 208 combines both illustrations into the full transfer path

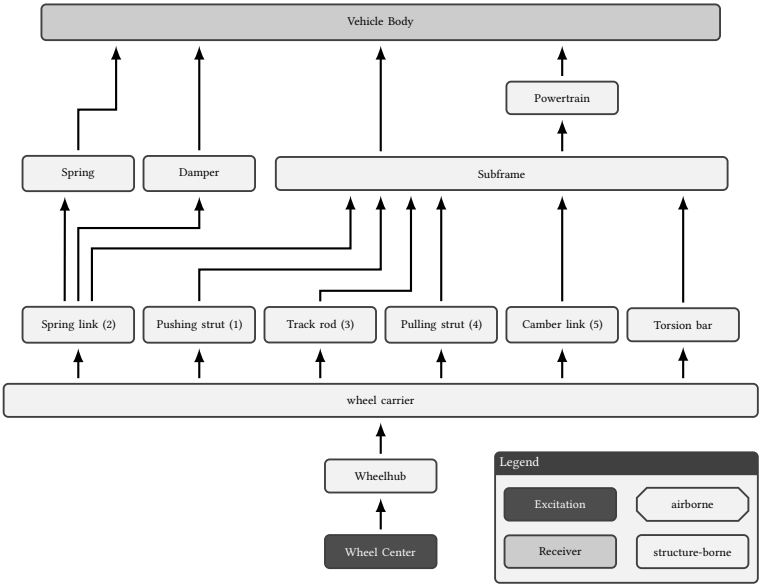

Figure 4.2: Transfer path of the five link rear suspension under investigation for road noise inducing vibrations from the wheel center to the passenger ears. The transfer path through the powertrain is omitted in this investigation. Usually all components are connected via elastomer elements. The numbers match the naming scheme in fig. 4.4

All connection points between the suspension links and wheel carrier on the one side and subframe on the other side represent kinematic hard points. Their locations are under investigation for their influence on road noise. Each kinematic hard point represents three degrees of freedom. In a Cartesian coordinate system, these are the x, y, and z direction.

The suspension under investigation uses the Cartesian coordinate system I presented in fig. 4.3. It is located in the center of the suspension, exactly in the middle between left and right wheel center points. The x axis points backwards with respect to the driving direction, the y axis to the right with respect to the driving direction, and the z axis to the top of the car.

In this coordinate system I, each kinematic hard point is defined as

$$\vec{P}_{\mathrm{n}} = \left[P_{\mathrm{n,x}}, P_{\mathrm{n,y}}, P_{\mathrm{n,z}}\right]^{\mathrm{T}} \tag{4.1}$$

Figure 4.3: Cartesian coordinate system I for the rear suspension. The origin is located on the center of the dashed connection line between left and right wheel center point. Vehicle image part of [Mer22d].

for the vehicle-side kinematic hard points and

$$\vec{R}_{\mathrm{n}} = \left[R_{\mathrm{n,x}}, R_{\mathrm{n,y}}, R_{\mathrm{n,z}}\right]^{\mathrm{T}} \tag{4.2}$$

for the wheel-side kinematic hard points.

Kinematics changes are stated by

$$\Delta\vec{P}_{\mathrm{n}} = \left[\Delta P_{\mathrm{n,x}}, \Delta P_{\mathrm{n,y}}, \Delta P_{\mathrm{n,z}}\right]^{\mathrm{T}} \tag{4.3}$$

$$= \left[P_{\mathrm{n,x,new}} - P_{\mathrm{n,x,old}}, P_{\mathrm{n,y,new}} - P_{\mathrm{n,y,old}}, P_{\mathrm{n,z,new}} - P_{\mathrm{n,z,old}}\right]^{\mathrm{T}} \tag{4.4}$$

and

$$\Delta\vec{R}_{\mathrm{n}} = \left[\Delta R_{\mathrm{n,x}}, \Delta R_{\mathrm{n,y}}, \Delta R_{\mathrm{n,z}}\right]^{\mathrm{T}} \tag{4.5}$$

$$= \left[R_{\mathrm{n,x,new}} - R_{\mathrm{n,x,old}}, R_{\mathrm{n,y,new}} - R_{\mathrm{n,y,old}}, R_{\mathrm{n,z,new}} - R_{\mathrm{n,z,old}}\right]^{\mathrm{T}} \tag{4.6}$$

respectively.

The naming scheme for each kinematic hard point is visualized in fig. 4.4. Each link in the suspension is represented by its own number n. For the five link suspension, each link holds one P and one R kinematic hard point. For the components spring and damper, n is replaced by S and D respectively. This forms the kinematic hard points $\vec{R}_{\mathrm{S}}$ and $\vec{P}_{\mathrm{S}}$ and $\vec{R}_{\mathrm{D}}$ and $\vec{P}_{\mathrm{D}}$ for the bottom and the top kinematic hard points, respectively. The torsion bar is connected to

the subframe at P_{TB} and the wheel carrier at R_{TB}. The linkage in between is named P_{TBL}. These locations result in 17 kinematic hard points with three displacement directions, which sums up to 51 possible DOFs. The left and right suspension half are considered as symmetrical, making one DOF modifying both suspension sides simultaneously. In order to reduce the parameter space, not all DOFs are selected in the following investigations.

It is to note that the wheel center is no degree of freedom and the location and orientation angle of the wheel hub is fixed in this investigation. Therefore, the wheel hub keeps its orientation regardless of the kinematics changes and the static suspension parameters camber and toe remain constant.

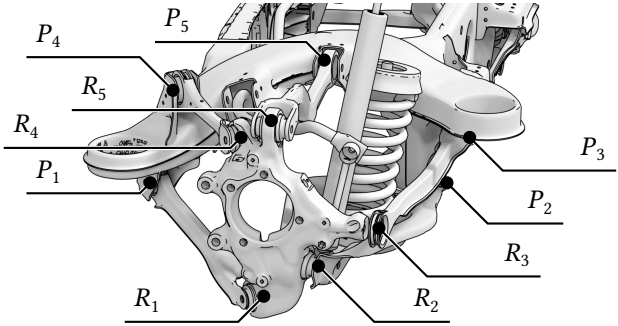

Figure 4.4: Naming convention for the used kinematic hard points. Each link is unambiguously identified by its number n. The letters P and R represent body and wheel side of the links, respectively. Spring, damper, and torsion bar kinematic hard points are not visualized here for simplification.

4.2 Utilized Types of Simulation Models

For the investigation, there are different kinds of simulation models. NVH simulation uses FE models for the calculation of eigenvalues, FRFs, and SPLs. These simulation models operate at different levels of detail, from component level to full vehicle level. The FE models are presented in section 4.3.

An analytical rigid body model is utilized for the calculation of suspension parameters. This simulation model is presented in section 4.4.

Further simulations regarding the effects of modified suspension kinematics could be carried out. This could include driving dynamics or durability analysis. In the vehicle development process, these calculations are performed by the corresponding development departments. As the modification of suspension kinematics due to improved NVH performance can only be a suggestion to the suspension development, these additional calculations are not considered here.

The investigation of the first research question[a] follows the V-Model. The implementation and investigation starts on component level and enlarges the scope afterwards onto subsystem and full vehicle level. On component level, eigenvalues and FRFs contribute to NVH performance. Component FRFs were investigated using the presented methodology in earlier publications [Wys20b, Wys21]. Eigenvalues and FRFs on suspension level were investigated as a proof of concept in the preceding publication [Wys20a]. Here, the focus is set to full vehicle SPL simulation, as presented on a conference in 2022 [Wys22].

4.3 Finite Element Simulation Model

For the presented investigation, full vehicle FE simulation models provide estimations for the NVH performance. The FE model consists of three types of subsystems, explained in detail in the following sections. The vehicle body

[a] Is it possible to modify dedicated road noise phenomena by changing the location of specific kinematic hard points?

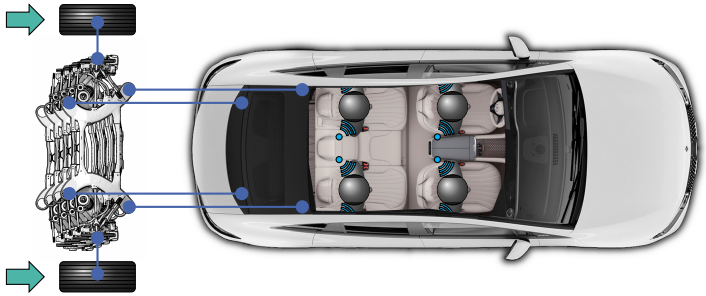

Figure 4.5: Different parts of the full vehicle model utilized for rear suspension kinematics investigations. Excitation, vehicle body and front suspension are the same for each kinematics configuration, only the rear suspension changes. Vehicle images by Mercedes-Benz Group Media [Mer22c, Mer22d].

includes bodywork, trim, and air cavity. The subsystem suspension includes suspension components, elastomer bushings, brake system, and wheel hub. The wheel model attaches at the wheel hub, including the excitation for SPL simulation.

The full vehicle SPL simulation model for suspension kinematics investigation is illustrated in fig. 4.5. It consists of the vehicle body subsystem, two subsystems for the front and rear suspension and four wheel subsystems including excitation. Modifying the kinematics of the rear suspension only changes the rear suspension subsystem. Therefore, vehicle body, front suspension and all wheels remain unchanged. In fig. 4.5 this is represented by multiple different rear suspension subsystems.

The subsystems are connected by coupling all six DOFs of a pair of coincident FE grids on both subsystems. The subframe mounts, damper top mounts, and spring top mounts couple the rear suspension to the body. The front suspension links are usually directly coupled to the subsystem body. The wheel center point couples the subsystem wheel to the subsystem suspension.

The full vehicle FE model is identical to the simulation model used for series development. It consists of 13 000 000 FE grids connected by 11 000 000 solid and 4 000 000 shell elements. Because this investigation is performed as a proof of concept after the series development of the vehicle, the FE model of

the last DPT loop is used. This guarantees a detailed simulation model, which is considered valid and suitable for SPL prediction.

4.3.1 Vehicle Body Model

For the vehicle body, there are different modeling approaches in FE simulation. They differ in the level of modeling detail. Common approaches use simplified representations like superelements or substructuring techniques [Har06, Sti10, Mor12, Gae14]. These simplified representations reduce calculation time while preserving the simulation result quality. They require additional model preparation effort, though.

For this investigation, the simulation resources to use full FE representations of the vehicle body are available. Therefore, there are no simplifications applied to the model. Using the most detailed model available for the fundamental investigation, possible effects resulting from model simplification can be prevented. Figure 4.6 shows the vehicle body FE model including the interior. Passengers are not considered in the simulation model.

The air cavity inside the passenger cabin includes the FE grids for SPL evaluation. In the used simulation model, there are SPL evaluations for both ears of the front left and right, as well as the rear left and right seating positions. This results in eight SPL evaluation points.

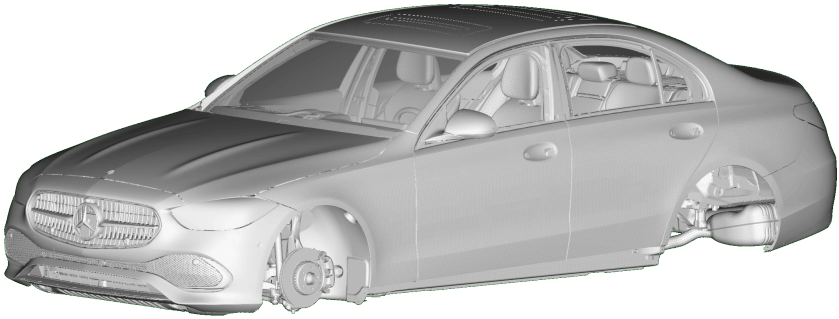

Figure 4.6: FE model of the vehicle body, including bodywork, trim, and air cavity.

4.3.2 Suspension Model

The FE model for the rear suspension includes the suspension components, modeled as solids or shells, depending on the shape and manufacturing technique of each component. The model consists of roughly 1 500 000 FE grids and 1 000 000 elements.

The suspension components are connected using simplified representations for the elastomer bushings. For each local direction, a stiffness and damping parameter is given. The local direction of each elastomer bushing is defined by the orientation of the attached suspension link. Figure 4.7 illustrates the orientation of the elastomer bushings for the pull rod kinematic hard points $R_{4,x}$ and $P_{4,x}$. Each bushing's local z-direction points towards the opposite bushing. The x-direction specifies the axial direction of the bushings. As the location of the kinematic hard points define the orientation of the elastomer bushings, the rotation of the kinematic hard points itself is no DOF for the investigation of kinematics changes.

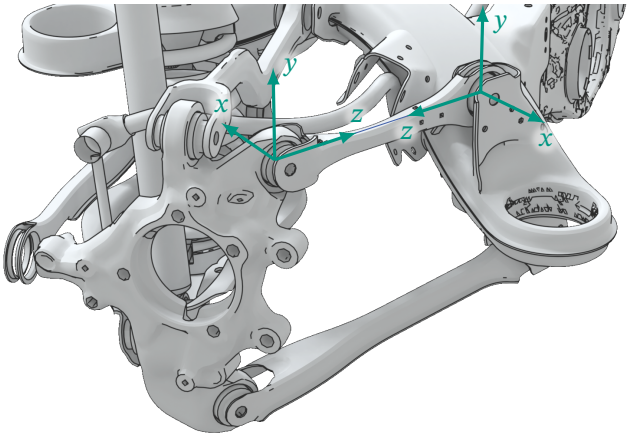

Figure 4.7: Orientation of the elastomer bushings for the pull rod. The local z directions point towards each other, the local x directions define the bushings' axial direction.

The location of the elastomer bushings is definied as centered at the kinematic hard point locations. These locations are defined using the coordinate systems presented exemplarily in fig. 4.7 and therefore exactly follow a displacement of a kinematic hard point.

When changing the location of single kinematic hard points and with it the position and orientation of the elastomer bushings, undesired kinematics configurations can occur. This is adressed by kinematics compensation in the optimization chapter in sections 6.2.3 and 6.2.4 and chapter 7.

4.3.3 Wheel Model

A wheel model is important for the simulation for two reasons. On the one hand, it provides the excitation for the calculation of SPLs, on the other hand the interaction between suspension and wheel is important for many road noise phenomena. For the fundamental investigation, the relative comparison between different kinematic layouts is most important. For the vehicle development process, the absolute prediction quality of the simulation also plays a crucial role and undergoes constant advancement [Sch12]. In FE simulation, there are different approaches for the modeling of vehicle wheels and the excitation for road noise simulation. There are approaches like applying synthetic loads [Bak87, Bak89, Wys20a] or measured spindle forces [Har06, Mat14] to the wheel hub, using simplified physical models [Oer01, Hei11, Nie12, Sch12, Wol14, cos, Fra, Her21, Sch21e, Uhl21a, Uhl21b, Uhl21c] or modal tire models [Kos14, Wol14, Gla17, Uhl21a] as well as full FE representations of Tire, Rim, and Cavity [Gro13].

The selection of the most suitable tire model depends on various different requirements to the simulation. One of the most crucial requirements is the desired frequency range. NVH simulation usually requires a frequency range up to 400 Hz. As the influence of the suspension kinematics is under investigation and the interaction between suspension and tire should not be omitted, a modal or full FE representation of the wheel is selected. For the vehicle under investigation, a modal model including tire, air cavity and a

flexible wheel is available. This model is based on the publications by Grollius and Glandier et al. [Gro13, Gla17] and is used for the SPL simulation.

4.3.4 FE Simulation Jobs

For NVH simulation, different types of jobs are generated from the previously described parts of the FE model. There are jobs using only a single component for eigenfrequency calculation, the subsystem suspension for the calculation of FRFs, or full vehicle SPL simulations using all the subsystems.

For full vehicle SPL simulation, the body simulation model is combined with both suspension simulation models and the attached modal wheel models. The excitation for the modal model applies a frequency dependent imposed displacement on the 2D representation of the contact patch between road and tire. This is a commonly used type of excitation for road noise [Kid11, Sch12, Gla17]. Each rib of tread blocks receives its own excitation. The excitation amplitudes at the different ribs and the phase relationship between ribs and also between tires are based on the stochastics of a road scan. This excitation modeling is based on the publication by Glandier et al. [Gla17]. For the investigation of the rear suspension kinematics, only the rear tires receive an excitation. This is possible, as the excitations are statistically uncorrelated [Kos14] and enables the targeted optimization of road noise phenomena originating from the rear suspension [Eis08].

The simulation results consist of sound pressure spectra at each ear position for each seating position. These results are then converted to dB

$$L_\mathrm{p} = 20 \log_{10} \left(\frac{p}{p_0} \right) \quad \text{with} \quad p_0 = 2 \times 10^{-5}\,\mathrm{Pa} \tag{4.7}$$

and A-weighted [DIN EN 61672-1:2014-07], resulting in A-weighted SPL spectra. For easier readability, these results are simply referred to as SPL spectra in the following.

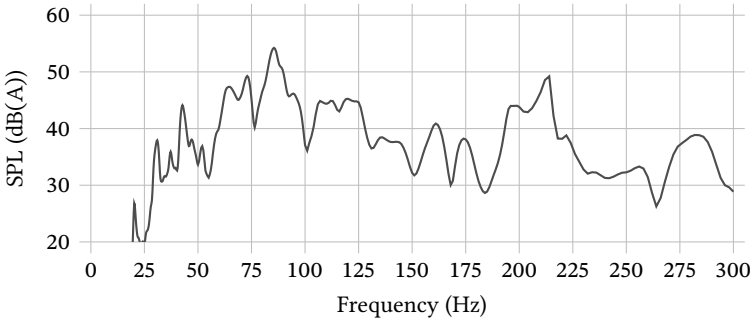

Figure 4.8: SPL spectrum for the initial full vehicle simulation model. Rear left seating position, right ear.

For the following fundamental investigation, most results are specific to one ear position. Figure 4.8 presents the SPL spectrum of the initial vehicle configuration for the right ear position of the rear left seating position[a]. This spectrum forms the reference curve for the following investigations and optimizations.

For series development, the optimization target should be a metric considering all seating positions, instead of a single SPL spectrum. A maximum metric is commonly used for this purpose [Uhl20a, Uhl21b], representing the maximum SPL value for each ear position at each frequency step. This could also include different load cases or vehicle types for each suspension configuration. As this approach is important for series development, but not for the fundamental investigation of the influences, a single SPL spectrum is used here.

Besides full vehicle simulation, NVH development also relies on subsystem simulation. A commonly used subsystem evaluation is the suspension as a blocked forces system. Both in simulation and testing, the subsystem suspension is fixed against ground at the attachment points to the body and excited at the wheel hub [Har06, Sel08, Gen10, Bin14, Ram17, Uhl20a, Uhl21a, Sel22]. These excitations range from full wheels on the test bench to synthetic loads on the wheel hub. NTFs using the transfer forces at the fixed coupling points

[a] This Spectrum was included as a reference curve in an earlier published conference paper [Wys22].

to the vehicle body, can lead to the vehicle interior noise for NVH performance evaluation [Dou06, Eis08, Ram17, Kim18, Llo18, Zel18].

Often, OEMs use the same suspension configuration in different vehicles. Investigating the suspension on subsystem level enables the investigation of effects for all of the relevant vehicles at the same time. This prevents an optimization from being beneficial to one vehicle but disadvantageous for another vehicle. The robustness of an optimization is discussed in section 8.2.3 after the fundamental investigation on one vehicle.

An earlier publication hinted potential for SPL improvement through suspension kinematics changes by targeted modifications to the FRFs of a suspension simulation model [Wys20a]. As this finding required further investigation on full vehicle level, the focus and optimization target in this investigation is the SPL inside the passenger cabin using full vehicle simulation models. The methodology does not differ for the investigation of subsystem or component levels, though.

On component level, investigations of durability or eigenfrequencies are common. For testing purposes, a component durability simulation was added to the data set. This enabled the resolvement of a target conflict between SPL and a buckling load case on a suspension link. The investigation of this buckling load case proved the possibility to easily integrate additional load cases to the investigation. Discussion of further possible load cases is omitted here, as the possibilities are unlimited, as long as the simulation input and output are externally accessible for scripting.

4.4 Suspension Parameter Calculation

Modifying suspension kinematics always implies modification to the suspension properties. Therefore, basic suspension parameters, quantifying these properties, need to be considered in addition to the NVH investigation.

The suspension parameters are calculated using an in-house vector analysis tool for the rigid suspension system, following the approach described by Matschinsky [Mat07, Hei11]. Using this tool, the relevant suspension parameters are calculated for each kinematics configuration. The suspension parameters[a] Toe angle, Toe angle gradient, Camber Angle, Camber angle gradient, Caster angle, Trail, Diagonal spring angle, Anti-Dive, Anti-Squat, Instant Center of Rotation (ICR) height, Damper ratio, Spring ratio, Scrub radius, Kingpin inclination (angle), Kingpin offset at wheel center, Kingpin offset[b], Wheel load lever arm, Lengths of track rod and steering arm, (overall) Steering ratio, and ICR gradient are used under their definitions presented in DIN ISO 8855:2013-11.

The suspension parameters divide into the two categories scalar initial values and curves. The scalar initial values describe the suspension without movement in the base state. Curves describe the suspension behavior for the deflecting body or steering maneuvers. Basically, they describe the change of the initial values for moving wheels. For the simplification in this investigation, only the gradients in the initial suspension configuration are under consideration, rather than the full deflection or steering curves. This represents the behavior tendency for small wheel movements out of the initial position.

As the attachment surface between wheel and wheel carrier remains fixed in place, the suspension parameters toe angle and camber angle remain constant for the kinematics modifications under investigation. This only applies for the parameters themselves; their gradients are subject to the kinematics modifications as the trajectory of the suspension DOF changes.

There are many more calculation and simulation possibilities for suspension and driving dynamics parameters. As the investigation focuses on the NVH performance and uses the presented suspension parameters only as basic check-parameters for the suspension kinematics, further investigation has to be performed by the respective development domains for each suggested kinematics modification. Therefore, further parameters or simulations are not under investigation here.

[a] German translations can be found in appendix D

[b] Short for the german *Stoßradius* (kingpin offset at wheel center cos (kingpin inclination))

4.5 Implementing Suspension Kinematics Modification

Investigating suspension kinematics modifications requires altering the simulation models. The translation of the kinematic hard points needs to be imposed on them. How to impose these modifications easily and quickly to existing simulation models is under investigation in Research Question 2[a].

For the calculation of the suspension parameters, only the location of the kinematic hard points is required. For the road noise FE simulation, the modification is much more complex. Figure 4.9 presents the components involved in a kinematic hard point investigation with all 51 DOFs. A modification of $\vec{P}_n$ and $\vec{R}_n$ with $n \in [1,5]$ affects the shape and hard point position of the colored components wheel carrier, suspension links, and subframe. The elastomer elements, highlighted in gray, are bound to the hard point locations and therefore require repositioning. Modifications of $\vec{P}_S$, $\vec{R}_S$, $\vec{P}_D$, $\vec{R}_D$, $\vec{P}_{TB}$, $\vec{R}_{TB}$, and $\vec{R}_{TBL}$ additionally affect the white components spring, damper, torsion bar,

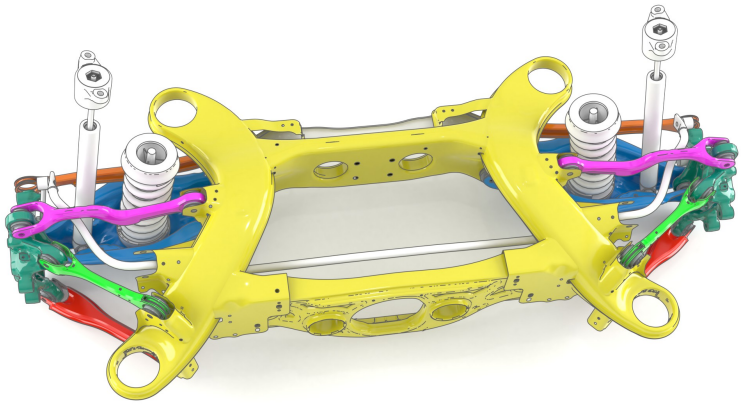

Figure 4.9: Components involved in changing the suspension kinematics.

[a] How can modified suspension kinematics be easily and quickly applied to road noise simulation models, enabling a systematic investigation of the correlations between suspension kinematics and road noise phenomena?

and torsion bar linkage. Modifications to the spring link $\vec{P}_2$ and $\vec{R}_2$ and to the lower spring and damper hard points $\vec{R}_S$ and $\vec{R}_D$ influence each other. The same applies to changes to the wheel carrier and the torsion bar linkage.

For the application of geometric modifications on FE simulation models, different approaches exist. So-called Multi Point Constraints (MPCs) connect single FE nodes on a force level without any geometric information. They are often used for the connection of non-fitting components, for example when compensating geometric incompatibilities between predecessor components and more recent parts of the simulation model. As the forces are transferred from one node to another, no lever arms between the nodes are regarded, as long as they are not considered in the mathematical formulation of the MPC. This prevents MPCs from being an adequate and easy to use modeling approach for kinematics modifications.

Another possibility to model kinematics changes are Rigid Body Elements (RBEs). These elements act as rigid material connecting FE nodes. They are massless and do not allow any deformation. Different to MPCs, they act as lever arms, though. For MBS the usage can only be successful, if the lost influence of mass changes is neglectable. For FE simulation the stiffness influence needs to be considered as well [Har06, p. 178]. For example, Harzheim et al. uses RBEs for the modeling of selected kinematics modifications [Har06].

For the present investigation, the usage of RBEs is problematic, though. Figure 4.10 illustrates the problematic behavior of RBEs for the planned kinematics adoption in the used FE model. The sketches represent a simplified suspension system in the top view. The vertical bar represents the wheel carrier, supported against the vehicle body by two suspension links.

Figure 4.10a illustrates the initial assembly configuration with the initial suspension kinematics. With $F/2$, the force attacking the wheel carrier is equally distributed to the two bearings. The two suspension links are loaded with push or pull forces only, no bending is present. This applies for both cases regarding the components as rigid bodies or as flexible bodies.

Figure 4.10b introduces the kinematics modification Δl, increasing the wheel carrier width including the distance between the two bearings. RBEs connect

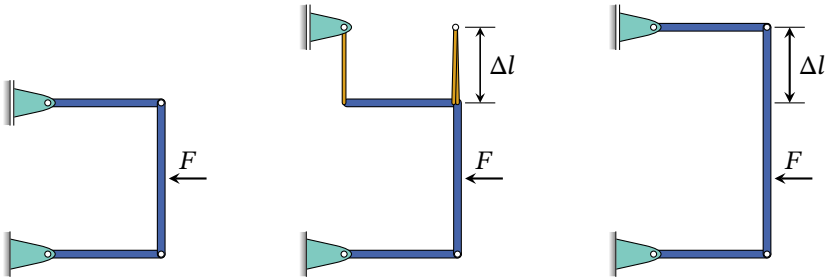

(a) Initial component configuration

(b) Modified component configuration

(c) Modified component shapes and positions

Figure 4.10: Illustration of rigid connection element disadvantage. The vertical bar represents a wheel carrier, the horizontal bars represent suspension links. Implementing a modified lever arm using a rigid connection element introduces torques into a suspension link. While being physically correct, a component designer would presumably modify the adjacent component.

the existing structure to the new kinematic hard points both at the wheel carrier–link connection and the link–bearing connection. Considering the components as rigid bodies, does not change anything to the load case of the links, except for different force values. The upper link is now loaded with $F/3$, assuming the original wheel carrier length was $2l$.

Assuming the upper link to be a flexible body changes the consideration drastically, though. Because the components are connected via rotational DOFs, representing the suspension elastomer elements, this induces bending into the suspension link. This changes the load case for the component completely and therefore the vibration system.

For a real world kinematics modification, the suspension design would be altered in a way, illustrated in fig. 4.10c. The link would be modified at least in its position, possibly also in its shape. Ideally, the link would still be loaded with push or pull forces only. Both the bearing and the wheel carrier need shape modification to adopt to the new suspension kinematics.

This example indicates the requirement for component position and shape modification in order to implement kinematics modifications to the FE simulation model. Additionally, this includes a first draft of real world design

changes, which need to be applied to the components in order to realize the kinematics modification.

Figure 4.11 presents the main components involved in suspension kinematics modifications. Additionally, there are spring, damper, and torsion bar (link) involved. The components are separated in relatively simple, slim components in fig. 4.11a and more complex components in fig. 4.11b. The slim components consist of nearly constant cross sections or at least easy to describe modifications. The red component's cross section for example is only scaled in one direction. The transition to the more complex components is fluent. For example, the pink camber rod is bent, making a description already more difficult. The blue spring link consists of piecewise constant cross sections with heavy modifications in the middle.

(a) Long and slim components

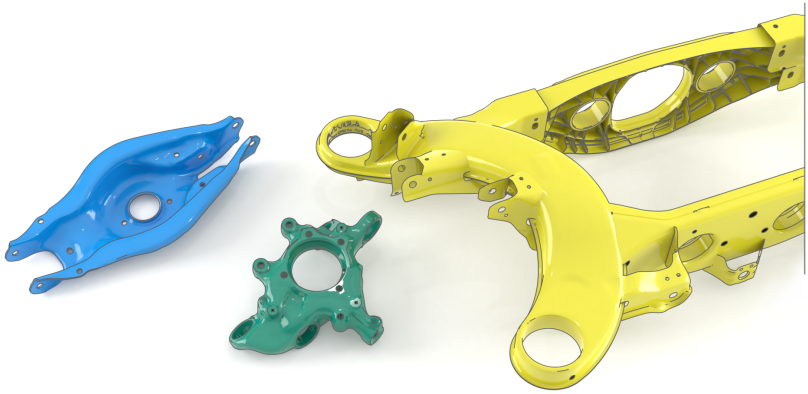

(b) Complex components

Figure 4.11: Separated suspension components involved in changing the suspension kinematics, identical color scheme to fig. 4.9.

Both types of components require alteration for the suspension kinematics modification. Depending on the complexity of the involved components, the required methodology differs.

4.5.1 Modifying Slim Components

The simple geometry of the slim components presented in fig. 4.11a is well suited for model simplification. For fundamental investigations in particular, this is a common technique for the reduction of model complexity while sustaining result quality [Sti10, Hel12, Mor12, Gae14, Tan18, Sch21e, Jeo22].

Within the present research project, the model reduction was investigated using the track rod of a trapezoidal suspension. In a master thesis, the reduction was implemented and investigated on component level NVH behavior [Cha19]. In a following publication, the simplified track rod was integrated into the full suspension transfer path and served the investigation of a kinematics modification [Wys20a].

The track rod was simplified using a parametric FE model, representing the link using beam elements. The simulation results for the FRFs proved valid, making the simplification a valid method for the exploration of kinematics modifications. [Wys20a]

The manual effort, required for each new component is quite high, though. Therefore, the method of creating simplified and parametric FE models for modified components is too time-consuming in a series development process.

4.5.2 Modifying Complex Components

A simplification of suspension components using beam elements like previously presented, is inconvenient for complex components. While possibly viable for the extended track rod attachment on the wheel carrier or the pipe-like parts of the subframe, the majority of the complex components need to be modified in a different way. The shape modification of complex components

requires significantly more effort compared to the modification of scalar parameters [Har19, Büt20]. Different to the slim components, creating parametric FE representations for the complex components is not feasible. Therefore, an existing component representation needs to be modified to resemble the desired kinematics modifications.

Modifying component structures divides into three domains. There is sizing, shape optimization and topology optimization. [Har19, S. 3] Sizing induces the smallest changes into the component. This includes for example changing metal sheet thicknesses. Topology optimization on the other hand drastically changes the component structure. In a mathematical sense, changing the topology creates holes in the component. Shape optimization is positioned in the middle changing the component shape by rearranging the material without creating a different topology. [Har19]

Modifying the suspension kinematics requires at least shape modifications. Moving the kinematic hard points moves the component material without necessarily changing the topology. This could be a second step to include for example weight reduction to the development process. As this is out of scope for the present investigation, a shape-changing algorithm is required.

There are different approaches for component shape modifications. The first method is the modification of parametric component CAD models [Har19, p. 188]. As road noise simulation relies on FE simulation, this would require a remeshing in order to obtain the FE mesh for the modified component [Auw07, Har19]. The second approach is to directly modify the existing FE mesh, without the step back to CAD [Har19]. Using this approach, only the position of the FE nodes is altered. Changing only the shape of the FE mesh allows the entire meshing, parametrization, and setup to remain unchanged [Auw07, Sta12, Gra14, Har19]. This makes the shape modification process completely independent from element types or modeling techniques, but limits the modifications to small displacements.

Changing the shape of a three-dimensional, digital representation of a component is often called morphing. To perform morphing on a component,

usually a commercial FE preprocessor is required [Büt20, p. 53]. The application of these multi purpose morphing tools usually requires manual effort and know-how to operate.

The desired application in the series development poses specific requirements to the methodology, indicated in Research Question 2[a]. Morphing directly on the FE model is favorable over modifying CAD models, as the FE models are present and required in any case. For a fast integration of the most recent simulation model, no manual preprocessing is desired. The modification of the complex components needs a meta-representation. This meta-representation reduces the complex description of the component modification on each FE node to few manageable variables [Gra14]. Most practically, the displacements at the kinematic hard points could form such a meta-representation. Additionally, there are specific points that are required to remain unchanged. For example, the attachment points for wheel hub or brake caliper must remain unchanged for the investigation of the suspension kinematics. The input of these imposed displacements and zero displacements should be convenient, for example a simple text file. This input, additionally to the FE mesh, should be all manual labor required for the creation of the new simulation model. This enables easy and fast integration of the suspension kinematics optimization into the series development process. Scripting the whole process enables the automated creation of data sets for later metamodeling.

Applying rotation to a component is achieved by a combined displacement of multiple FE nodes [Har19]. The requirement of component rotation needs to be elaborated for suspension kinematics modifications. Figure 4.12 illustrates a suspension kinematics modification with and without rotation.

Figure 4.12a presents the initial component configuration. The two circles represent the kinematic hard point locations with the box representing a component connecting them. The two arrows indicate the orientation of the elastomer

[a] How can modified suspension kinematics be easily and quickly applied to road noise simulation models, enabling a systematic investigation of the correlations between suspension kinematics and road noise phenomena?

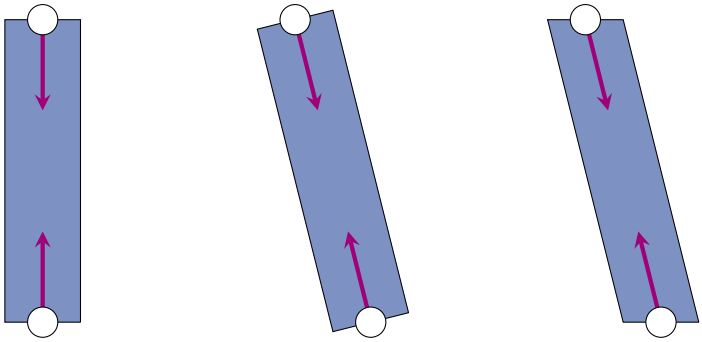

(a) Initial configuration **(b)** Rotating the component **(c)** Sheering the component

Figure 4.12: Geometric component modification to model kinematics changes.

element according to section 4.3.2 and fig. 4.7. Figure 4.12b introduces a modification of the suspension kinematics. The modified component still connects the two kinematic hard points. The modified kinematics is realized by a rotated connection component. The vertical length change introduced by rotating the component is omitted in this example. Figure 4.12c implements the modification by solely translational morphing which results in a sheered component. For the track rod the required rotation angle α for the maximum investigated translation of 10 mm at the wheel-side kinematic hard point amounts to

$$\alpha = \tan^{-1}\left(\frac{\Delta R_{3,\mathrm{x}}}{l_3}\right) = \tan^{-1}\left(\frac{10\,\mathrm{mm}}{466.5\,\mathrm{mm}}\right) = 1.2° \tag{4.8}$$

with the displacement $\Delta R_{3,\mathrm{x}}$ and the length of the track rod l_3. This rotation is neglected in the following investigation. The neglection only affects the rotation of the component FE mesh, though. The elastomer elements follow both the translation and the rotation as indicated by the arrows in fig. 4.12 and described in section 4.3.2.

The investigation of the suspension kinematics requires a process, for shape modification of given FE models. The imposed translations and zero translations need to be interpolated onto each FE node of the component. This process is referred to as *mesh morphing*, *mesh warping*, or *mesh moving* [Sta12], in the following simply called *morphing*. Morphing is a common methodology

for design evaluation, in particular for fundamental investigations in early development phases [Sta12].

Originating from computer graphics applications [Bru18], morphing is often used in movies for animating the transition between a source shape and a target shape [Ale02]. From these animation applications, morphing found its way into technical optimization of components and complex systems.

For example, in the automotive NVH development, morphing is commonly used for design exploration. For example, Moroncini et al. use a beam and shell FE model of the vehicle body for early stage NVH development. The connection elements between beams and shells are fitted using a morphing approach [Mor12]. Maressa et al. design NVH affecting bead layouts using a mesh morphing approach on a vehicle body FE simulation model [Mar11]. Similar to that, Balasubramanian et al. perform panel bead and curvature optimization for NVH objectives using morphing techniques in *ANSA* [Bal15]. Auweraer et al. investigate the influence of roof curvature, windshield angle, wheel base increase, and subframe shape on NVH characteristics using a morphing approach [Auw07]. Harzheim et al. uses a combined approach of morphing and RBEs to modify selected kinematic hard point coordinates. The approach is then used to identify and optimize significant coordinates for reduced transfer forces between suspension and vehicle body [Har06, Har10]. In multiple publications, Nunes et al. use a morphing approach to investigate the robustness of brake squeal against geometric imperfections [Nun09, Nun13, Nun15]. In a previous publication originating from the present research project, two different morphing approaches were compared for FRF optimization on a suspension component level [Wys20b]. In non-NVH related applications, morphing is also present [Har10, Gra14, Cal18, Har19, Cla22].

There are many different morphing approaches and implementations under different names available. Basically, all implementations break down to interpolating a displacement field for all nodes of the mesh, which corresponds to the given boundary conditions.

Boundary conditions for the morphing process consist of imposed or forbidden displacements. Depending on the morphing methodology, these displacements

are set either at FE nodes or at arbitrary points in the design space. The points can also extend to boundary condition surfaces or volumes. One of these methods, a *control-based approach*, is implemented for example as *Domain Morphing* or *Box Morphing* [Auw07, Mor12, BET22b]. An abstract control domain specifies the desired morphing behavior and links it to the FE nodes. For complex components in particular, the creation of the control domains is often time-consuming and complicated [Har19]. Another method is *Mesh Morphing*, *Direct Morphing*, or *Free Form Morphing* [Auw07, Mor12, Har19, BET22b]. Here, the displacements are defined at specific FE nodes and the algorithm transfers the displacement onto the remaining FE nodes. These morphing methodologies are often implemented into commercial FE preprocessors [Büt20].

For the modification of suspension kinematics, imposing displacements at the kinematic hard points and preventing displacements at connection consoles is required. This enables the usage of a *Direct Morphing* algorithm with the desired kinematics modifications as boundary conditions.

As the target is an easy and fast kinematics modification methodology, the setup of the morphing workflow also needs to be easy and fast to use. In order to create large data sets for the desired metamodeling, the morphing process must be completely automated. Therefore, the target is to create a morphing tool, dedicated to suspension kinematics modification on FE meshes. Ideally, the methodology relies completely on openly accessible tools without any preprocessors. The following sections describe the implemented methodology in detail. In an earlier publication [Wys20b], the methodology was presented and compared to a semi automated *Box Morphing* approach. The latter was implemented by Leupolz in a master thesis originating from the present research project [Leu20]. The *Box Morphing* approach resulted in good morphing quality, required extensive manual labor, though, which is why the approach was omitted.

4.5.3 Implementation of a Dedicated Suspension Kinematics Morphing Algorithm

A dedicated suspension kinematics modification algorithm is required to morph complete suspension assembly FE models. The morphing process should not require any manual setup, exceeding the definition of the kinematics boundary conditions. The following sections describe the morphing algorithm in detail and form an extended explanation to the previously published description [Wys20b].

The definition of the morphing boundary conditions orients on the discussed separation into *control nodes*, *fixed nodes* and *deformable nodes* [Auw07]. Figure 4.13 presents the different FE node types for the wheel carrier example. The n_c *control nodes*

$$\mathbf{x}_c = \left[\vec{x}_{c,1}, \vec{x}_{c,2}, ..., \vec{x}_{c,n_c}\right] \tag{4.9}$$

$$= \left[\begin{pmatrix} x_{c,1,1} \\ x_{c,1,2} \\ x_{c,1,3} \end{pmatrix}, \begin{pmatrix} x_{c,2,1} \\ x_{c,2,2} \\ x_{c,2,3} \end{pmatrix}, ..., \begin{pmatrix} x_{c,n_c,1} \\ x_{c,n_c,2} \\ x_{c,n_c,3} \end{pmatrix}\right] \tag{4.10}$$

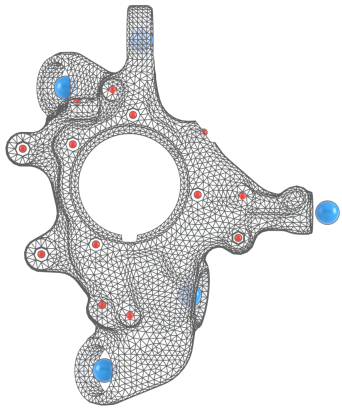

Figure 4.13: Illustration of *control nodes* (blue), *fixed nodes* (red), and *deformable nodes* (intersections of the FE mesh lines) on the wheel carrier FE mesh.

are located at the kinematic hard points. They define the center points of the elastomer elements connecting the suspension components. In fig. 4.13 they are marked as blue points. It is clearly visible that the *control nodes* do not necessarily lie coincidentally to the FE nodes, as there are no FE nodes in the center of the elastomer elements. The *control nodes* are P_1 through P_5, R_1 through R_5 and the additional kinematic hard points R_D, R_S, and R_TB. Their displacements

$$\mathbf{v}_\mathrm{c} = \left[\vec{v}_{\mathrm{c},1}, \vec{v}_{\mathrm{c},2}, ..., \vec{v}_{\mathrm{c},\mathrm{n_c}}\right] \tag{4.11}$$

form the kinematics modifications. The n_f *Fixed nodes*

$$\mathbf{x}_\mathrm{f} = \left[\vec{x}_{\mathrm{f},1}, \vec{x}_{\mathrm{f},2}, ..., \vec{x}_{\mathrm{f},\mathrm{n_f}}\right] \tag{4.12}$$

with their displacements

$$\mathbf{v}_\mathrm{f} = \left[\vec{v}_{\mathrm{f},1}, \vec{v}_{\mathrm{f},2}, ..., \vec{v}_{\mathrm{f},\mathrm{n_f}}\right] \tag{4.13}$$

$$= \left[\vec{0}, \vec{0}, ..., \vec{0}\right] \tag{4.14}$$

mainly control connections to peripheral components like the brake caliper or the wheel hub bearing. These nodes must not be moved. In fig. 4.13 they are marked as smaller red points. The combination of *control nodes* and *fixed nodes*

$$\mathbf{x}_\mathrm{d} = \left[\vec{x}_{\mathrm{c},1}, \vec{x}_{\mathrm{c},2}, ..., \vec{x}_{\mathrm{c},\mathrm{n_c}}, \vec{x}_{\mathrm{f},1}, \vec{x}_{\mathrm{f},2}, ..., \vec{x}_{\mathrm{f},\mathrm{n_f}}\right] \tag{4.15}$$

forms the set of displacement boundary conditions with the displacements

$$\mathbf{v}_\mathrm{d} = \left[\vec{v}_{\mathrm{c},1}, \vec{v}_{\mathrm{c},2}, ..., \vec{v}_{\mathrm{c},\mathrm{n_c}}, \vec{0}, \vec{0}, ..., \vec{0}\right] \tag{4.16}$$

for the morphing process. The n_m *deformable nodes*

$$\mathbf{x}_\mathrm{FE} = \left[\vec{x}_{\mathrm{FE},1}, \vec{x}_{\mathrm{FE},2}, ..., \vec{x}_{\mathrm{FE},\mathrm{n_m}}\right] \tag{4.17}$$

form the nodes of the FE mesh and form the material performing the actual morphing movement. For the *deformable nodes*, the displacements

$$\mathbf{v}_{\mathrm{FE}} = \left[\vec{v}_{\mathrm{FE},1}, \vec{v}_{\mathrm{FE},2}, ..., \vec{v}_{\mathrm{FE},n_m}\right] \tag{4.18}$$

need to be interpolated from the neighboring *control node* and *fixed node* boundary conditions.

The positions of the *deformable nodes* $\mathbf{x}_{\mathrm{FE}}$ directly originate from the FE nodes and do not require any additional specification. The positions $\mathbf{x}_{\mathrm{c}}$ and displacements $\mathbf{v}_{\mathrm{c}}$ of the *control nodes* directly originate the desired suspension kinematics modification. Their numeric values are defined in a table of the form, presented in table 4.1. The locations of the *fixed nodes* $\mathbf{x}_{\mathrm{f}}$ require manual definition, depending on the component shape. The combined boundary conditions $\mathbf{x}_{\mathrm{d}}$ and $\mathbf{v}_{\mathrm{d}}$ could be provided for example in a simple text file.

The interpolation from the boundary conditions $\mathbf{x}_{\mathrm{d}}$ and $\mathbf{v}_{\mathrm{d}}$ to the displacements $\mathbf{v}_{\mathrm{FE}}$ at the FE nodes $\mathbf{x}_{\mathrm{FE}}$ is a two-step process, illustrated in fig. 4.14[a]. First, the boundary conditions are used to create a morphing object. Then, this morphing object is used for the calculation of the mesh displacements $\mathbf{v}_{\mathrm{FE}}$. The creation of

Table 4.1: Input for displacement boundary conditions $\mathbf{x}_{\mathrm{d}}$ and $\mathbf{v}_{\mathrm{d}}$.

Name	Location	Displacement
$P_{1,\mathrm{x}}$	$x_{\mathrm{c},1,1}$	$v_{\mathrm{c},1,1}$
$P_{1,\mathrm{y}}$	$x_{\mathrm{c},1,2}$	$v_{\mathrm{c},1,2}$
$P_{1,\mathrm{z}}$	$x_{\mathrm{c},1,3}$	$v_{\mathrm{c},1,3}$
$P_{2,\mathrm{x}}$	$x_{\mathrm{c},2,1}$	$v_{\mathrm{c},2,1}$
⋮	⋮	⋮
$R_{\mathrm{TBL,z}}$	$x_{\mathrm{c},n_c,3}$	$v_{\mathrm{c},n_c,3}$
$F_{1,\mathrm{x}}$	$x_{\mathrm{f},1,1}$	0
⋮	⋮	⋮
$F_{n_f,\mathrm{z}}$	$x_{\mathrm{f},n_f,3}$	0

[a] fig. 4.14 details the *Model preparation* block from fig. 3.3. Figure C.1 on page 214 combines the two figures into one.

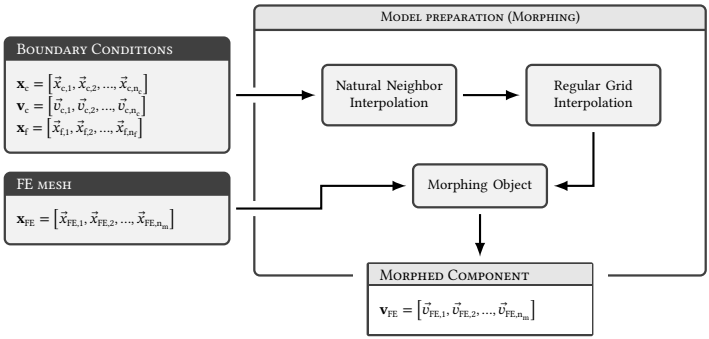

Figure 4.14: Process for the component morphing algorithm.

the morphing object is a two-step process as well, combining two different existing interpolation methods. This is due to an easy implementation in python using existing open source interpolation packages. This enables a simple morphing process, which does not require any commercial FE preprocessor.

The two-step morphing object creation combines the two morphing approaches *Natural Neighbor Interpolation* and *Regular Grid Interpolation*. The natural neighbor interpolation, provided by the *Python* package `naturalneighbor`[a], interpolates the imposed displacements onto a regular grid $\mathbf{x}_g$. The regular grid interpolation, provided by the *Python* package `scipy`[b] then interpolates from the regular grid onto the FE nodes $\mathbf{x}_{FE}$.

Natural Neighbor interpolation was introduced by Sibson in 1980 [Sib80]. It is based on a voronoi diagram indicating weighting factors for the nearest boundary conditions to an interpolation point [Par06]. Figure 4.15 illustrates the voronoi approach for the Natural Neighbor interpolation. Figure 4.15a presents the used suspension in top view. 5 kinematic hard points are highlighted and serve as exemplary locations for kinematics modifications. In the real problem, these points are more numerous and additional zero displacements come into play. For easier illustration, the number of points is reduced, though. Additionally, the problem is assumed to be two-dimensional for this

[a] Version 0.2.1 from [pyp18, Par06], released under MIT license [Ope22b]
[b] Version 1.8.0 [Sci22a, Vir20], released under the 3-Clause BSD License [Sci22b, Ope22a]

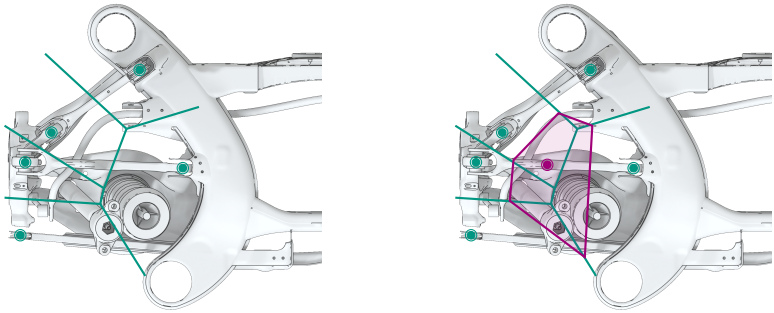

(a) Voronoi Grid for the modified kinematic hard points

(b) Voronoi-Cell for the interpolation on an FE node

Figure 4.15: Voronoi Grid illustrating the Natural Neighbor Interpolation for the example of five modified kinematic hard point locations. The kinematic hard points are assumed to have the same z coordinate for simpler illustration.

illustration with identical z coordinates for all kinematic hard points. Later, the voronoi diagram would be needed in three dimensions. The voronoi cells indicate the nearest kinematic hard point for each point in space [Par06].

The Natural Neighbor interpolation generates an interpolation value for specific additional points. This is illustrated in fig. 4.15b. For the additional point, the additional voronoi cell is generated. The percentage of overlapping between the new cell and each of the existing green cells defines the weighting factor for the neighboring kinematic hard point displacements. The interpolation is performed for each direction separately, resulting in three interpolations for each additional point.

For the present investigation, the Discrete Natural Neighbor interpolation algorithm by Park et al. is used [Par06]. The algorithm is available as *Python* package `naturalneighbor`[a]. The discrete variation of the original Natural Neighbor algorithm reduces the required calculation effort and enables the calculation on a Graphics Processing Unit (GPU) [Par06]. As the implementation is developed for the interpolation on a regular grid—an equidistant arrangement of grid points—instead of arbitrary points in space, the natural neighbor interpolation

[a] Version 0.2.1 [pyp18, Par06], released under MIT license [Ope22b]

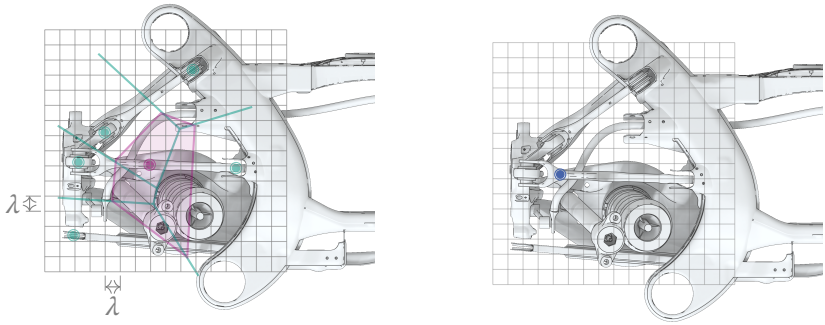

(a) Regular grid with equidistant spacing λ in all directions containing the component

(b) Interpolation from regular grid to FE nodes

Figure 4.16: 2D-visualization of the regular grid interpolation.

interpolates the displacements at the kinematic hard points onto the regular grid nodes $\mathbf{x}_g$ first, illustrated in fig. 4.16.

The regular grid with the displacement at the regular grid nodes $\mathbf{x}_g$ is presented in fig. 4.16a. The distancing of the grid is marked as λ. The grid only includes the components to morph. Increasing the grid raises calculation times without any advantages. In order to keep the grid as small as possible, the suspension symmetry is utilized. Only one grid for one suspension half is calculated. Figure 4.16b presents the interpolation from the regular grid onto the FE nodes. For the interpolation from $\mathbf{x}_g$ to $\mathbf{x}_{FE}$, the function `RegularGridInterpolator` provided by the *Python* package `scipy`[a] is used with *linear* interpolation.

4.5.4 Morphing Accuracy

The nature of the selected interpolation process introduces a small morphing deviation at the kinematic hard point locations. If the location $\vec{x}_{c,i}$ of an imposed displacement does not coincide with a regular grid node $\vec{x}_{g,j}$, all adjacent regular grid nodes form an interpolation between $\vec{x}_{c,i}$ and another

[a] Provided by SciPy [Sci22a, Sci22c, Vir20], released under the 3-Clause BSD License [Sci22b, Ope22a]

imposed displacement. Therefore, none of the regular grid nodes exactly matches the desired displacement. This leads to a small deviation between desired displacement and actual displacements on the regular grid.

One approach to increase morphing accuracy would be to decrease the regular grid spacing λ. This massively increases the calculation time for the generation of the natural neighbor interpolation, though. Figure 4.17 presents the required calculation times for different grid spacings and the achieved morphing accuracy. The evaluation tracks the displacement of an FE node coinciding with the connection point R_3 between wheel carrier and track rod. Figure 4.17 shows little improvement in calculation time for $\lambda > 3\,\text{mm}$. The Morphing deviation almost linearly increases with increased λ.

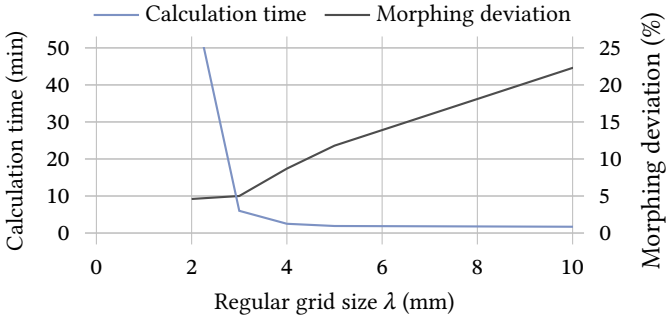

Figure 4.17: Calculation times and Morphing Accuracy for different regular grid sizes λ.

Another approach introduces additional control nodes $\mathbf{x}_c$, placed in a small distance around the kinematic hard points. The desired displacements are mapped to all of these additional control nodes. This makes the regular grid nodes around the actual control node interpolate between the actual control node displacement and the identical displacement at the additional nodes. This makes the interpolation at the center of the area exact but comes with additional effort of defining the additional control nodes.

A third approach is to perform the morphing twice. After the first combination of Natural Neighbor and Regular Grid Interpolation, the relative deviation between the desired kinematics modification displacements and the actual

morphed kinematic hard point locations is evaluated[a]. For the three Cartesian directions i the relative deviation

$$\Delta v_{\mathrm{c,rel,i}} = \frac{v_{\mathrm{c,actual,i}}}{v_{\mathrm{c,desired,i}}} \quad \text{, for i in } [1,3] \tag{4.19}$$

is calculated. As the Regular Grid Interpolation is performed as a linear interpolation, compensated displacements

$$v_{\mathrm{c,compensated,i}} = \frac{v_{\mathrm{c,desired,i}}}{\Delta v_{\mathrm{c,rel,i}}} = \frac{v^2_{\mathrm{c,desired,i}}}{v_{\mathrm{c,actual,i}}} \tag{4.20}$$

can be evaluated in a way that the final morphed position of the kinematic hard point matches the desired position for the kinematics modification. If the altering leads to leaving the regular grid cell, this process might require an additional compensation cycle.

The discussed morphing deviation only applies to the component material FE nodes. The kinematic hard point FE nodes, forming the connection between suspension components, are moved to the exact location without morphing. This is the case, as they are positioned in a separate coordinate system coincident with the hard point location as introduced in section 4.3.2. Therefore, the small morphing deviation is compensated by RBEs connecting the component FE nodes to the connection node. These modified RBEs introduce a slightly deviating component stiffness resulting from the sub millimeter morphing deviation. This differs compared to the data set of the earlier publication, in which the real displacements after morphing were used for the metamodeling [Wys21].

To investigate if the morphing error is relevant for the simulation results, an experiment with maximum displacements is performed. All kinematic hard points receive an absolute imposed displacement of 10 mm in each direction away from the wheel center. The resulting morphing errors are presented in table 4.2 The numbers clearly show that the morphing error can be reduced

[a] A detailed derivation can be found in appendix B.2

Table 4.2: Morphing error after morphing once compared to morphing twice.

		Morphed once		Morphed twice	
Coordinate	**Target**	**Actual**	**Error**	**Actual**	**Error**
$R_{1,x}$	−10.00 mm	−9.58 mm	4.25%	−9.99 mm	0.11%
$R_{1,y}$	−10.00 mm	−9.83 mm	1.68%	−10.00 mm	0.03%
$R_{1,z}$	−10.00 mm	−9.84 mm	1.64%	−10.00 mm	0.03%
$R_{2,x}$	10.00 mm	8.85 mm	11.49%	10.03 mm	0.32%
$R_{2,y}$	−10.00 mm	−9.61 mm	3.95%	−9.99 mm	0.08%
$R_{2,z}$	−10.00 mm	−9.59 mm	4.14%	−9.99 mm	0.11%
$R_{3,x}$	10.00 mm	9.14 mm	8.57%	10.01 mm	0.09%
$R_{3,y}$	−10.00 mm	−9.14 mm	8.57%	−9.99 mm	0.12%
$R_{3,z}$	10.00 mm	8.78 mm	12.20%	10.01 mm	0.13%
$R_{4,x}$	−10.00 mm	−9.44 mm	5.63%	−10.00 mm	0.02%
$R_{4,y}$	−10.00 mm	−9.48 mm	5.22%	−10.00 mm	0.01%
$R_{4,z}$	10.00 mm	9.46 mm	5.38%	10.00 mm	0.00%
$R_{5,x}$	10.00 mm	8.75 mm	12.48%	10.03 mm	0.35%
$R_{5,y}$	−10.00 mm	−9.64 mm	3.58%	−10.01 mm	0.10%
$R_{5,z}$	10.00 mm	9.64 mm	3.61%	10.01 mm	0.12%

significantly by morphing twice following eq. (4.20). To investigate the effects from morphing once, the effects in the SPL simulation need to be addressed.

Figure 4.18 presents the SPL at one ear position for the initial kinematics and the modified kinematics from table 4.2. The curves for morphing once and morphing twice differ less than 1 dB(A) for the frequency range up to 290 Hz with only one larger deviation with 1.1 dB(A) at 218 Hz. The Root Mean Square (RMS) value of the deviation up to 220 Hz, the main frequency range under investigation here, is 0.08 dB(A) and 0.29 dB(A) for the full frequency range up to 300 Hz.

Using the presented dedicated suspension kinematics morphing algorithm, new suspension models can be prepared quickly without any preprocessing except the definition of $\mathbf{x}_c$, $\mathbf{v}_c$, and $\mathbf{x}_f$. Accelerating the morphing process is possible by using the symmetry of the suspension. The Natural Neighbor Interpolation needs to be performed once only, if the morphing is performed with the absolute value of the y-coordinates. Increasing the grid size λ reduces

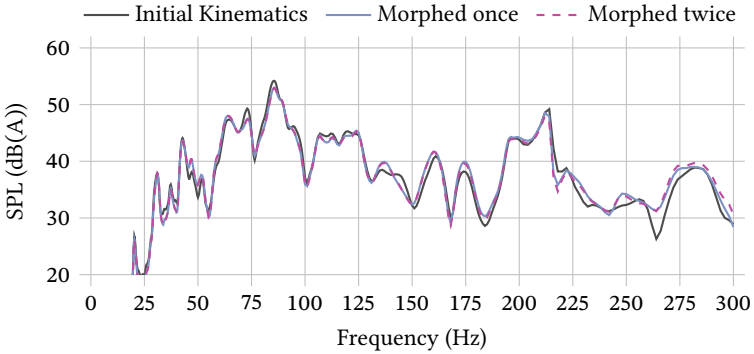

Figure 4.18: SPL compared from initial suspension kinematics to an extreme kinematics variation. For the comparison, the suspension kinematics modification is performed by morphing once and twice.

calculation time with the cost of reduced morphing accuracy. For the creation of larger numbers of suspension kinematics variations, a parallelization of the morphing process is suggested.

The presented morphing procedure is restricted to small kinematics changes in the range of few millimeters. This excludes suspension topology and configuration investigations. Introducing extensive deviations into the FE mesh could decrease the FE mesh quality and therefore alter the simulation results. This problem is discussed in the next section.

4.5.5 Mesh Quality

Morphing becomes problematic, when the displacements become too large. As long as there are no remeshing algorithms implemented, morphing the FE mesh can potentially distort the elements leading to decreased element quality. Therefore, at least an element quality check needs to be performed in order to ensure proper simulation result quality [Auw07, Sta12, Nun15, Har19].

For the assessment of the mesh quality, many different criteria exist. For example, the element aspect ratio or skewness are commonly used [Kle15, S. 308]. In the present investigation, these two quality criteria are evaluated

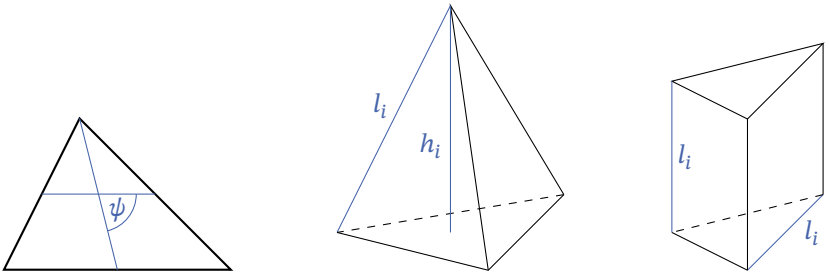

(a) Skewness **(b)** Aspect Ratio Tetra **(c)** Aspect Ratio Hexa

Figure 4.19: Selected element quality criteria.

using the built-in *ANSA* checks. Figure 4.19 illustrates the selected quality criteria after their definition in *ANSA* [BET22a].

The skewness, illustrated in fig. 4.19a, checks distorted diagonal lengths. The criterion calculates the skewness

$$s = 90° - \psi \tag{4.21}$$

for each combination of the element's diagonals and returns the worst value. The larger the skewness value, the worse the element quality. [BET22a]

The Aspect Ratio checks the variance in edge lengths. For tetra elements in fig. 4.19b the Aspect Ratio

$$a = \frac{\max(l_i)}{\min(h_i)} \tag{4.22}$$

compares the maximum edge length to the minimum element height. For penta or hexa elements in fig. 4.19c, the Aspect Ratio

$$a = \frac{\max(l_i)}{\min(l_i)} \tag{4.23}$$

compares the maximum to the minimum edge length. The higher the aspect value a, the worse the element quality. [BET22a]

In order to ensure a sufficient model quality, the mesh quality for maximum morphing displacements needs to be acceptable. Here, the mesh quality investigation does not aim at the evaluation of the general mesh quality, though. Only the change in mesh quality is under investigation, as the utilized full vehicle FE development simulation model is considered valid.

For the investigation, the mesh quality for the worst case morphing example from table 4.2 is observed. As the mesh quality is expected to decrease with strong deformations [Auw07], maximum displacements are investigated. Each kinematic hard point of the wheel carrier—the most complex part regarding adjacent kinematic hard points—is moved in three dimensions away from the wheel center point. This induces the maximum morphing displacements, which by far exaggerate the displacements in the DoE, as the DoE tries to prohibit correlating displacements. This makes simultaneous maximum displacement of all three directions unlikely.

In order to compare the mesh quality before and after the morphing process, the number of bad elements is monitored. Table 4.3 presents the number of elements, violating a certain mesh quality rating. The two previously presented quality criteria *Aspect Ratio* and *Skewness* are observed. The investigation threshold values for bad element quality is selected using the criteria values for the second worst element in the original model. This allows one outlier element. For an aspect ratio of 8, the second worst value in the original model, the number of violating elements does not increase. For the skewness, the number of elements violating 64° doubles. As expected, the morphing induces mesh quality deterioration, but the general mesh quality threshold remains nearly constant.

Table 4.3: Mesh quality for two selected quality criteria.

	Original	Morphed	Delta
Aspect Ratio 8	2	2	0.0%
Aspect Ratio 5	14	22	57.1%
Skewness 64°	2	4	100.0%
Skewness 60°	9	29	222.2%

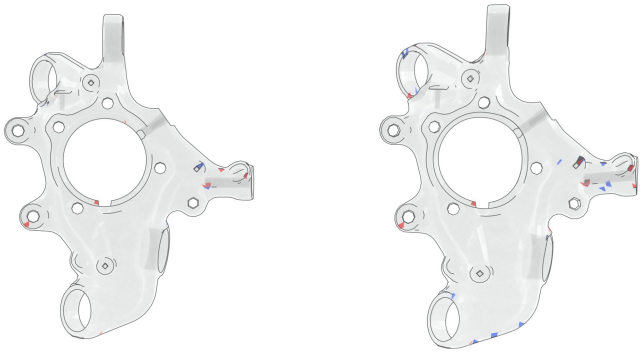

(a) Initial component **(b)** Morphed component

Figure 4.20: Comparison between original and morphed component regarding FE mesh quality. Aspect ratio violating elements in red, skewness violating elements in blue.

For the lower values 5 for *Aspect Ratio* and 60° for *Skewness*, also presented in table 4.3, the distribution of violating elements is presented in fig. 4.20. These lower criteria give more insight in the broader mesh quality changes. Figure 4.20a presents the distribution for the original component, fig. 4.20b for the component after morphing. Red elements indicate *Aspect Ratio* 5 violations, blue elements indicate *Skewness* 60° violations. Especially in the area around the track rod R_3, the number of violating elements increases. This is due to the close boundary conditions with maximum displacement at R_3 and fixed position of R_{TBL}.

The presented violation of mesh quality criteria can occur for multiple criteria in one element. This reduces the absolute value of violating elements from the sum of *Aspect Ratio* and *Skewness* elements in table 4.3. Table 4.4 presents the number of violating elements for the combined quality criteria. The morphed component preserves the combined mesh quality by keeping one element that violates both quality criteria. The number of elements violating the weakened criteria increases from one to seven.

The investigation shows that the number of elements violating the original worst element quality does not increase for the aspect ratio and increases by only two elements for the skewness. As expected, the mesh quality is decreased,

Table 4.4: Mesh quality for the combination of two selected quality criteria.

	Original	Morphed
Aspect Ratio 8, Skewness 64°	1	1
Aspect Ratio 5, Skewness 60°	1	7

though. Hereby it is to note that the original component originates from the development simulation model and is not suspicious of bad mesh quality, at all.

In order to create a last safety barrier for bad mesh quality, an additional check is performed. *NX Nastran* built-in quality criteria automatically assess the model mesh quality before starting every single simulation run. With threshold values for these mesh quality criteria, a calculation of a kinematics modification with unacceptable mesh distortion is prohibited. This reduces the number of calculated samples, while increasing the data set quality. For the present investigation, no sample violated these additional pre-calculation quality checks. If this would have been an issue, for example automatic local mesh modifications could be implemented, fixing the deteriorated mesh quality [Auw07, Sta12].

4.5.6 Application to Different Components

The previous sections presented two different methodologies for altering suspension kinematics in the FE simulation model. Model simplification is mainly suitable for simple slim components, whereas morphing is able to alter all types of components. One of the requirements after Research Question 2[a] is to implement kinematics modifications with as little manual effort as possible. Morphing with the dedicated suspension kinematics morphing algorithm seems to be most promising for all suspension components.

Using the morphing approach for all suspension components requires the set of morphing boundary conditions to be split into a separate set for each

[a] How can modified suspension kinematics be easily and quickly applied to road noise simulation models, enabling a systematic investigation of the correlations between suspension kinematics and road noise phenomena?

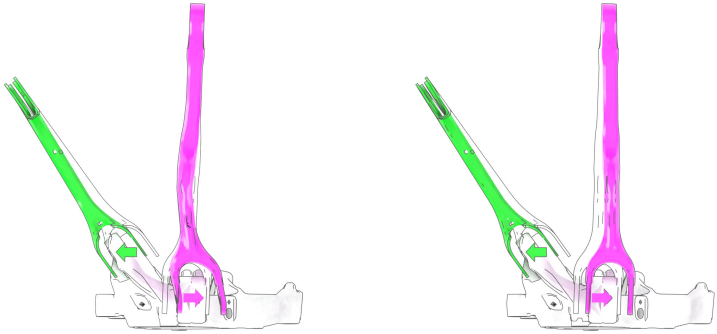

(a) Full set of boundary conditions **(b)** Reduced set of boundary conditions

Figure 4.21: Morphing Suspension links with different sets of boundary conditions.

component, though. The points $\mathbf{x}_d$ need to be reduced to the points adjacent to each component. This is illustrated in fig. 4.21. In the example, only displacements to R_4 and R_5 are considered. As the wheel carrier needs to adapt to both changes, it requires both boundary conditions. Using both boundary conditions for the links results in the undesired behavior illustrated in fig. 4.21a. The pink camber rod is bent due to the boundary condition of the green link. Using only the link-adjacent boundary conditions leads to the desired behavior illustrated in fig. 4.21b. Both links are not bent and only adapt to their own kinematics modification.

In the long term, using morphing to create different suspension kinematics could provide a component database for the investigation of suspension configurations as well. Having the possibility to utilize previously morphed components, new suspension concepts could be assembled enabling more advanced suspension kinematics investigations.

5 Identification of Correlations

The introduced simulation models help answering Research Question 1[a]. Correlations between design variables and SPLs could indicate first possibilities. In this chapter, a simulation data set is created and used to identify general correlation rules, which describe the correlations between suspension kinematics and the SPLs for the given vehicle example.

5.1 Creating the Data Set

Before creating the data set, the design variables have to be selected. With an appropriate DoE method, the data set can be prepared and evaluated.

5.1.1 Selection of the Design Variables

Section 4.1 presented all possible DOFs in the suspension under investigation. In order to keep the problem simpler and reduce the required processing power, the fundamental investigation is performed on the wheel-side kinematic hard points only. Less design variables require less samples in the data set, additionally the morphing on the subframe is more complex due to more adjacent components with displacement restrictions. The reduced design space results in the five variable kinematic hard points R_1 to R_5, connecting the wheel carrier to the suspension links.

[a] Is it possible to modify dedicated road noise phenomena by changing the location of specific kinematic hard points?

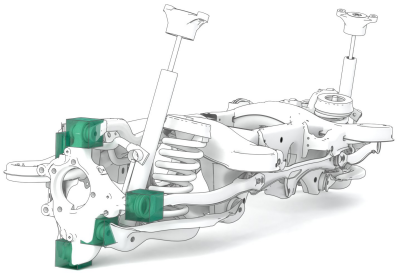

Figure 5.1: Design space for the used five link rear suspension. The design space of the left and right suspension half is symmetrical. For better visualization, the boxes are exaggerated by factor 3. Similar visualisation to an earlier conference paper [Wys22].

The design space for each kinematic hard point is represented by green design space boxes in fig. 5.1[a]. The design space for each kinematic hard point is the same size with a possible displacement of $\pm 10\,\mathrm{mm}$ in x-, y-, and z-direction[b]. The three directions for each kinematic hard point add up to 15 design variables for the full system under investigation.

5.1.2 Method Selection

Creating large simulation data sets requires systematic parameter variation. The so-called DoE methods split into classical DoE methods and modern DoE methods. An example for classical DoE is full factorial investigation of the design space. One disadvantage of full factorial investigations is the large number of required samples. The number of required samples increases exponentially with the number of design variables [Har19, Dyn20]. For the presented problem, the design space contains $n_\mathrm{v} = 15$ design variables. With only $n_\mathrm{l} = 2$ levels per design variable this results in

$$n_\mathrm{r} = n_\mathrm{l}^{n_\mathrm{v}} = 2^{15} = 32\,768 \tag{5.1}$$

[a] A similar visualisation of the design space was published in a previous conference paper [Wys22].

[b] The size of the boxes in fig. 5.1 is exaggerated by factor 3 in order to clearly illustrate the design variables without hiding the boxes inside the components.

samples [Sie17, S. 6]. As each sample requires about 3 hours of calculation time, this results in—considered no parallelization—11.2 years of simulation.

This is not practical, which is the reason why there are more modern DoE methods. So-called space filling DoE methods include for example Monte Carlo Sampling or Latin Hypercube Sampling, which are commonly used DoE methods for simulation [Wil04, Sie17, Har19].

Monte Carlo Sampling is suitable especially for large numbers of samples [Wil04, Sie17, Mos11]. For smaller number of samples the design variables can correlate and holes can emerge in the design space [Wil04, Sie17, Har19, Dyn20]. Latin Hypercube Sampling optimizes the design distribution reducing the correlation and number of required samples, at the same time [Wil04, Sie17]. As the calculation times are high for the presented example, the number of samples should be kept low. This is why Latin Hypercube is selected as the sampling method here.

The commercial optimization tool *Ansys optiSLang* is used to create the DoE using Space Filling Latin Hypercube Sampling. For the required number of samples n_r *Ansys optiSLang* suggests to evaluate

$$n_\mathrm{r} = \max(500, 2n_\mathrm{v}) \tag{5.2}$$

samples with n_v being the number of design variables. Following this suggestion, the 15 design variables require 500 samples. This corresponds to investigations in literature using similar numbers of design variables or calculation rules [Wil04, Gra14, Har19]. There are some investigations, though, which use significantly more samples relative to their numbers of design variables [Har19]. Keeping this in mind, the data set is composed of 500 samples, in a first attempt.

5.1.3 Creating the DoE

For the data set, the five kinematic hard points R_1 to R_5 with their directions x, y and z form the 15 design variables. Each design variable varies in the domain $\pm 10\,\mathrm{mm}$, which is small enough to perform well in the morphing process

and large enough to cover common kinematics changes in the suspension kinematics development phase. The 500 samples DoE for the 15 design variables is identical to the one used in an earlier publication [Wys21]. There, the data set was created using component structure-borne noise transfer simulation for the wheel carrier only. Here, the data set consists of full vehicle SPL simulations and suspension parameter simulation, described in sections 4.3.4 and 4.4. To verify the quality of the created DoE, the Pearson correlation values between all 15 design variables are observed. No design variables show absolute correlation values above 0.02 between each other.

5.1.4 Obtaining the Simulation Data Set

Using the created DoE, the next step is obtaining the simulation data set. This data set consists of simulation results for each sample of the DoE. For each sample, the SPL and suspension parameter simulation models are created. This requires morphing a new suspension FE simulation model for each sample.

As presented in section 4.5.4 the morphing process is not exact, if performed once. For the creation of the data set, the time required to morph the suspension simulation models for each sample is notable, so the required time should be as low as possible. In order to decrease morphing time, morphing once is selected for the creation of the data set. This reduces the required preparation time for the data set by the factor two, which corresponds to approximately 10 min per sample or 3.5 days, considering a business notebook without parallelization. For validation simulations, morphing twice ensures the validity of optimized suspension kinematics. The calculation of rigid body suspension parameters is independent from the morphing error, as these calculations use the desired displacement values as an input.

For each sample of the data set, specific simulation models are created. These include SPLs at all seating positions in the frequency range 20 to 300 Hz for rolling on rough asphalt, eigenvalues for the subassembly suspension, FRFs for the subassembly suspension for unified load at the wheel hub to the body connection points, and calculation of suspension parameters. The simulation models for the SPLs and the suspension parameters are solved for all samples.

All other simulation models are created for further investigations of specific samples if required. This results in eight SPL curves, one for each ear position of the four passenger seats, omitting the middle seat in the back row, and 22 suspension parameters. Each sample requires approximately 3 hours for the SPL calculation and few seconds for the suspension parameters.

The specific road noise or suspension parameter optimization targets are irrelevant at this point. The data set includes the full SPL frequency range and all suspension parameters. Therefore, the optimization target frequency or suspension parameter can be selected after generating the simulation data set.

5.2 Processing the Data Set

After the simulation run, the data set consists of 500 samples containing the values for the 15 design variables, SPLs for eight ear positions and 22 suspension parameters. These results are only a brief representation of the requirements to the suspension design. Therefore, there exists no obvious target function for an optimized suspension kinematics. In this section, simplifications on the data set enable a holistic optimization approach, not only numerical, but also qualitative in the form of design rules.

5.2.1 Reduction of the Data Set Complexity

In a first step, the complexity of the eight SPL spectra needs to be reduced. A common procedure to handle multiple spectra is to combine them into one spectrum using an envelope curve [Uhl20a, Uhl21b]. An envelope curve picks the highest amplitude of all spectra for each frequency bin separately. The main advantage of optimizing on an envelope curve is to ensure that an optimum is only achieved, if global maximum amplitudes are reduced.

The first target of this investigation, defined in the first Research Question[a], is to identify the correlations between kinematics changes and road noise phenomena. Therefore, the focus is not finding a globally optimized suspension kinematics but connections and design rules for the suspension design. As combined SPL spectra could hide correlations, the use of envelope curves is not effective here. Therefore, the following investigations are performed on single SPL curves. If required in the series development process, the lessons learned can be combined to an envelope curve investigation.

For a first investigation, one ear position needs to be selected. The noise of the rear suspension dominates on the rear seats. Consequently, one of the rear ear positions is selected. To avoid optimization for one seat only, the inner ear is selected, as it is closer to the other seating position. For consistency with the suspension modeling, the left seating position is selected. From this point on, all SPL spectra originate the right ear of the rear left seating position, if not stated otherwise.

Figure 5.2 presents the selected SPL spectrum. The single line represents the initial suspension kinematics. The gray area in the background represents the scatter band of the 500 samples. The scatter band marks the minimum and

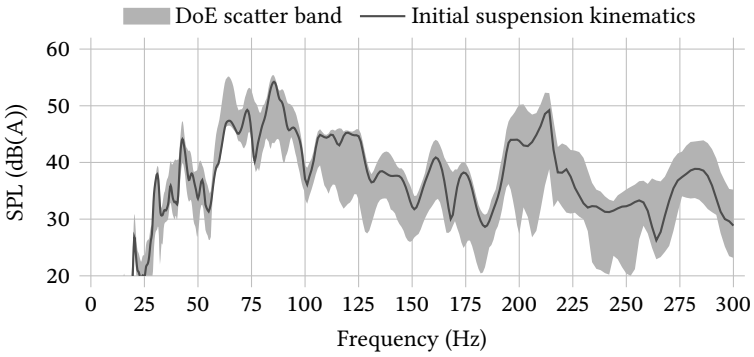

Figure 5.2: SPL for the initial suspension kinematics with scatter band of all 500 samples.

[a] Is it possible to modify dedicated road noise phenomena by changing the location of specific kinematic hard points?

maximum value for each frequency bin in the data set. It is important to note that there is no single sample following the bottom or the top end of the scatter band. The scatter band clearly reveals frequency ranges with large deviation in both directions, ranges in which only improvement or only deterioration is possible and small ranges without any potential for modification. The next section selects appropriate frequency ranges for the further investigation and the Research Question 1[a], if specific phenomena might be modified by kinematics changes.

5.2.2 Selection of Relevant Frequency Ranges

As seen in the previous section, the SPL spectrum scatters around the curve of the initial suspension kinematics. Figure 5.3 marks prominent frequency ranges. They were selected because of either high initial amplitudes (80 to 90 Hz, 190 to 220 Hz), promising optimization potential (105 to 125 Hz) or worryingly high amplitudes of the scatter band (58 to 68 Hz).

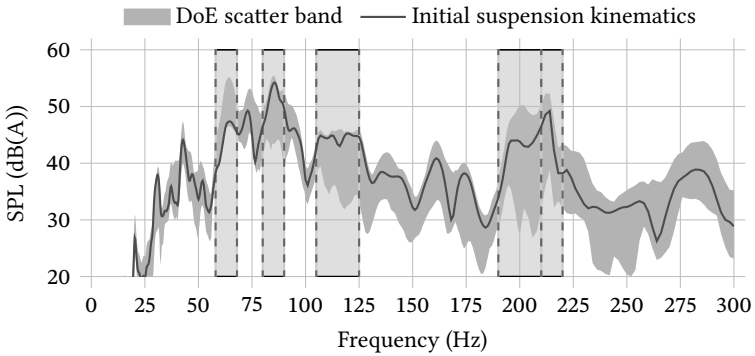

Figure 5.3: SPL for the initial suspension kinematics with scatter band of all 500 samples and highlighted relevant frequency ranges.

[a] Is it possible to modify dedicated road noise phenomena by changing the location of specific kinematic hard points?

The frequency range 80 to 90 Hz dominates the lower frequency range of the spectrum and represents the droning noise. Next to this peak, the range 58 to 68 Hz only shows potential for deterioration whereas the frequency range 105 to 125 Hz only shows potential for improvement. The right half of the spectrum is dominated by the 190 to 220 Hz peak, which represents the cavity noise. This frequency range is segmented into two parts, which is explained in fig. 5.4.

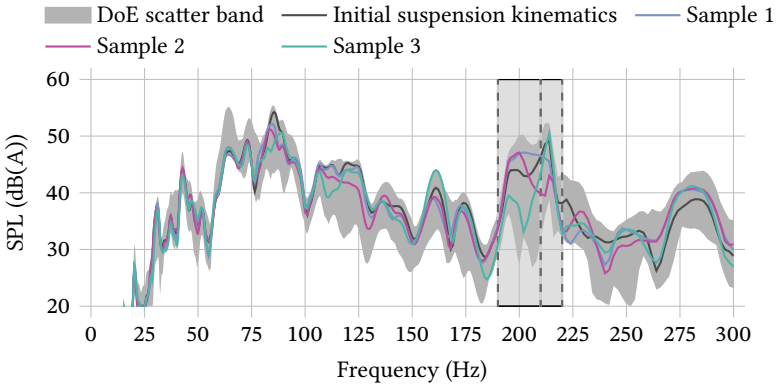

Figure 5.4: SPL for the initial suspension kinematics with scatter band of all 500 samples and 3 selected sample examples. Three different curve behaviors exist in the frequency range 190 and 220 Hz.

From the 500 samples, three example samples with interesting curve behavior are picked and illustrated in fig. 5.4. The three samples illustrate the necessary separation of the frequency range 190 to 220 Hz into the lower frequency range 190 to 210 Hz and the upper frequency range 210 to 220 Hz. Sample 1 shows a flat top curve with deterioration in the frequency range 190 to 210 Hz and improvement in the range 210 to 220 Hz. For sample 2, the peak switches from the upper frequency range to the lower one, switching the dominating frequency range. Sample 3 improves the lower frequency range whereas the upper one stays unchanged.

For further investigation, each frequency range is reduced into one scalar value for each sample. In acoustics, third or octave bands accomplish such reduction. Here, prominent phenomena and frequency ranges determined

from the SPL graphs are used, which is also common in acoustics [Ref15, p. 10]. The average SPL amplitude[a]

$$\bar{L}_{\mathrm{p}} = \frac{1}{n}\left(\frac{1}{2}\left(L_{\mathrm{p}}\left(f_1\right) + L_{\mathrm{p}}\left(f_2\right)\right) + \sum_{i=1}^{n-1} L_{\mathrm{p}}\left(f_1 + i\Delta f\right)\right) \quad \text{, with } n = \frac{f_2 - f_1}{\Delta f} \tag{5.3}$$

sums up the discrete SPL amplitudes for each frequency bin in the frequency range with the lower frequency border f_1, the upper frequency border f_2, and the frequency bin width Δf.

For a better insight into the data set, fig. 5.5 illustrates the Pearson correlation coefficients between the scalar representations of the selected frequency ranges for all 500 samples. There is no fixed threshold value indicating the existence of correlations, but in literature, values above 0.7 are considered as strong correlations [Mos08]. Especially the frequency ranges 58 to 68 Hz and 105 to 125 Hz correlate by −0.89 hinting a target conflict for the road noise optimization. The frequency range 190 to 210 Hz dominates the cavity noise frequency range 190 to 220 Hz. The droning frequency range shows

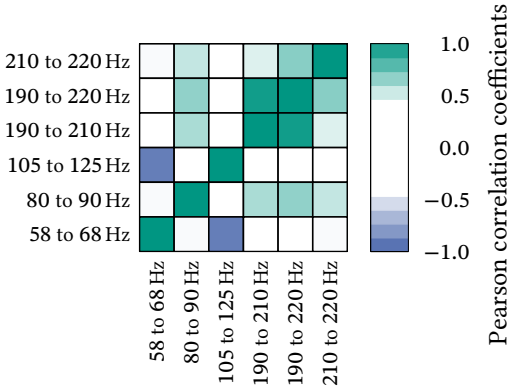

Figure 5.5: Pearson correlation coefficients of the scalar frequency band average values for the selected frequency ranges.

[a] The derivation can be found in appendix B.1.

a positive correlation to the cavity noise frequency range. It is to note, that the correlation values only evaluate changes in the frequency range mean values. They do not hint to subjective perception or absolute amplitude, as visible in the cavity noise frequency range in fig. 5.4. The correlation plot proves the necessity to create metamodels for each frequency range itself. If negatively correlating frequency ranges would be combined in one metamodel, the metamodel could not differ between the two effects.

5.2.3 Selection of Relevant Suspension Parameters

Following the selection of relevant frequency ranges, the relevant suspension parameters need to be identified. For each of the 500 samples there are 22 suspension parameters. Figure 5.6 presents the suspension parameters of the initial suspension kinematics as gray bars. In order to visualize them in one single graph, a logarithmic ordinate is used with absolute suspension

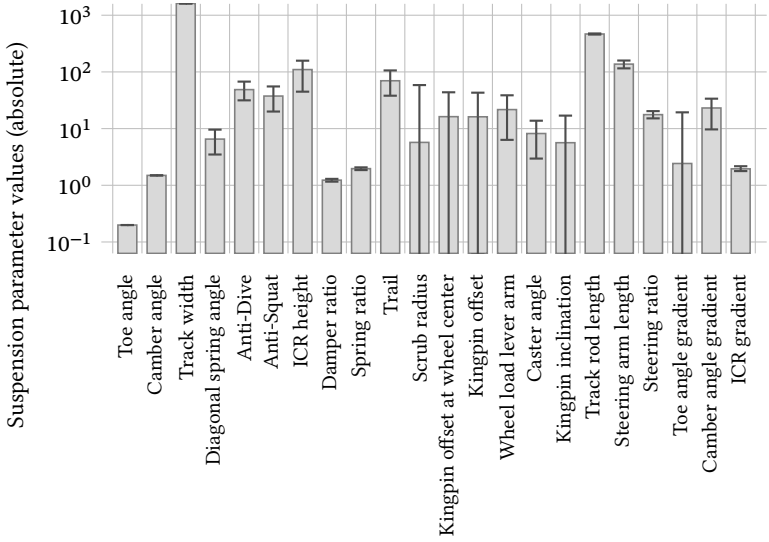

Figure 5.6: Absolute values for the suspension parameters. Bars represent the initial suspension kinematics, scatter indicators the scatter band for the 500 samples data set. Scatter indicators reaching to the bottom of the bars indicate sign changes.

parameter values. Error bars represent the variance in the data set, analogical to the scatter band in figs. 5.2 to 5.4. Error bars reaching down to zero represent sign conversions within the data set. Changing only the kinematic hard points at the wheel carrier without any changes to the wheel flange or the location of the wheel with respect to the wheel carrier, does not affect the kinematic parameters camber, toe, and track width. Therefore, none of the 500 samples differs from the initial suspension kinematics and there are no error bars for these suspension parameters. In the following investigations, these three parameters are omitted.

5.3 Correlations between Suspension Parameters and SPLs

The suspension parameters are not directly modified in the data set, but result from the modified hard point locations. As multiple hard point location configurations could lead to similar suspension parameters, their variance is lower compared to the hard point locations. Therefore, the correlations between suspension parameters and SPLs, as well as hard point locations and SPLs could differ. Low correlations between suspension parameters and SPLs and high correlations between kinematic hard point locations and SPLs at the same time, could hint an optimization opportunity. Modifying hard point locations with high correlations to SPL could improve specific road noise phenomena. Simultaneously, additional hard point location modifications could then revert negative changes to the suspension parameters, as there are no direct correlations between them and SPLs.

Figure 5.7 presents the Pearson correlation coefficients between the selected suspension parameters and the scalar SPL average values of the selected frequency bands[a]. The correlation values are below 0.5 and therefore do not show clear effects. This indicates the possibility to modify road noise phenomea

[a] Note, that the frequency range 235 to 255 Hz is added here due to interesting correlation values. Section 8.1 shows, that in this frequency range elastic effects dominate the kinematics changes, though.

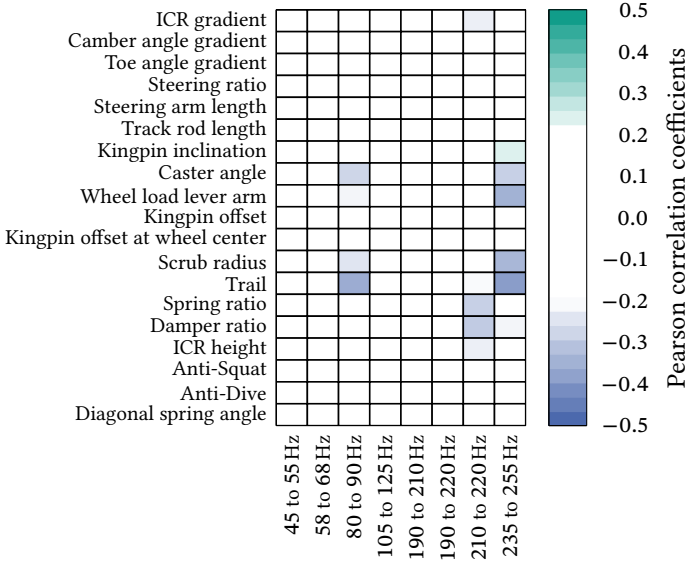

Figure 5.7: Pearson correlation coefficients between the selected scalar suspension parameters and selected scalar frequency band average values.

by changing kinematic hard point locations, while compensating suspension parameters by additional hard point location changes. This opportunity is investigated in detail in the following sections.

5.4 Metamodels Describing the Data Set

In order to direct design choices regarding the suspension kinematics, metamodels should indicate the correlations between suspension kinematics and SPLs. Both connecting the design variables to scalar frequency range representation values and suspension parameters is a regression problem. Common scalar regression metamodels include, but are not limited to (piecewise) polynomials, Kriging, Support Vector Machines, or ANNs [Mos08, Sie17].

Polynomials are the simplest type of metamodels performing well for linear and smaller problems [Wil04, Har19]. Non-linear problems in particular are difficult

to represent using polynomial metamodels [Wil04]. Higher polynomial orders do not necessarily improve the global approximation quality, though [Mos08]. A Moving Least Squares (MLS) approach extends the polynomial approach and uses variable coefficients for different design space sections, in order to find the best local fit for the metamodel [Mos08].

In an earlier publication, polynomial metamodels were successfully used for the optimization of a single component transfer path [Wys20b]. Therefore, polynomial metamodels are selected as one possible type of metamodels for the investigation on the full vehicle SPL.

Kriging, a metamodel originating from geostatistics [Chi18], is another commonly used metamodel [Har06, Hem09, Har10, Chi18]. It provides good interpolation for few parameters but is slow in the creation [Hem09]. Kriging is investigated here, as a possible alternative metamodel.

In recent years, increasing processing power enabled widespread usage of machine learning algorithms in engineering applications [Nol21]. In automotive NVH development, ANNs become popular [Tso21]. ANNs connect input and output parameters via multiple layers of neurons, connected by synapses-like edges [Nol21]. The full network is able to represent a non-linear system behavior, overcoming the disadvantages of the previously discussed polynomials [Nol21]. Cunha et al. summarize the current state of the art of Machine Learning Methods in Structural Dynamics and Vibroacoustics [Cun22]. Regarding the present work, the following research is of special interest. Acerbi et al. interpolate irregularly sampled FRFs at previously unseen inaccessible points from measurements at accessible points [Ace21]. Tsokaktsidis et al. use ANNs to represent component [Tso19] and full vehicle [Tso21] transfer paths. Büttner et al. use ANNs as a metamodel for the creation of a vehicle sensitivity matrix from a large number of FE simulations [Büt21]. Rade et al. reduce the computational effort for FE topology optimization both in 2D and 3D representations [Rad21]. In a previous publication, ANNs were used for targeted design of component FRFs from a FE simulation data set [Wys21]. Based on this pre-study, ANNs become one of the used methods for metamodeling the suspension kinematics changes. Whereas the pre-study used a *Python* implementation [Wys21], here the software *Ansys optiSLang* [Ans21]

is used. This allows an easy to use examination of different kinds of metamodels in one software tool and easy integration into the suspension series development process.

Selecting the best fitting type of metamodel is a long process. In order to select a fitting metamodel, the data set is represented by different metamodels from which the best is selected. As tuning a metamodel to the best performance is its own study [Ran13] and beyond the scope of this investigation, basic metamodels are used for the investigation. In the end, this shows the possibility to extract design rules and perform optimization, even with an non-optimized metamodel.

For the prediction quality evaluation of different metamodels, the Coefficient of Prognosis (CoP) is used. CoP is a metric first introduced by Most et al. [Mos08] and used by *Ansys optiSLang* [Ans21]. First, the data set is split into a training data set and a test data set. The test data set is used for the CoP calculation

$$\mathrm{CoP} = 1 - \frac{S_{\mathrm{E}}^{\mathrm{Prediction}}}{S_{\mathrm{T}}} \tag{5.4}$$

with the sum of squared prediction errors $S_{\mathrm{E}}^{\mathrm{Prediction}}$ and the equivalent to the total variation S_{T} [Mos11]. The full mathematical derivation of the CoP can be found in the publications by Most et al. [Mos08, Mos11]. The CoP value is usually presented in percent from 0 to 100% and indicates the amount of explainable variation in the data set. Higher values indicate better prediction quality with 100% being the maximum value. [Mos08, Mos11]

Table 5.1 presents the performance for three different types of metamodels. The used approach for the metamodel configuration can be found in appendix C.2. The prediction quality for different frequency ranges using polynomials of order two, Kriging and ANN metamodels is indicated by the CoP value. Clearly, Kriging and ANN outperform the polynomials. As the ANN metamodels require less training time and provide slightly better prediction quality compared to Kriging, especially in the higher frequency ranges, ANNs are used for the further investigation of the road noise phenomena.

Table 5.1: Comparison of metamodel prediction quality, indicated by CoP, for different metamodel types and different SPL frequency ranges.

Frequency	Polynomial	Kriging	ANN
58 to 68 Hz	37.7%	51.5%	48.8%
80 to 90 Hz	60.4%	65.5%	78.1%
105 to 125 Hz	44.9%	54.9%	54.0%
190 to 210 Hz	29.2%	46.2%	57.1%
190 to 220 Hz	37.2%	46.9%	56.2%
210 to 220 Hz	34.2%	37.1%	46.7%

Whereas the values presented in table 5.1 are mainly used to compare the different types of metamodels, the overall prediction quality can be improved. In an additional investigation on another vehicle, using a larger data set results in better performing metamodels. Table 5.2 presents the results of additional investigations with five link rear suspensions for two different vehicles. Both additional investigations are based on 1500 samples each investigating similar frequency ranges. The ANN metamodel quality improved to CoP mean values around 90% with identical ANN configurations as before. Additionally, the variance in prediction quality for the individual frequency ranges and seating positions was halved. This shows the potential to improve the prognosis quality by enlarging the data set. An improvement of the network architecture could also lead to improved prognosis quality, but is out of scope for this research.

Table 5.1 only presents the metamodel quality for the metamodels connecting kinematic hard point locations to SPLs in the selected frequency ranges. Metamodels connecting the kinematic hard point locations to the suspension

Table 5.2: Comparison of ANN metamodel prediction quality, indicated by CoP, for different five link rear suspensions and different frequency ranges with varied numbers of samples.

Value	Vehicle A (W206)	Vehicle B	Vehicle C
Samples	500	1500	1500
CoP min	46.7%	73.4%	76.8%
CoP max	78.1%	98.6%	96.8%
CoP mean	56.8%	93.5%	89.7%
CoP median	55.1%	96.6%	91.5%
CoP std	11.2%	6.0%	5.7%

parameters perform above 97% CoP independently of the metamodel type, as the correlations are much simpler compared to the full vehicle acoustic transfer path. For consistency, ANNs are used for both the road noise and the suspension parameter metamodels.

The creation of metamodels for the connections between suspension parameters and SPLs was discontinued, as the metamodel prediction quality was unacceptably low. This again hints to the possibility of modifying road noise phenomena independently from suspension parameter changes by modifying hard point locations.

5.5 Insights into the Data Set

Using the previously selected ANN metamodels, this section provides an insight into the data set. Conclusions regarding sensitivities and correlations are presented.

5.5.1 Sensitivities

In Engineering, sensitivities and design rules are often preferred over single optimized designs. They can lead an optimization based on the most significant design variables and additional requirements.

Figure 5.8 presents the sensitivity analysis using *Ansys optiSLang*. The metamodeling approach discussed in section 5.4 additionally provides importances for each design variable by rating their contribution to the overall variance. Most et al. describe the approach in detail [Mos11]. Both frequency range and suspension parameter metamodels provide the presented sensitivities as design variable individual CoP values. Darker colors indicate high sensitivities.

It is clearly visible that each target value has its unique set of significant design variables. For example, most of the frequency ranges are dominated by the design variables $R_{2,x}$ and $R_{3,x}$. Lower frequency ranges additionally depend on $R_{5,x}$. This hints the possibility to influence different frequency ranges by

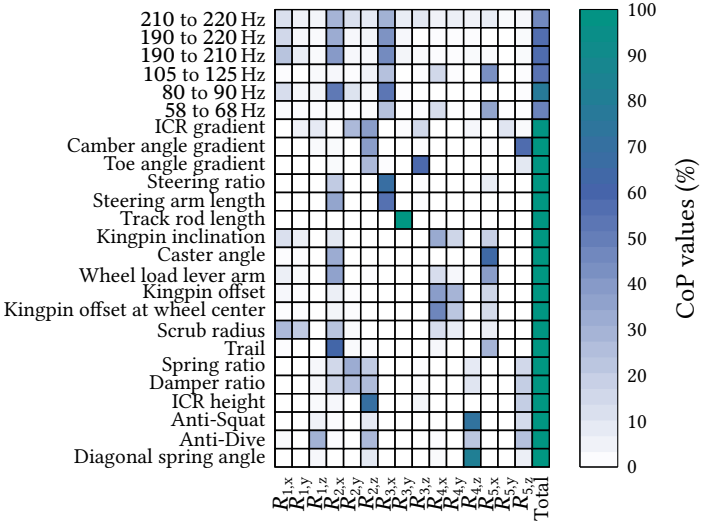

Figure 5.8: Sensitivities between kinematic hard point locations and both road noise phenomena and suspension parameters.

different design variables up to a certain extent. Additionally, hard points not influencing the acoustic effects at all dominate many of the suspension parameters. For example, $R_{2,z}$ or $R_{5,z}$ only determine suspension parameters. This indicates the possibility to compensate disadvantageous behavior resulting from the acoustic optimization. Additionally, this indicates the possibility to change suspension parameters without influencing road noise phenomena.

5.5.2 Graphical Metamodels

Each metamodel considers all 15 design variables. Therefore, a 15-dimensional graphical representation would be required to fully represent the correlations. As this is impossible with an easy to interpret visualization, each plot is always a simplification. For a graphical representation, the 15-dimensional parameter space is reduced onto a two-dimensional parameter space. Two of the 15 variables are selected as plot variables whereas the remaining variables are kept constant.

The selection is guided by the sensitivities in fig. 5.8. This way, the graphical representations in fig. 5.9 show the correlations between a target parameter and the two most important design variables regarding the respective target parameter. The colored surfaces represent the metamodels' fitted approximation for the correlations between design variables and result values. The fewer sensitive parameters there are, the better the visual representation represents the full relationships.

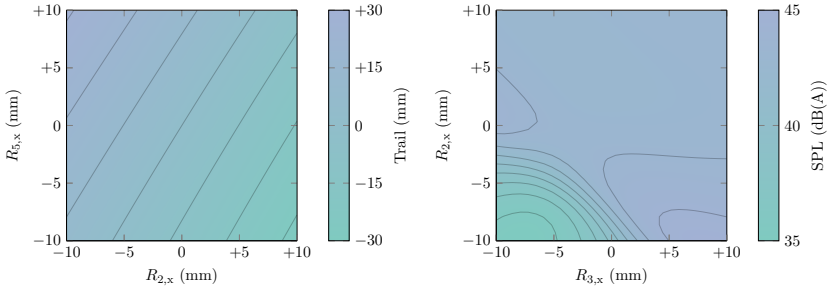

(a) Metamodel for trail as a function of the design variables $R_{2,x}$ and $R_{5,x}$

(b) Metamodel for frequency range 190 to 210 Hz as a function of the design variables $R_{2,x}$ and $R_{3,x}$

Figure 5.9: Two example metamodels. Graphical representation of the target parameter as a function of their two respective dominating design variables. Isolines indicate constant target parameter values.

Figure 5.9a represents the almost linear correlation between the two design variables $R_{2,x}$ and $R_{5,x}$ and the deviation for the suspension parameter trail with respect to its initial value. The metamodel clearly indicates a linear behavior with two dominating design variables.

Figure 5.9b indicates a highly nonlinear dependency between the design variables $R_{2,x}$ and $R_{3,x}$ and the amplitude in the frequency range 190 to 210 Hz. The graphical representation indicates reduced $R_{2,x}$ and $R_{3,x}$ coordinates as promising for noise reduction. Figure C.2 in the appendix presents further metamodels in relation to their most dominating design variables.

These graphical representations are able to direct or assist design choices in the suspension development process, regarding the boundary conditions of many

different development domains. Instead of suggesting single optimized suspension kinematics designs, the metamodels can indicate promising optimization directions for specific design variables. The different development domains can then compromise on the final design using these metamodel-based design rules.

5.5.3 Possible Optimization Criteria

Combining the insights resulting from sensitivities and metamodels, the complexity of the system becomes visible. There are design variables contributing massively to specific frequency ranges, there are design variables contributing contrary to different frequency ranges and suspension parameters, and there are design variables without any influence on specific target values. For these observations, the main target is to create design rules from the metamodels that can direct a cross-domain suspension optimization. Nevertheless, a numerical optimization for a best performing road noise kinematics is also possible. For that, the high complexity of the system requires working with a multi-target optimization problem.

To simplify the optimization problem, the optimization can be split into the different development domains. This results in an optimization function for the road noise phenomena and another optimization function for the suspension parameters. Utilizing the n_p averaged road noise phenomena frequency ranges determined in eq. (5.3), the optimization function for the SPL

$$\bar{L}_\mathrm{p,res} = \sum_{\mathrm{j}=1}^{8} \sum_{\mathrm{i}=1}^{n_\mathrm{p}} w_{\mathrm{L_{i,j}}} \bar{L}_{\mathrm{p_{i,j}}} \quad \text{, with } w_{\mathrm{L_{i,j}}} \in \mathbb{R} \tag{5.5}$$

weighs the eight ear positions. The weighting factors $w_{\mathrm{L_{i,j}}}$ allow prioritization of specific phenomena and ear positions. Zero or negative weighting factors could ignore or increase the SPL in some frequency ranges if this is necessary for benefits in other frequency ranges.

Weightings for the suspension parameters allow targeted optimizations. Contrary to the SPL values, the suspension parameter values are of different orders of magnitude and different measurement units. Therefore, the suspension

parameter changes have to be normalized [San10]. The relative suspension parameter changes

$$k_{\mathrm{i,rel}} = \frac{k_{\mathrm{i,abs}} - k_{\mathrm{i,abs,orig}}}{k_{\mathrm{i,abs,orig}}} \tag{5.6}$$

are standardized relative to their values within the initial suspension kinematics. The n_{k} standardized suspension parameters $k_{\mathrm{i,rel}}$ are combined to an optimization function

$$k_{\mathrm{res}} = \sum_{i=1}^{n_{\mathrm{k}}} w_{\mathrm{k_i}} \left| k_{\mathrm{i,rel}} \right| \quad \text{, with } w_{\mathrm{k_i}} \in \mathbb{R} \tag{5.7}$$

weighting the different suspension parameter deviations against each other. Weighting factors smaller and larger than one take into account different desired suspension behaviors. Zero as a weighting factor represents a degree of freedom in the suspension parameters. This is a simplified optimization function, only regarding suspension parameter changes without their sign. For the acoustic suspension kinematics optimization, this target function is able to ensure minimal changes to the suspension parameters, rather than actively designing them.

A set of weighting factors $w_{\mathrm{L_{i,j}}}$ and $w_{\mathrm{k_i}}$ represent a desired suspension behavior regarding road noise and suspension parameters. It is not effective to create one metamodel per optimization function but one for each weighted summand in the optimization functions. The resulting target value is then calculated during the optimization run. This improves the quality of the target function prognosis and thus the quality of the optimization.

5.6 Conclusions to the Correlations

In the previous sections, examples for quantitative and qualitative conclusions from the data set were presented. Sensitivity analyses provide numeric correlations between design variables and SPLs or suspension parameters. The usage of this knowledge can be split into two scenarios, which is indicated in fig. 3.3.

The first application is numerical optimization, which means searching a single optimal suspension design. This requires a combined optimization target function including each single boundary condition and requirement to the suspension regarding all development domains. For a holistic suspension development, this is not possible. There are too many boundary conditions, load cases, and even experimental investigations to include. Therefore, a numerical optimization will always need manual postprocessing by different development domains.

A more realistic and relevant application are design rules. Graphical and numerical metamodels provide the different development domain's suspension designers with insights into SPL modification. They can consider them and find a suspension design regarding the road noise comfort as far as possible. Therefore, these qualitative correlations can be more important in a holistic development process compared to finding a single optimization. For one- or two-dimensional correlations, the graphical representations offer an easy to interpret insight. Interactive plotting is required for more complex correlations, as the plotting becomes difficult for more than two dimensions. Here, numerical metamodel evaluation can direct the design choices.

6 Optimizing Suspension Designs

Sections 5.2 and 5.5 provided a first insight into the data set and the correlations between suspension kinematics and SPLs. In this chapter, multiple suspension design optimizations are presented regarding different optimization criteria. Elaborating Research Question 4[a], the optimizations illustrate different application examples possibly occurring in suspension development.

Even though the optimization using metamodel design rules in cooperation with the different development domains seems to be most promising, this chapter starts by picking designs in section 6.1 and then proceeds to numerical optimization in section 6.2. This enables a first evaluation of the targeted modification of SPLs by modifying suspension kinematics. After this, the holistic optimization using metamodel design rules is presented in section 6.2.4.

6.1 Picking Suspension Designs

Figure 5.4 on page 88 presented selected designs indicating the existence of local optimal designs. Designs following the lower boundary of the scatter band are unlikely, though.

The existence of such global optimal designs can be investigated using parallel coordinates plots and the data set as a kind of brute force method[b]. Each black line in fig. 6.1 represents one of the 500 data set designs. On the abscissa,

[a] Do suspension kinematics optima exist for road noise and how can such optima be integrated into the development process?

[b] It is to mention that this approach works particularly well using digital and interactive parallel coordinates plots, rather than printed static ones.

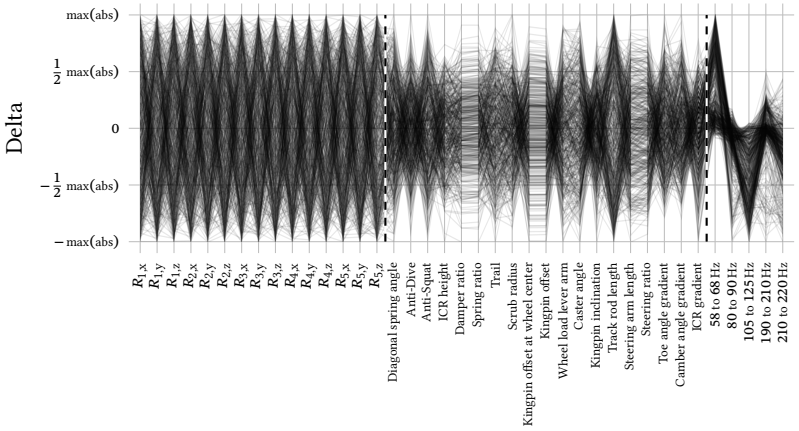

Figure 6.1: Parallel coordinates plot for the full data set consisting of 500 samples. From left to right, separated by dashed lines, hard point coordinates, suspension parameters, and SPLs scaled to their maximum absolute deviation.

the design variables, suspension parameters selected in section 5.2.3, and the SPL frequency ranges selected in section 5.2.2 are listed. Black and white dashed lines separate the three groups. A horizontal line at zero deviation could represent the initial suspension kinematics. On the ordinate, the design space relative to the maximum absolute deviation of each variable or parameter is given.

Limiting specific suspension or SPL parameters to desired ranges enables design picking from the data set. In fig. 6.2 the SPLs in the ranges 58 to 68 Hz, 80 to 90 Hz, 190 to 210 Hz, and 210 to 220 Hz are limited to the lower design space, indicated by green bars. This results in two possible designs included in the data set fulfilling the requirements. Figure 6.3 presents the SPL curves for the two selected designs from fig. 6.2. Clearly, an improvement was achieved for the three frequency ranges to the right. In the frequency range 58 to 68 Hz, the deterioration in SPL was limited to a minimum.

The picked designs modify all 15 design variables. As this is a drastic modification to a suspension kinematics, it is obvious that the suspension parameters would differ clearly from the reference suspension kinematics. Figure 6.4 compares the suspension parameters to the reference suspension kinematics. For

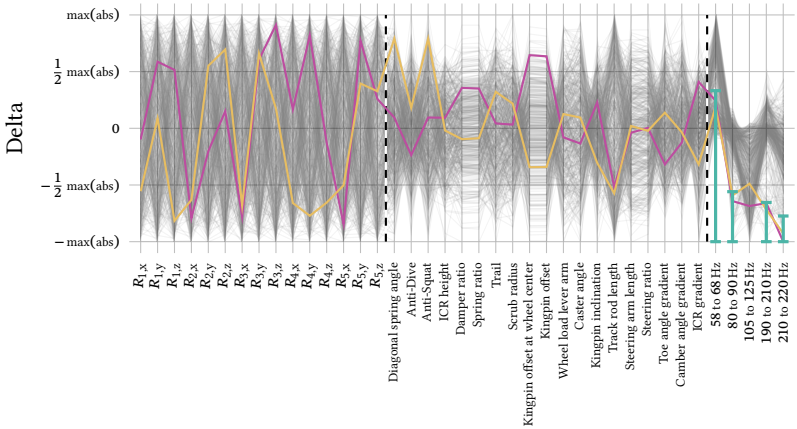

Figure 6.2: Reducing the design space by limiting SPL intervals to the green ranges until only few feasible samples remain visible.

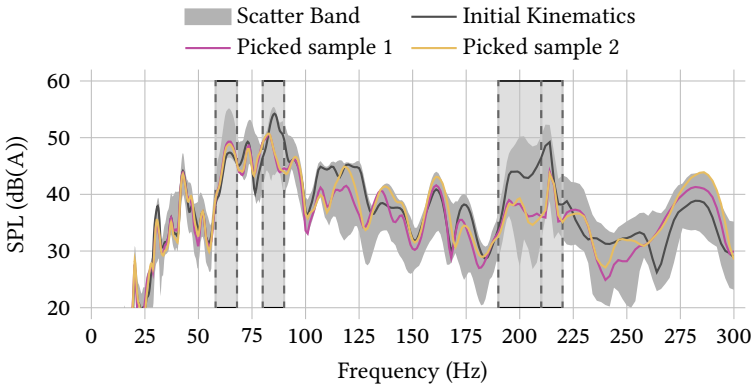

Figure 6.3: SPL for the selected samples from fig. 6.2.

better illustration, the suspension parameters are indicated with their absolute values. Missing bars indicate changed signs and therefore large deviations. Multiple of the suspension parameters changed by large amounts. Therefore, a more specific optimization needs to be found for further investigations.

A more systematic approach compared to reducing and picking samples in the parallel coordinates plots, is clustering. For example a K-Means clustering can

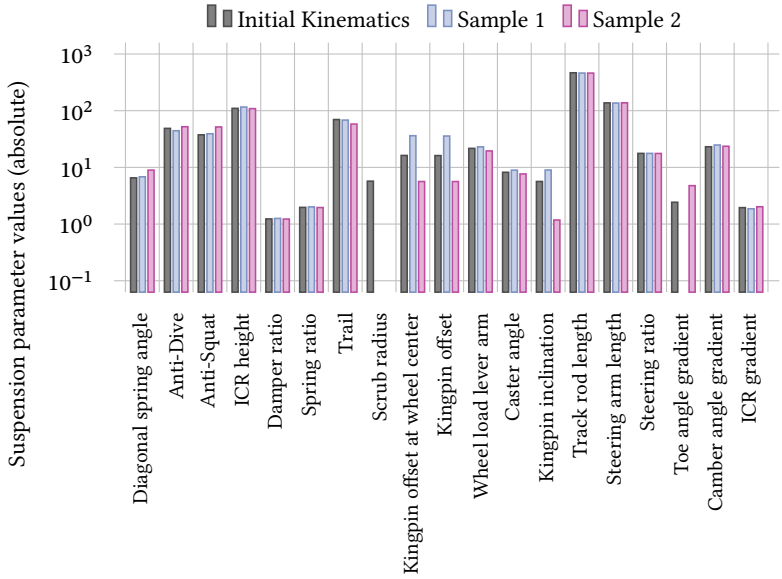

Figure 6.4: Absolute suspension parameter values for the selected samples from fig. 6.2.

identify connected samples and identify simple connections between design variables, suspension parameters and SPLs. An evaluation of this method lead to insights that could also be identified by selecting samples in the parallel coordinates plots. Therefore, this approach was discontinued.

6.2 Suspension Kinematics Modification Examples

After picking designs from the data set by selecting specific design properties, this section presents a systematic optimization of various SPL parameters considering different restrictions to suspension parameters. In the real development process, qualitative optimization using visual metamodel representations would be of more relevance. For the presented investigation, numeric optimization is mainly used to showcase the possibility to modify the suspension kinematics to receive optimized SPLs. Nevertheless, section 6.2.4 presents

the possibilities of optimizing suspension kinematics in a holistic way using metamodel design rules. The investigations utilize the previously generated data set containing 15 design variables with a design space of ±10 mm.

The optimization is based on the previously presented ANN-based metamodels for both suspension parameters and SPL parameters. Their parameters are specified in appendix C. The metamodel prediction quality is reduced towards the parameter limits, as the sample density is lower there [Har19, S. 137]. Instead of decreasing the optimization range, each optimization is verified by an additional FE simulation run. If the FE simulation run does not confirm the desired behavior, the optimization range is reduced afterwards.

The selected examples simulate different scenarios in the vehicle development process. Different development stages and possibilities originating from driving automation affect the optimization boundary conditions. Therefore, the optimization case study is separated into multiple scenarios with changing boundary conditions and suspension parameter restrictions. The first scenario in section 6.2.2 imposes no suspension parameter restrictions and focuses solely on the SPL optimization. As these boundary conditions are similar to picking a design, this is the first scenario under investigation. The second scenario in section 6.2.3 represents set suspension parameters and provides road noise optimization with as little changes to the suspension parameters as possible. The last scenario in section 6.2.4 presents the optimization using metamodel design rules.

6.2.1 Optimization Strategy

The combined optimization of multiple SPL frequency ranges and suspension parameters forms a multi-target optimization. As previously shown, the data set hints the absence of a global optimum suspension kinematics, optimizing all SPL frequency ranges without deterioration in the suspension parameters. Therefore, the multi-target optimization results in a multi-dimensional pareto front indicating the target conflicts between different optimization criteria [Har19].

In the case of two or three optimization targets, the pareto front is graphically representable. With more targets, the same difficulties as for the graphical metamodel representations emerge [Har19]. Cost functions combine multiple optimization criteria into one scalar target value, reducing the complexity of the optimization [Har19]. Equations (5.5) and (5.7) represent the utilized cost functions for the presented optimizations. In the present investigation, SPL targets are mainly used on their own, whereas the suspension parameter targets are combined into a cost function, following eq. (5.7).

The combination is done on the optimization level, not on metamodel level. If the cost function results would be fitted by a metamodel, the individual information would be lost. Therefore, the overall optimization performs better when combining multiple metamodels into one cost function.

For the numerical optimization, an evolutionary algorithm is used. These optimization algorithms are specifically suitable for complex multi-target optimizations with many local optima [Har19]. This fundamental investigation does not aim at identifying the best performing optimization algorithm, but a suitable general optimization strategy for road noise suspension kinematics optimization. Therefore, the implementation and configuration details are not in focus here and all metamodel optimization results are verified by FE simulations.

6.2.2 Road Noise Optimal Suspension Kinematics

The first optimization scenario imposes no restrictions to the suspension parameters. This could be a futuristic scenario when most of the boundary restrictions are compensated by Drive-by-Wire systems, automation or active actuation. The scenario enables the possibility to fully focus the optimization onto the SPL without regards to the suspension parameters. This way, target conflicts between different frequency ranges may be resolved. The scenario

combines Research Question 1[a] and the first part of Research Question 4[b], identifying suspension kinematics optima for specific road noise phenomena.

In section 5.2.2, the target conflict between the two frequency ranges 58 to 68 Hz and 80 to 90 Hz was identified. Figure 6.5 presents an attempted optimization for the frequency range 80 to 90 Hz. The existence of the target conflict with the frequency range 58 to 68 Hz is clearly visible. The improvement of approximately 8 dB(A) in the optimization frequency range comes with a deterioration of approximately 6 dB(A) in the frequency range 58 to 68 Hz. If the optimized frequency range clearly dominates the SPL in the vehicle, this could be a valid optimization result. Nevertheless, resolving target conflicts is usually desired.

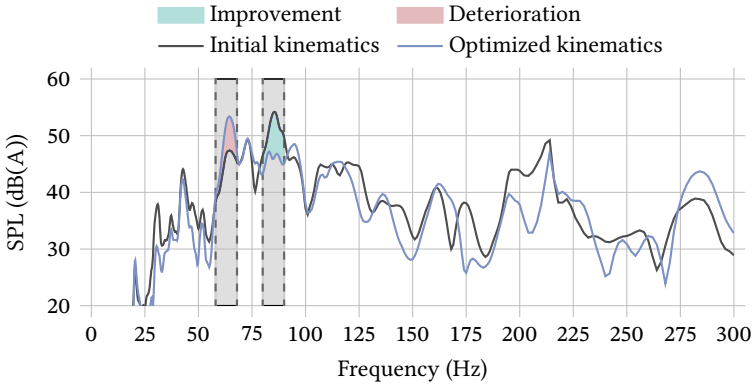

Figure 6.5: Optimization result for an SPL reduction in the frequency range 80 to 90 Hz. Clearly visible is the target conflict with the frequency range 58 to 68 Hz.

Resolving the target conflict is a two-target optimization. Without restrictions to the suspension parameters, this creates a pareto front for both frequency ranges, visualized by the anthill plot in fig. 6.6. Each dot represents one design,

[a] Is it possible to modify dedicated road noise phenomena by changing the location of specific kinematic hard points?

[b] Do suspension kinematics optima exist for road noise and how can such optima be integrated into the development process?

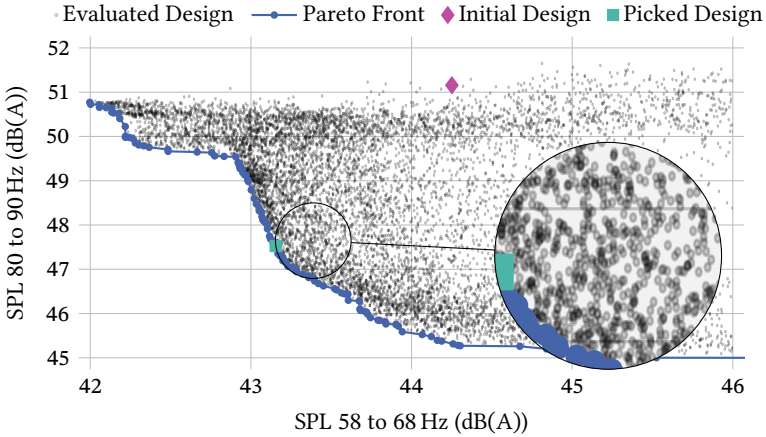

Figure 6.6: Pareto front for SPL optimization without any restrictions to the suspension parameters. The optimization target is to resolve the target conflict between the frequency ranges 58 to 68 Hz and 80 to 90 Hz. For better visualization, the plot is cut at 46 Hz on the abscissa.

obtained via ANN metamodel evaluation. The connection of the leftmost and lowest points creates the pareto front. The metamodels clearly hint an optimization potential in both target frequency ranges. The selected optimization result is marked on the pareto front. This design indicates a possible improvement in both frequency ranges. Figure 6.7 presents the design variables for the selected design.

Each gray bar, represents the displacement for one kinematic hard point direction. The blue bars are discussed in a following paragraph. Figure 6.8 presents the verification simulation result for the selected design.

The optimized design reduces the SPL in both frequency ranges. In the frequency range 80 to 90 Hz a peak to peak reduction by 3.2 dB(A) was achieved. Between 58 and 68 Hz the peak to peak reduction is 0.6 dB(A). As fig. 5.8 identifies the metamodel for 80 to 90 Hz as better performing compared to the one for 58 to 68 Hz, the better performing optimization for the frequency range 80 to 90 Hz is not surprising. Additionally, the potential for improvement in the frequency range 58 to 68 Hz is lower, indicated by the scatter band in fig. 5.2 on page 86. The optimization example shows the possibility to resolve

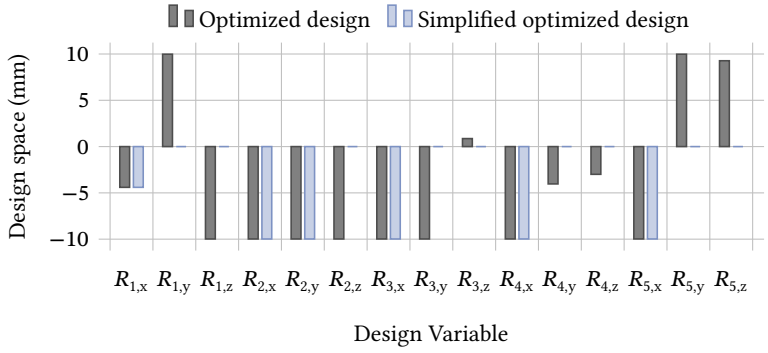

Figure 6.7: Design variable distribution for the selected design from fig. 6.6 in gray and a simplified version in blue.

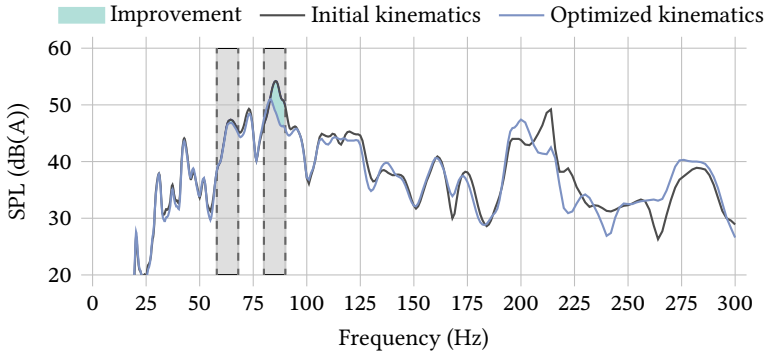

Figure 6.8: SPL for the selected design from figs. 6.6 and 6.7. The optimization potentials in the target frequency ranges 58 to 68 Hz and 80 to 90 Hz are colored in green.

target conflicts in the SPL systematically. The example also indicates possible deterioration in frequency ranges not under optimization focus. For example, the frequency range 190 to 210 Hz deteriorates.

The presented optimization modifies all 15 design variables. In the actual suspension development process, this might not be feasible. The combination of the optimized design, indicated by gray bars in fig. 6.7, with the sensitivity analysis in fig. 5.8 indicates differing relevance of the design variables. Reducing the design space by picking only the most relevant design variables could therefore result in a similar optimization result. As a selection criterion,

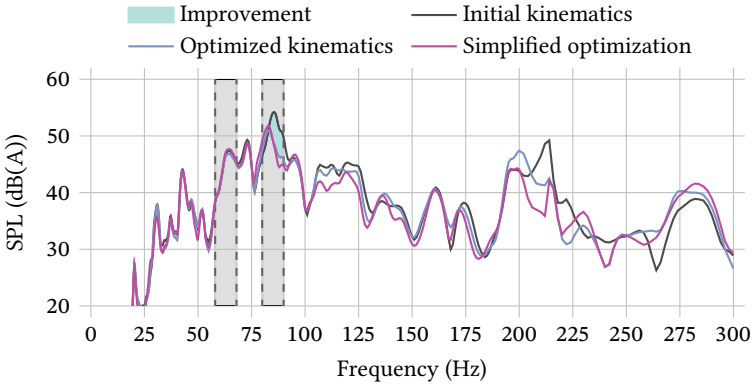

Figure 6.9: SPL for the optimized and simplified optimized suspension kinematics. Optimization frequency ranges 58 to 68 Hz and 80 to 90 Hz marked in green.

design variables with at least one CoP value larger than 0.1 in one of the selected frequency ranges are considered as most relevant. The blue bars in fig. 6.7 represent the selected design variables $R_{1,x}$, $R_{2,x}$, $R_{2,y}$, $R_{3,x}$, $R_{4,x}$, and $R_{5,x}$. The remaining design variables are set to zero displacement. This is a design variable reduction by 60%.

The resulting SPL is presented in fig. 6.9. The small benefit between 58 and 68 Hz is lost with 0.2 dB(A) above the original value. The amplitude in the frequency range 80 to 90 Hz is still reduced by 2.5 dB(A). This improves the target conflict, as fixing the frequency range 58 to 68 Hz is not trivial, indicated by the SPL scatter band. In the remaining frequency ranges, the cavity noise region in particular, the results differ significantly. Using additional optimization targets, these differences could be addressed separately.

6.2.3 Including Suspension Parameters into the Optimization

The optimization phase for the suspension kinematics mainly takes place in the early development phase, after the concept evaluation. After the suspension topology and configuration are set, only small changes are implemented into the suspension. In this phase, the suspension parameters are mostly fixed. In

the following investigations, this fact is translated to the optimization boundary condition of minimal changes to the suspension parameters.

While changing the suspension kinematics for optimized SPLs, it is inevitable to change the suspension parameters. As not all kinematic hard points are sensitive to SPLs, indicated by fig. 5.8, the remaining hard points may be used for kinematics compensation. With the compensation measures, the suspension parameters and design can be brought back to acceptable values.

For the first optimization examples, constant suspension parameters are desired. Therefore, the optimization target is to minimize the suspension parameter deviation while decreasing the SPL. Figure 6.10 presents a pareto front using the suspension parameter deviation cost function eq. (5.7) on page 100 and the SPL in the frequency range 190 to 210 Hz. The pareto front apparently indicates an optimum design on the left of the lower horizontal part of the pareto front.

Figure 6.11 presents the SPL curve originating from the FE simulation of the optimum picked in fig. 6.10. An amplitude reduction in the desired frequency range was clearly achieved. Figure 6.12 presents the corresponding suspension parameters. It is clearly visible that the changes in the suspension parameters is small, but present.

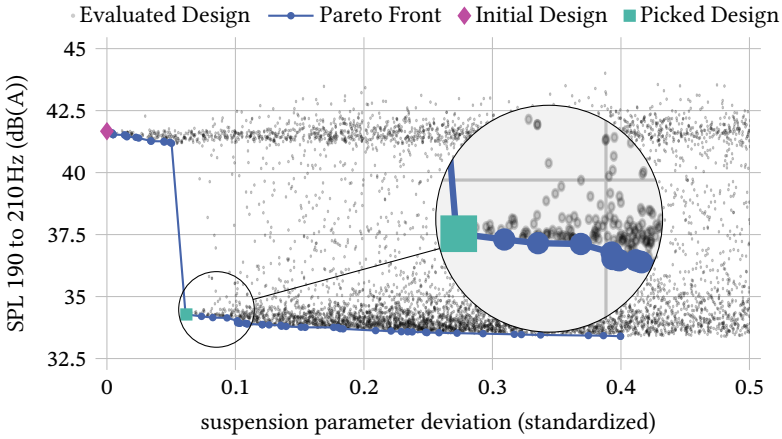

Figure 6.10: Pareto front for SPL optimization in the frequency range 190 to 210 Hz and restricted modifications to the suspension parameters.

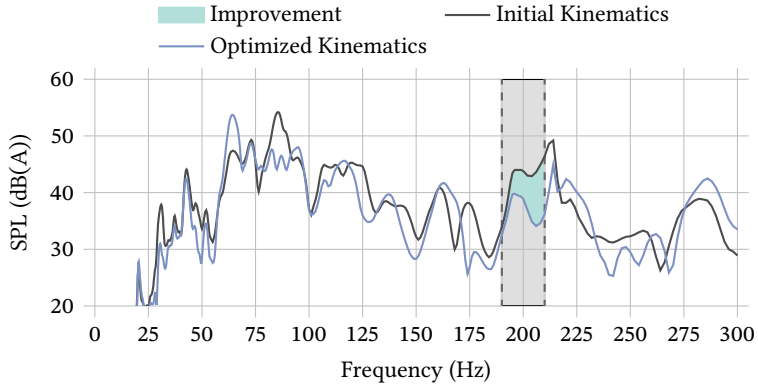

Figure 6.11: SPL for the selected optimum design from fig. 6.10.

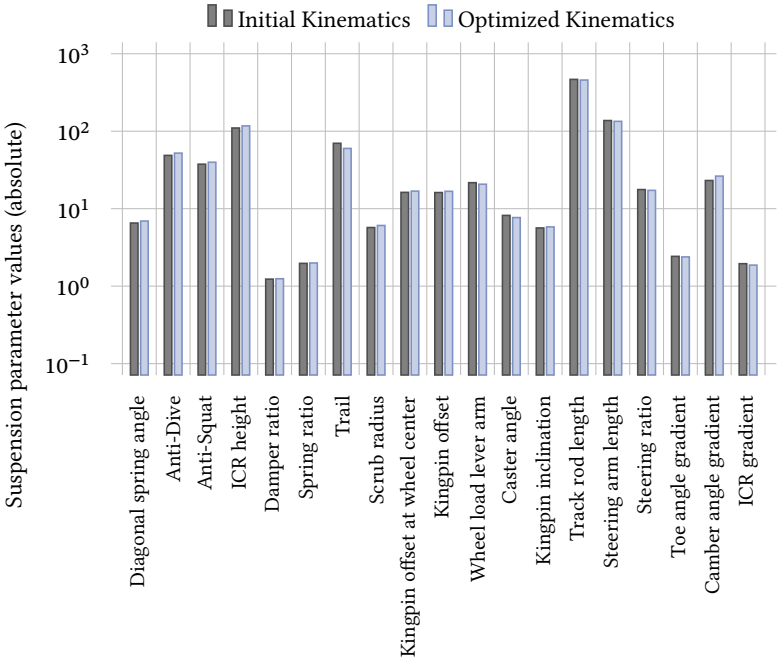

Figure 6.12: Absolute suspension parameter values for the selected optimum design from fig. 6.10.

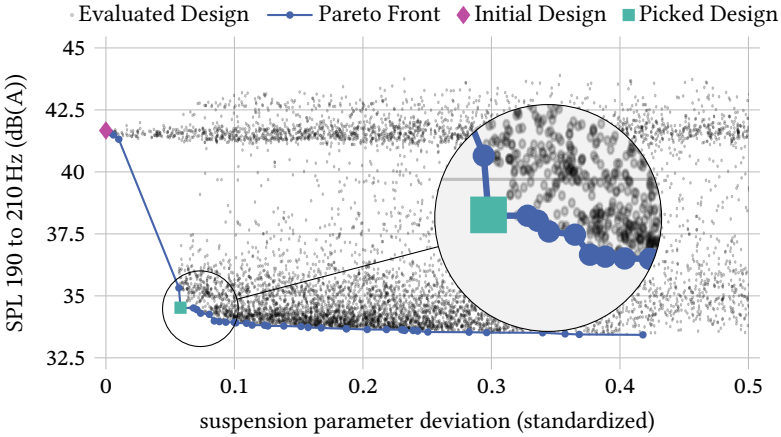

Figure 6.13: Pareto front for SPL optimization in the frequency range 190 to 210 Hz and restricted modifications to the suspension parameters with extra penalization for trail deviations.

There are certain suspension parameters of particular importance. For example, the trail is an important suspension parameter for driving dynamics. This raises the question, if the deviation of the trail could be reduced, while keeping the positive effect in the SPL. For this investigation, an additional penalty is introduced for suspension parameter deviations by increasing w_{k_i} for the trail. Figure 6.13 presents the pareto front for the same optimization target as before, this time containing additional trail penalty.

Figure 6.14 confirms the successful reduction of the trail deviation. Whereas some suspension parameter deviations became larger, the trail is nearly at the original value.

Figure 6.15 presents the new SPL curve. Clearly the optimization is still possible with changed boundary conditions.

For both optimization examples, it is apparent that with the optimization of one frequency range the deterioration of another may occur. Here, the frequency range 58 to 68 Hz is increased. This again confirms the target conflict under investigation in the previous example. The target conflict between

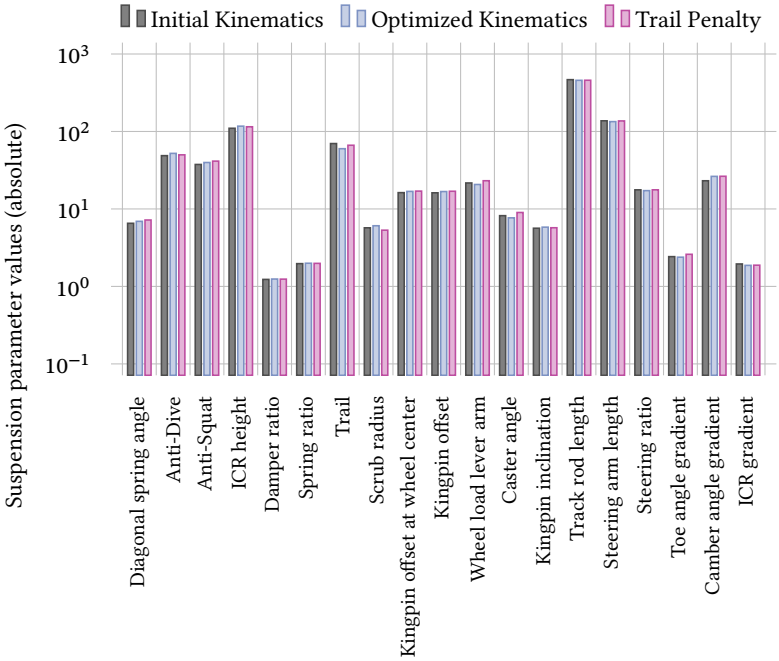

Figure 6.14: Absolute suspension parameter values for the selected optimum design with trail deviation penalty from fig. 6.13.

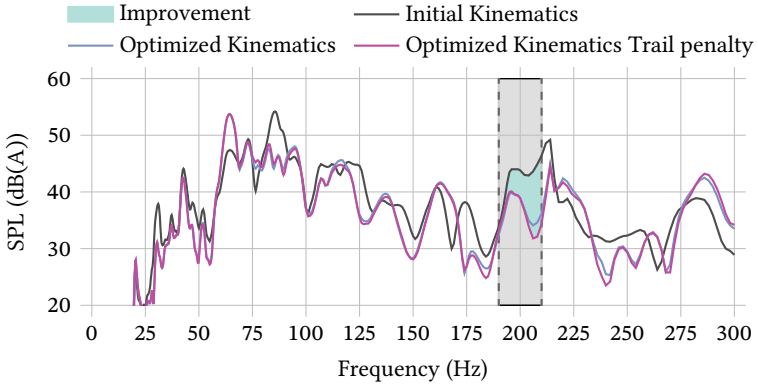

Figure 6.15: SPL for the selected optimum design with trail deviation penalty from fig. 6.13.

different frequency ranges is a commonly observed phenomenon in NVH development [Uhl21b].

6.2.4 Optimization Using the Visual Metamodels

In suspension development, there are that many requirements and restrictions to the suspension kinematics that one single development domain is not in the position to define new suspension kinematics. While being viable as a proof of concept, numerically optimized suspension kinematics using many design variables are difficult to implement into the design process. Therefore, in the next application example, metamodel visualizations are used to determine optimization directions which can then be integrated in a holistic and collaborative way into the suspension development.

The tire cavity noise frequency range between 190 and 220 Hz shall be subject to optimization in this example. The evaluation of a SPL optimized design is performed on the graphical metamodel representations. As the graphical representation can only illustrate two design variables at once, the other 13 need to be fixed to one value. In an iterative process, the final design is determined. Figure 6.16 presents the graphical representation for the last

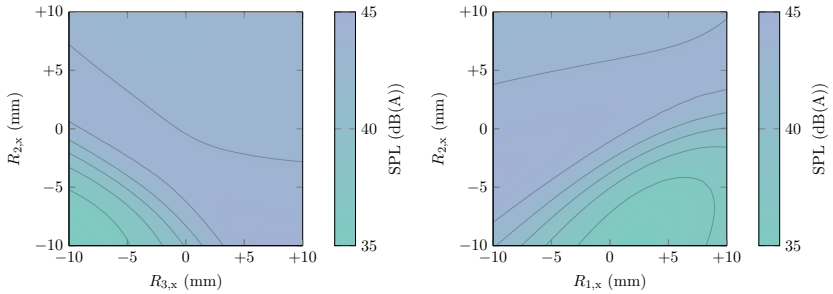

(a) Metamodel for frequency range 190 to 220 Hz as a function of the design variables $R_{2,x}$ and $R_{3,x}$.

(b) Metamodel for frequency range 190 to 220 Hz as a function of the design variables $R_{1,x}$ and $R_{2,x}$.

Figure 6.16: Graphical representation of the metamodel describing the correlation between SPL between 190 and 220 Hz and the coordinates $R_{1,x}$, $R_{2,x}$, and $R_{3,x}$. The optimum is located at $R_{1,x} = +2.7$ mm, $R_{2,x} = -10$ mm, and $R_{3,x} = -10$ mm.

iteration. It is to note that the process works best using digital interactive representations of the metamodels, instead of the static images presented here.

The iterations are performed as follows: The sensitivity analysis in fig. 5.8 indicates the coordinates $R_{2,x}$ and $R_{3,x}$ as most sensitive in the frequency range 190 to 220 Hz. The graphical representation for all 15 design variables at a fixed value of ± 0 mm hints a displacement of -10 mm for both coordinates as optimum. In the next step the graphical representation for the next most important design variable $R_{1,x}$ is created. For this, the graphical representation for $R_{3,x} = -10$ mm is created. As the target for this optimization is to use as few design variables as possible, the process is stopped after the three most important design variables. Fine tuning of the optimized design variables is performed by iterating through the graphical representations again with the selected design variables as fixed values. In this example, this does not change the values any more, making the first iteration the final one. The final iteration for both metamodel representations is presented in fig. 6.16. These specify the ideal kinematics modification at the displacement values presented in fig. 6.17. The arrows indicate the direction of the modification, driving direction being to the left.

Figure 6.18 confirms the hypothesis for an optimum design regarding the desired frequency range. Again, the plot is best evaluated as a digital interactive visualization. The plot shows the 500 sample design space with their $R_{1,x}$, $R_{2,x}$,

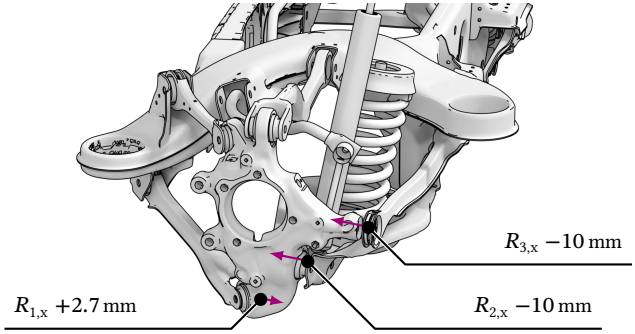

Figure 6.17: Desired suspension kinematics after metamodel optimization. Driving direction to the left.

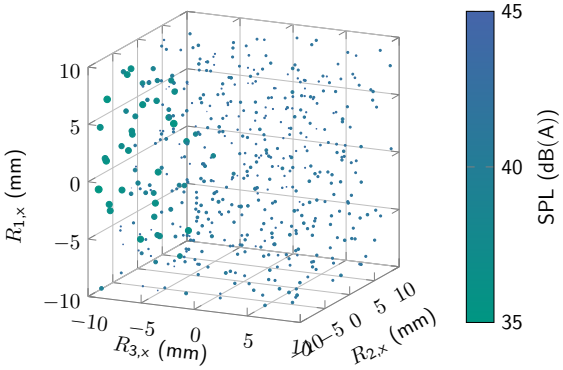

Figure 6.18: Three dimensional design Space for the three most important design variables in the frequency range 190 to 220 Hz. Larger greener dots indicate low SPLs.

and $R_{3,x}$ coordinates. The color and size represent low SPL values in the frequency range. These low values accumulate in the region of low $R_{2,x}$, and $R_{3,x}$ values. The influence of the $R_{1,x}$ coordinate seems to be low. It is to remember that each of the 500 samples is varied in all 15 design variables. Despite this large deviation, the correlation in the presented three dimensions clearly exists. The figure also shows potential negative effects despite the clear correlation in two dimensions. If $R_{1,x}$ is raised or lowered up to ± 10 mm, the clear correlation between low values for $R_{2,x}$ and $R_{3,x}$ and low SPL does not exist anymore. This shows the relevance of adjusting the metamodel representations to the desired design variable values.

The selected set of design variables leads to the SPL presented in fig. 6.19. The three displacements lead to a reduced SPL in the desired frequency range 190 to 220 Hz.

For a development compromise, the remaining DOFs are important. The sensitivities in fig. 5.8 show high significances for $R_{2,x}$ in most suspension parameters. This hints undesired modification of the suspension parameters if the modifications are used without any additional compensation modifications. As there are many sensitivities to the suspension parameters in the coordinates except the modified ones, this indicates the possibility to compensate the

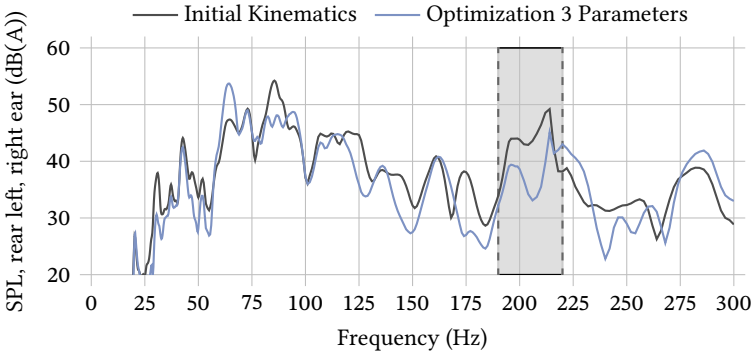

Figure 6.19: Optimized SPL using three design variables.

undesired effects. These additional requirements for a holistic optimization are further investigated in the next chapter.

6.3 Conclusion to the Kinematics Optimization

This chapter presented the possibility to extract correlation information directly from the data set and by generating metamodels. The larger the data set, the more possibilities exist to directly pick samples, which fulfill given requirements. Selecting from parallel coordinates plots allows first insights into systematic connections between kinematic hard point locations and simulation results of different development domains. Targeted creation of kinematics changes was demonstrated for different optimization use cases.

The simulation results of the optimization examples demonstrated the possibility for optimization of NVH phenomena by changing the suspension kinematics. The possibility to perform targeted reduction for specific road noise phenomena or frequency ranges was demonstrated. The optimization was performed via both numeric optimization and qualitative metamodel optimization. The suspension kinematics modification can be based on few design variables, enabling the remaining design variables to serve as compensation to changed suspension properties.

The prediction quality of the metamodels still allows improvement. The examples showed that roughly optimized metamodels on a particularly small set of samples could lead to holistic and aimed SPL optimization. The metamodel predictions were verified using FE simulation. This proved the predicted optimization to be present in the actual simulation model. This still does not prove that the optimization is present in the final hardware, though. This is investigated in detail in the next chapter.

7 Validation

For a holistic suspension kinematics optimization regarding road noise, the metamodel design rule optimization is extended in this chapter. The optimization result from section 6.2.4 is modified for better feasibility in collaboration with mentioned additional development domains. Kinematics compensation is considered and the final variant of the optimized suspension kinematics is manufactured in hardware. In full vehicle validation measurements, the effectiveness of the optimization to reduce road noise in the cavity frequency range is examined. The results and investigations presented in this chapter were obtained in cooperation with the experts of the corresponding development domains [Bus21].

7.1 Optimized Suspension Kinematics

The selected suspension kinematics optimization shows reduction in the cavity noise frequency range between 190 and 220 Hz. The simulation results indicate a possible optimization using three kinematic design variables, indicated as *first iteration* in table 7.1.

In order to simplify the design space and keep the changes as small as possible, the design space is further reduced in a *second iteration*. Figure 5.8 clearly identifies the design variables $R_{2,x}$ and $R_{3,x}$ as the most important design variables in the optimization frequency range. Thus, the design variable $R_{1,x}$ is omitted from the original optimization. This reduces the number of modified kinematic hard points to two, also reducing the required changes to the wheel carrier, the track rod (R_3) and the spring link (R_2). Figure 7.1 presents the

Table 7.1: Suspension kinematics evolution for hardware validation. All remaining kinematic hard points stay unchanged.

Coordinate	1st iteration	2nd iteration	Final iteration
$R_{1,x}$	+2.70 mm	0.00 mm	0.00 mm
$R_{1,y}$	0.00 mm	0.00 mm	0.00 mm
$R_{1,z}$	0.00 mm	0.00 mm	0.00 mm
$R_{2,x}$	−10.00 mm	−10.00 mm	−9.73 mm
$R_{2,y}$	0.00 mm	0.00 mm	+2.16 mm
$R_{2,z}$	0.00 mm	0.00 mm	+1.31 mm
$R_{3,x}$	−10.00 mm	−10.00 mm	−10.00 mm
$R_{3,y}$	0.00 mm	0.00 mm	0.00 mm
$R_{3,z}$	0.00 mm	0.00 mm	0.00 mm

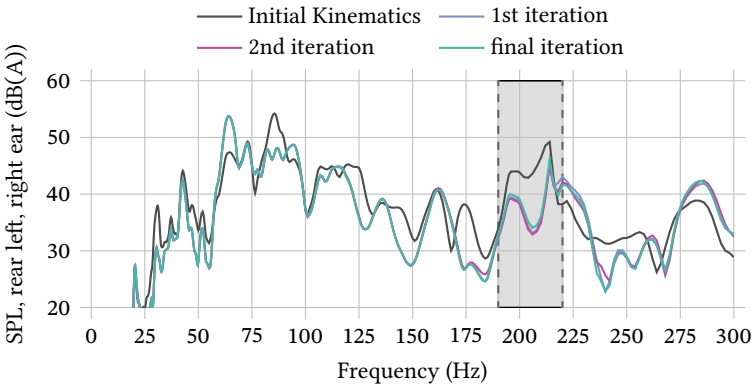

Figure 7.1: SPL for the optimization iterations towards hardware validation presented in table 7.1.

predicted optimization loss in the FE simulation. For both peaks in the cavity noise frequency range, the loss is approximately 0.5 dB(A)

The second optimization iteration using two design variables shifts both $R_{2,x}$ and $R_{3,x}$ by 10 mm in negative x-direction, towards the front of the vehicle. As this would impose a length change to the adjacent suspension links, the proposed kinematics changes are further simplified in the final iteration. Figure 5.8 hints a lower sensitivity for the $R_{2,y}$- and $R_{2,z}$-directions of the spring link wheel-side hard point R_2. Moving the kinematic hard point in these directions, compensates the length change of the spring link resulting from

moving $R_{2,x}$. This enables the usage of the original spring link in the optimized suspension kinematics.

As the track rod is used to adjust the toe, the length change can be compensated by shifting the track rod slightly on the subframe-side kinematic hard point P_3. This leaves the wheel carrier the only component to be modified. Figure 7.2 illustrates the kinematics modification in the suspension context.

The simplifications to one changed component further reduce influences added by changing component materials or manufacturing methods in the prototyping process. Figure 7.1 presents the SPL for this further simplified kinematics optimization. As indicated by the significances, the changes in the cavity noise frequency range are neglectable.

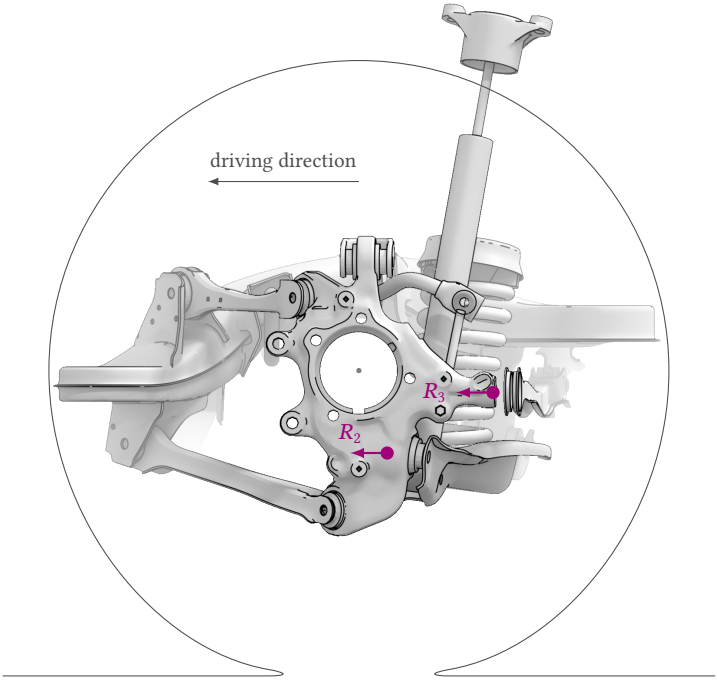

Figure 7.2: Illustration of the validation Kinematics for points $R2$ and $R3$, viewed from the left vehicle side. All other kinematic hard points remain unchanged.

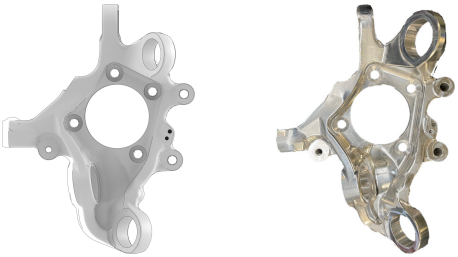

(a) Virtual modified wheel carrier. Lines indicate initial wheel carrier shape

(b) Machined modified wheel carrier.

Figure 7.3: Digital and hardware wheel carrier for the modified validation suspension kinematics.

The modified geometry of the wheel carrier is presented in fig. 7.3. Figure 7.3a presents the modification on the digital wheel carrier. The black outline represents the wheel carrier geometry used in the initial suspension kinematics, the white geometry represents the component for the modified suspension kinematics.

Figure 7.3b presents one of the two final machined wheel carrier prototypes. Compared to the morphed wheel carrier, the hardware component requires a few small changes. For example, the depth of the threaded hole for the screw fixing the track rod elastomer bushing to the wheel carrier needs to be adjusted. As the modified wheel carrier is milled from a solid block of aluminum, the material parameters differ compared to the forged series production wheel carrier. The aluminum was chosen so the Young's Modulus does not differ from the forged aluminum. This prevents a different component stiffness to interfere with the vibration transmission. As other material parameters such as the yield strength differ, an assessment of the component's endurance strength is required, though. For the required use cases some small changes are required to curve radii or the wall thickness of the bushing bore. The path from the first optimization result to the final hardware components confirm the benefit of metamodels instead of generating the one optimized result.

In order to include another development domain, first driving dynamics simulations are included in the preparation for hardware validation. This prevents

the test drivers from facing unexpected vehicle behavior on the test track. The required maneuvers do not include extreme driving maneuvers, as the comfort improvement is in focus here. Therefore, only a small set of basic driving dynamics simulations are included. Figure 7.4 presents the results. None of the calculated driving dynamics parameters differ from the initial suspension kinematics. This leads to the conclusion that the road noise optimized suspension kinematics is viable for comfort test track evaluation.

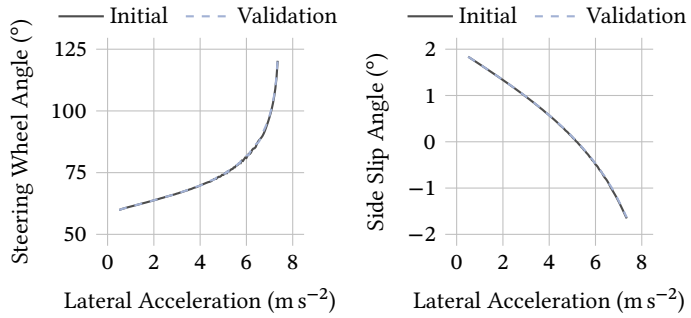

(a) Steady-state constant radius maneuver

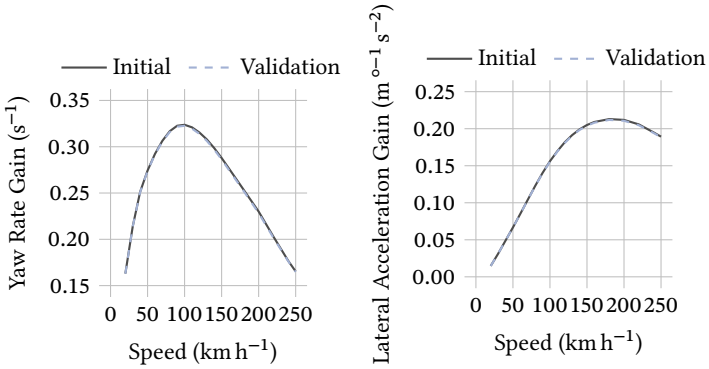

(b) Stationary gains

Figure 7.4: Driving dynamics simulation results for the final iteration of the validation suspension kinematics.

7.2 Validation Measurements

Following the vehicle under investigation for the simulation investigation, a 2021 C-Class Sedan C200 (W206) with M254 4-cylinder gasoline engine and rear wheel drive serves as the validation vehicle. According to the utilized simulation model, the vehicle is equipped with steel coil springs and no rear steering. The front tires are filled with Helium in order to shift the cavity resonance frequency. This sets the focus on the changes resulting from the changed rear suspension configuration only.

The measurements take place on the rough asphalt test track of the comfort module at the Mercedes-Benz Test and Technology Center Immendingen [Mer19]. An artificial head is placed on the rear left seating position. Before starting measurements, a subjective identification of the relevant speed range for the cavity noise phenomenon is performed. With the initial suspension kinematics, the audible tire cavity noise occurs in the speed range 60 to 100 $\mathrm{km\,h^{-1}}$. According to this, the measurement procedure is defined as a coasting measurement. The vehicle enters the test track at 100 $\mathrm{km\,h^{-1}}$ and slows down to 60 $\mathrm{km\,h^{-1}}$ in neutral position (N). Five identical measurement runs are then averaged in the resulting Power Spectral Densities (PSDs).

After the measurements with the initial suspension kinematics, the new suspension kinematics is installed by swapping the wheel carrier and adjusting spring link and track rod. After the modification, the suspension is aligned again on the test bench. The new wheel carrier is equipped with new elastomer bushings. The bushing stiffness is checked to lie in the series production tolerance range. With the modified suspension kinematics, the same measurement procedure with five measurement runs and averaging the PSDs is repeated.

7.3 Validation Measurement Results

Figure 7.5 presents both the results for the initial and the modified suspension kinematics. Figure 7.5a presents the SPL for the coasting measurement with the initial suspension kinematics. Figure 7.5b presents the results for the

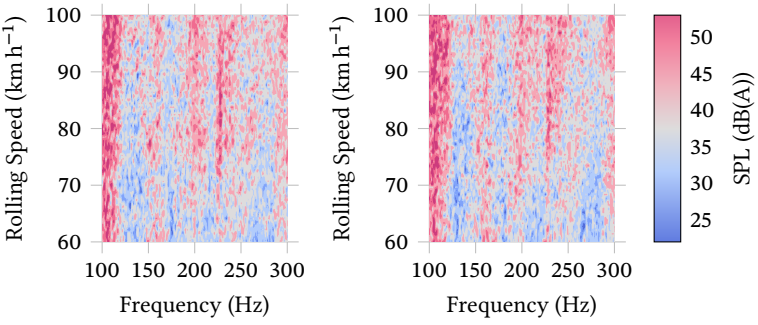

(a) Initial Suspension Kinematics. **(b)** Modified Suspension Kinematics.

Figure 7.5: Spectrographs for both suspension kinematics variations in coasting measurements from 100 to 60 km h^{-1}.

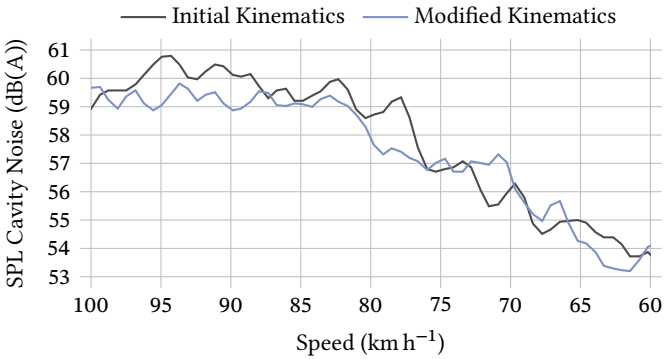

Figure 7.6: Amplitude of the cavity noise SPL for different rolling speeds resulting from coasting measurements. Modified diagram from an earlier conference paper [Wys22].

modified suspension kinematics. The cavity noise phenomenon is visible as the slightly tilted vertical line around 225 Hz.

To easier illustrate the amplitude difference of the cavity noise, fig. 7.6[a] extracts the maximum amplitude in the frequency range 200 to 240 Hz for the full speed from 100 km h^{-1} down to 60 km h^{-1}.

[a] These results were presented in an earlier conference paper [Wys22].

7.4 Discussion of the Validation Measurement Results

The measurement results from fig. 7.6 show a positive trend in wide speed ranges. Especially in the speed range above 75 km h^{-1}, the positive trend dominates. There is an amplitude reduction between 1 and 2 dB(A). This is less compared to the simulation results from fig. 7.1, nevertheless it is a perceptible difference. In the lower speed ranges the effect varies between positive and negative change. In the broad speed range between 100 and 60 km h^{-1} the effect can be classified as positive.

A single measure to improve the NVH performance often reduces amplitudes by up to 2 dB(A). As the presented optimization acts in an earlier development phase compared to classical virtual or experimental NVH measures, the possibility to improve NVH performance optimizing the suspension kinematics should be used to improve the product maturity and robustness as early as possible.

8 Generalization of the Suspension Kinematics Road Noise Optimization

The previous chapters presented dedicated simulation and optimization results and a first approach for an integrated kinematics optimization. For a holistic integration into the suspension development process, some further, general investigations need to be performed and development process integration needs to be defined.

8.1 Differentiation between Kinematics and Stiffness Changes

Previous chapters demonstrated the possibility to alter SPLs by changing suspension kinematics. This answers the first Research Question[a] partly only. The question remains, if the achieved modification is due to the kinematics changes itself, or if the changed component stiffnesses play a crucial role in the modification.

Morphing the suspension components in the suspension kinematics modification process also changes their stiffnesses. In the context of an actual suspension kinematics development process, this is the desired behavior. A proposed kinematics modification needs to be integrated into the suspension

[a] Is it possible to modify dedicated road noise phenomena by changing the location of specific kinematic hard points?

design. For that, the component designers need to alter the suspension components in order to assemble the new suspension kinematics. While doing so, the stiffness of the suspension components inevitably changes, if not compensated explicitly. Of course, the characteristics of these changes are defined by the component designers and might differ from the changes introduced by the morphing approach. Nevertheless, morphing provides a first guess and argumentation basis for real kinematics modifications.

For the investigation, whether the optimization is based on kinematics or stiffness changes, the opposite assumption is nullified. If the changes would be due to component elasticity changes only, a simulation model without component elasticities could not represent the changes in SPLs.

For this evaluation, the optimization result presented in fig. 6.5 in section 6.2.2 is evaluated. Figure 8.1 presents the hard point modifications for the optimized suspension kinematics. Using this modification, four FE simulations are compared. The SPLs for the initial and the modified suspension kinematics already exist from the optimization. Additionally, both simulation models are altered to omit the effects of changed component stiffnesses. For this, a Young's modulus of 10 000 GPa for both steel and aluminum changes the suspension components to nearly ideal stiff components. The results of these simulations are presented in fig. 8.2.

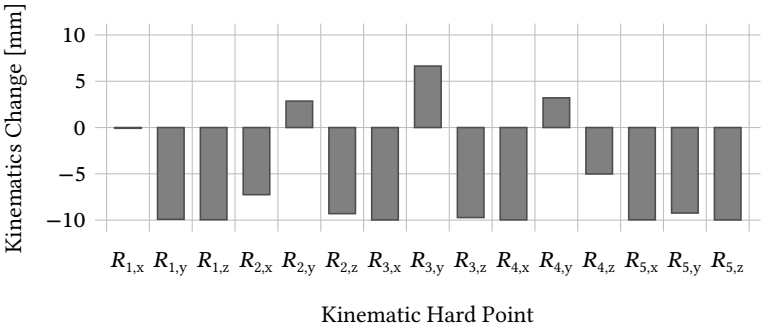

Figure 8.1: Suspension kinematics modification for the investigation of the stiffness influence compared to the kinematics influence.

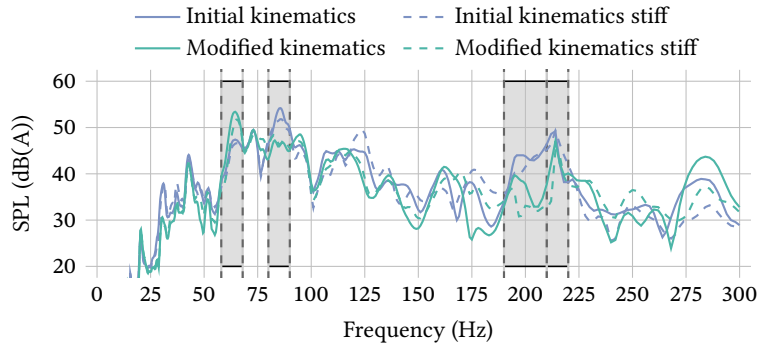

(a) SPLs for initial and modified suspension kinematics for both elastic and stiff compnent modeling.

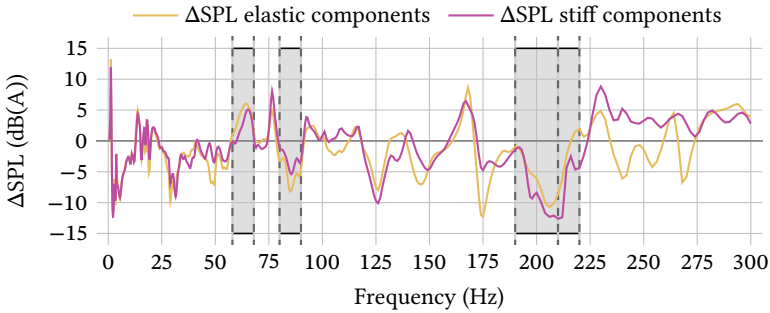

(b) Delta in SPL between initial suspension kinematics and modified suspension kinematics for both elastic and stiff component modeling.

Figure 8.2: Comparison between initial and optimized kinematics using both physically accurate elastic components and stiff components.

Figure 8.2a presents the SPL values for the four simulation results. The difference between the two Young's moduli for the initial suspension kinematics demonstrates the necessity for the evaluation using elastic components. Especially the amplitude of peaks in the SPL spectrum deviates between the two modeling approaches.

Figure 8.2b presents the differences between initial and modified suspension kinematics for both modeling approaches. The discussed optimization frequency ranges are marked in fig. 8.2b as well. If both delta curves match, the

influence of kinematics changes is due to the changed kinematics alone. Then, the changed component stiffness does not influence the effects from changing the suspension kinematics. If the two delta curves do not match, the delta between them represents the influence of the changed component stiffnesses. For example in the first selected frequency range 58 to 68 Hz, the effect with elastic components is 6.0 dB(A), whereas the effect with stiff components is 4.8 dB(A). This indicates that the kinematics changes are responsible for 4.8 dB(A), the stiffness changes for additional 1.2 dB(A). The effects due to kinematics changes are highly relevant for most of the peaks below 220 Hz in particular. Additionally, the differing delta curves confirm the necessity to model kinematics changes by morphing suspension components instead of rigid body elements. From around 215 Hz the elastic effects start to dominate.

The simulation example shows large effects in the SPLs for wide frequency ranges with stiff suspension components. This disproves the hypothesis that changes in SPLs are solely due to changes in component stiffnesses.

The investigation indicates possible road noise modification by changing suspension kinematics up to the cavity noise frequency range. Above, kinematics modifications can still be beneficial to road noise perfomance, the underlying physical principle changes, though.

8.1.1 General Effects in the Suspension Vibration System

All previous chapters and sections proposed a methodology to create suspension kinematics modifications, enabeling targeted modification of specific road noise phenomena. The design rules and numeric optimizations originating from the metamodels only provided the hints, what to change, but omitted the question, why the kinematics changes modify SPLs as they do.

The resulting effects in the subsystem suspension were investigated in detail in an earlier publication [Wys20a]. In this publication, the force transfer through a trapezoidal rear suspension was under investigation. Changing the location of the kinematic hard point between the track rod and the wheel

carrier by 10 mm in positive x-direction[a], caused a remarkable effect in the transfer functions. All transferred forces below 88 Hz were reduced, while all transferred forces above 88 Hz were increased.

An analytical investigation leads to the hypothesis that a changed steering eigenmode in the suspension vibration system could lead to the observed effect. A Modal Assurance Criterion (MAC)-based eigenmode-tracking investigation endorsed this hypothesis. Figure 8.3 illustrates the tracked eigenmodes of the subsystem suspension.

Each dot on the upper row represents an eigenmode frequency of the initial suspension kinematics. The connected dots on the lower row indicate the frequency of the same eigenmode on the modified suspension kinematics. Clearly visible is exactly one eigenmode—it is the steering-eigenmode—changing its eigenfrequency drastically from 86.7 Hz up to 89.3 Hz. The frequency of the observed force shifting phenomena lies exactly in between, at 88 Hz and was explained by Equation 13 in the previous publication [Wys20a].

This investigation shows that changing the suspension kinematics can change the vibration system suspension locally. With that behavior, changing the suspension kinematics enters the regular tool belt of road noise optimization. Like changing component stiffnesses or elastomer element properties, changing the suspension kinematics modifies the vibration system suspension and

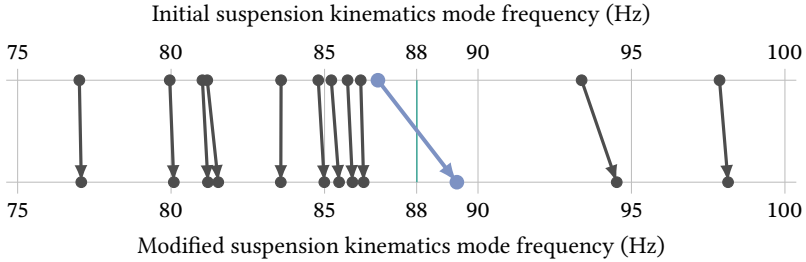

Figure 8.3: Eigenmode-tracking for a trapezoidal rear suspension for a kinematics modification on one kinematic hard point. Reduced figure from an earlier publication [Wys20a].

[a] The same coordinate system was used, as in the present investigation. The positive x-direction points backwards, when looking in driving direction

therefore modifies the transfer path and ultimately the road noise inside the vehicle. In contrast to the other mentioned measures, modifying the suspension kinematics is placed at an earlier development phase, though.

8.2 Transfer into Series Development

Up to this point, this research presents investigation results regarding a five link rear suspension. Additionally, a previous publication used a trapezoidal rear suspension for the prove of concept [Wys20a]. All these results can be seen as fundamental research, mostly done on a finished suspension. For a holistic and sustainable success of NVH kinematics optimization, an integration into the suspension development process needs to be established. Such a process has to be suitable for different suspension types and development phases.

8.2.1 Additional Suspension Topologies

Additionally to the investigated five link rear suspension and trapezoidal rear suspension the methodology has to be easily and fast applicable into the suspension development process. For this, the process has been under investigation for additional five link rear suspensions and three link front suspensions.

The additional five link rear suspensions—the dominating rear suspension topology at Mercedes-Benz—proved the process to be fast applicable to new FE models. The three link front suspension uncovered additional challenges when changing the suspension kinematics for NVH purposes. The reduced number of DOFs combined with additional requirements for the steering makes the kinematics modification much harder compared to the five link rear suspension. There were less DOFs for the optimization due to the fewer suspension links, while having less DOFs for greater kinematics compensations.

None of the investigated suspension concepts revealed a showstopper for the application of the process, though. This encouraged the development of a series integration process for future suspension development projects.

8.2.2 Integration into the Development Process

Compared to the fundamental investigation presented previously, NVH optimization of suspension kinematics requires much more additional requirements and restrictions. Instead of optimizing one seating position, series development requires consideration of all seating and ear positions in the car. This may go up to 14 SPL curves for seven seating positions in large Sport Utility Vehicles (SUVs), instead of one. As previously mentioned, this is usually approached using maximum metrics reducing the highest SPL for each frequency band. As presented in the optimization examples, the development has to focus on multiple frequency ranges at once. Additionally, the design space is significantly decreased. Besides obvious package restrictions like component intersections, assembly restrictions like tool accessibility needs to be considered as well. If all these requirements and restrictions are fulfilled, all development domains still need to approve the kinematics modification.

The series development follows the DPT process, described in section 2.3.4. Each development loop contains its own V-Model development cycle transferring the development from the starting state to the final state of each loop. Included into this V-Model, another V-Model inspired process is introduced to implement the kinematics optimization into the series development process. Figure 8.4 presents the established process for systematic kinematics optimization regarding road noise.

The presented V-Model process can be integrated into each DPT loop. The kinematics optimization process starts with the most recent FE model on the top left defining the optimization system. The optimum stage of the development depends on the required changes to the kinematics development. In the early concept phase, the suspension topology and configuration change a lot. Even when for example the decision between pull rod or push rod suspension is set, the kinematics changes can be magnitudes larger, compared to the evaluated optimization kinematics changes. Therefore, the main optimization process should not start too early. On the other side, too late changes are impossible to integrate into the development process. This could be the case, if for example

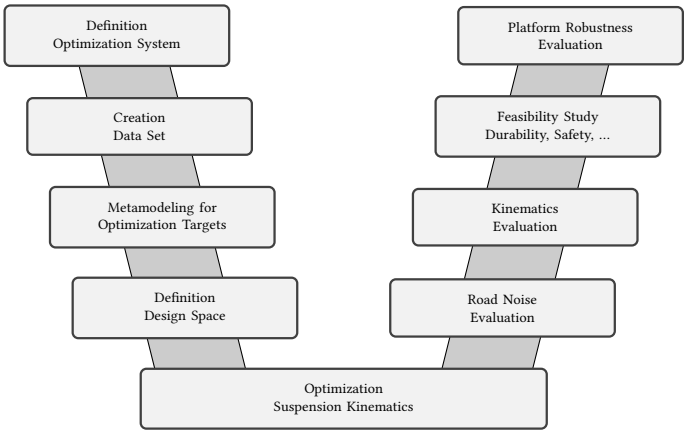

Figure 8.4: V-Model for the series integration of kinematics changes.

tools for the suspension components are already specified or even ordered and in the manufacturing process.

The most recent development state, containing NVH and other simulation models, is the base for the metamodel creation. The creation of the DoE can already contain strict package restrictions like for example an intersection with the wheel. For smaller changes in the final kinematics defining development phase, a DoE of ± 15 mm proved effective. With all direct suspension link kinematic hard points in the DoE, this results in 30 design variables for a five link rear suspension. A data set of 1000 samples provides very good metamodel prediction quality.

With the metamodels created, the next step is performed together with the suspension development department. The sensitivities and general tendencies originating from the metamodels are compared with detailed package and assembly restrictions for each kinematic hard point coordinate. This results in a smaller approved design space for the kinematics optimization.

Using this design space, the NVH performance optimization is performed containing as few kinematics changes, as possible. This includes combining seating and ear positions, as well as different road noise phenomena. With these ideal optimization results, kinematics compensation is performed in the

next step. The relevant deviations in suspension parameters are compensated using the NVH independent kinematic hard point coordinates. This results in a compensated kinematics modification proposal. If this proposal still fulfills the desired NVH benefits, the process can enter a feasibility study. This includes—but is not restricted to—durability, ride, handling, safety, packaging, assembly, and NVH again. The investigation should include evaluation of different vehicle derivatives of the same platform, if they use the same suspension as the optimized one. In theory, all these evaluations could be included into the initial metamodel creation. For testing purposes, this was successfully evaluated using a buckling load case for durability evaluation.

If the proposed suspension kinematics does not affect any other development domain, or the advantages outweigh the disadvantages, the new suspension kinematics can be implemented.

8.2.3 Robustness Regarding Platform Development

In the previous section, the required feasibility investigation regarding the NVH performance in additional vehicle derivatives was mentioned. In the last investigation of this work, the necessity of this investigation shall be elaborated.

In the early development stages, usually only the lead car—the first derivative on a newly developed platform—is under development. Additional derivatives emerge over time forming the platform family. If the derivatives base on the same platform, they often share the same suspension concept with no or only small modifications. Nevertheless, the NVH comfort needs to be ensured for all these derivatives.

Additional variance occurs for different road noise phenomena and driving situations. Passengers experience NVH comfort not only at one moment in time, but integrate the perception over different driving states [Mat14]. This requires additional robustness in the NVH development.

Here, the performance of a developed kinematics optimization is under investigation for a full platform family and differing excitation. This includes

robustness investigation for variance in vehicle type and road excitation. The suspension kinematics of the lead car is optimized for a better road noise performance in the cavity noise frequency range. The optimization is performed using a maximum metric for all seating positions in the car. As the front seats receive the higher SPLs in the selected frequency range, the optimization mainly reduces those SPLs. The optimization is performed on the lead car of the platform. In fig. 8.5 this vehicle's optimization is marked as *B1–A*, which stands for Battery Electric Vehicle (BEV) with body shape 1. The *A* stands for one specific modal tire excitation model. In the figure, the position of the center of the ring represents the original maximum SPL of all seating positions and the delta of the maximum metric between initial and modified suspension kinematics. The SPL of the optimization car *B1–A* was reduced by 1.4 dB(A) at an original SPL of 48.5 dB(A). The four inner shapes represent the modification in SPL for the four seating positions with driving direction

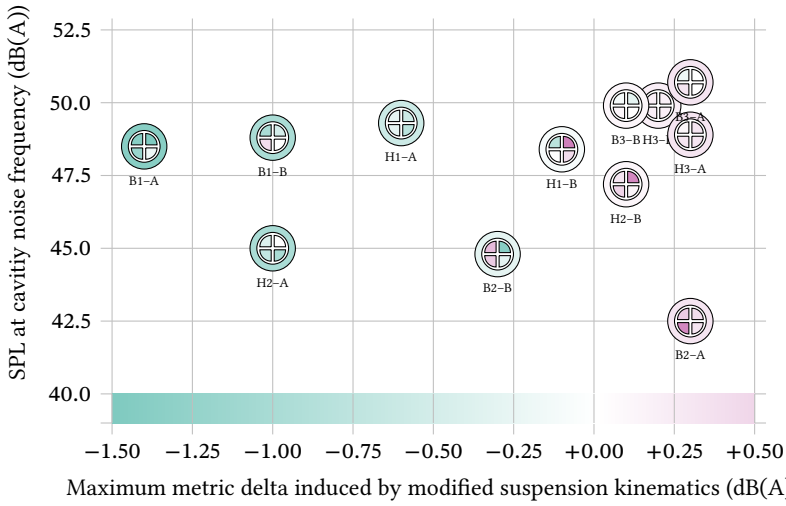

Figure 8.5: Results of the robustness investigation for three different vehicle derivatives (*1* to *3*) as BEV (*B*) or Hybrid Electric Vehicle (HEV) (*H*) and two different modal tire models (*A* and *B*). The colorbar represents the abscissa value for both maximum metric delta and individual seating position deltas. The symbols are positioned on the abscissa following their maximum metric delta value, indicated also by the outer ring. The inner four shapes represent the amplitude values at the four seating positions with driving direction upwards.

upwards. For the optimization vehicle this shows an improvement on all four seating positions with less improvement on the rear right.

All other derivatives of the platform are also marked in fig. 8.5. The naming scheme is *B* and *H* for BEV and HEV respectively, three different body shapes including a coupé and an SUV, indicated by the numbers *1* to *3* and finally the letter *A* or *B* for two different modal tire excitations. The different tire models represent different tire dimensions, which shift the frequency of the cavity noise. This ensures a robustness for not only different tire dimensions, but also different driving speeds, as the cavity noise frequency changes with the driving speed [Gen10, San02].

The 12 different vehicle combinations show a mixed performance of the optimized suspension kinematics. For 6 variants the effect is positive, for the other 6 the effect is negative. Nevertheless, the positive effect of −1.4 dB(A) in the maximum metric is much larger, compared to the 0.3 dB(A) deterioration on the right side of the figure.

The robustness analysis shows the difficulty to optimize a full vehicle portfolio sharing one suspension kinematics. Especially in the early development phases, where only the lead car is under development, optimization has to find a way, to consider upcoming derivatives. In the series development process the platform simulation results were considered positive, as modifications less than 0.3 dB(A) are insignificant as it is below the digital prognosis tolerance.

The optimization was performed following the V-Model methodology presented in section 8.2.2. The required feasibility study considered the kinematics modification suitable regarding durability, assembly, ride, handling, and other development domains. The kinematics compensation successfully reverted all unwanted changes to the suspension parameters, proving the possibility to include suspension kinematics modifications for NVH optimization into the series development process.

9 Conclusion and Outlook

Recent trends in the automotive industry impose new challenges to road noise and suspension development. On the one hand, electrification changes the composition of vehicle interior noise. On the other hand, reduced engine noise enhances the perception of road noise, especially in the speed range up to $100\,\mathrm{km\,h^{-1}}$. For comfort-oriented vehicles in particular, this requires additional effort to reduce road noise. With CO_2 reduction being one of society's most demanding challenges, weight intensive NVH measures are costly on different levels. Additionally to changing noise sources, automation shifts the passenger focus at least temporarily away from driving to alternative activities. In these situations, this increases the demand for comfort over perceivable driving dynamics, changing the requirements to vehicle feedback via the suspension. New vehicle concepts like people movers introduce completely changed requirements and boundary conditions to the suspension. This includes wheel modules, new space concepts or even exchangeable bodies. The drastically changing boundary conditions require fast tools to create and evaluate new solutions in the suspension development.

9.1 Conclusion

The investigation of the research hypothesis *Small changes in suspension kinematics enable the optimization of specific road noise phenomena in an early development phase* was separated into four main research questions.

Is it possible to modify dedicated road noise phenomena by changing the location of specific kinematic hard points?

In order to identify the potential of suspension kinematics modifications to change dedicated road noise phenomena, a data set consisting of 500 samples with modified suspension kinematics was created. The locations of the five kinematic hard points connecting the wheel carrier to the suspension links were used as design variables. The Latin Hypercube based data set contained FE road noise simulation results and suspension parameters for each sample.

Selecting designs from the data set indicated the possibility to find suspension kinematics modifying dedicated road noise phenomena. A sensitivity analysis showed that few specific kinematic hard point directions are sensitive to dedicated road noise phenomena.

ANN metamodels describing the connections between kinematic hard point locations and road noise frequency ranges were created. These metamodels provided insights into optimization potential and target conflicts regarding different road noise phenomena. Different application examples showed the potential to optimize specific road noise phenomena and to resolve target conflicts in between different phenomena. Optimization simplifications showed the possibility to reduce the number of design variables, enabling the remaining design variables to compensate undesired suspension parameter changes. A hardware validation in a full vehicle using a road noise optimized suspension kinematics confirmed a positive effect in testing.

Further investigations divided the positive effects to road noise phenomena between effects based solely on the suspension kinematics changes and effects based on component stiffness changes due to the changed component shapes. The investigation showed significant kinematics effects up to the cavity noise frequency range around 215 Hz. Above, elastic effects start increasing.

Investigations in an earlier publication [Wys20a] indicated modification of specific eigenmodes in the suspension leading to a changed transfer path through the suspension. Like most classical NVH measures, changing the suspension kinematics therefore changes the transfer path, resulting in dedicated changes in road noise phenomena.

How can modified suspension kinematics be easily and quickly applied to road noise simulation models, enabling a systematic investigation of the correlations between suspension kinematics and road noise phenomena?

As the suspension kinematics definition takes place in an early development phase, there is no hardware available yet. Therefore, the investigation of both road noise and suspension parameters need to take place in the digital world.

Changing suspension kinematics in the suspension parameter calculation is easily possible, as only the location of the kinematic hard points is considered. For the adaption of road noise simulation models, FE simulation models needed modification. The investigated suspension kinematics modifications affect the wheel carrier and the suspension links. Applying the kinematics modifications to the simulation model via MPCs is not possible, since this connection methodology does not consider geometrical changes of lever arms. Using RBEs changes the load case to the suspension links, which makes them unfavorable as well. Changing the actual component shape is required to adequately model kinematics changes.

The suspension components are of varying complexity, making different approaches for changing their shape possible. Slim components such as most suspension links can be simplified into parametric beam formulations. This enables easy shape modifications. For the more complex components, a morphing approach was chosen. The main requirement to this approach was fast and easy application to new kinematics investigations in order to enable later deployment into the development process. Only FE representations of the components $\mathbf{x}_{\mathrm{FE}}$, the location of the kinematic hard points $\mathbf{x}_{\mathrm{c}}$ and their modification displacements $\mathbf{v}_{\mathrm{c}}$, and coordinates of fixed points $\mathbf{x}_{\mathrm{f}}$ are required. An interpolation algorithm calculates the displacement for each FE node changing the component shapes to the new suspension kinematics.

Changing the suspension kinematics by morphing suspension components restricts the investigation to small kinematics changes in the range of few millimeters. Here, $\pm 10\,\mathrm{mm}$ were investigated, which reduced mesh quality deterioration to a minimum. To ensure no simulation artefacts occur in the data set, the mesh quality is checked for each processed sample. The restriction

to small kinematics changes excludes suspension topology and configuration investigations, which were not in scope for this investigation.

The created data set includes data regarding SPLs at each ear position in the vehicle for the full simulation frequency range and the suspension parameters. Using this approach, the definition of optimization targets, for example specific road noise phenomena, can be determined after creating the data set. This makes the approach suitable for fast changing boundary conditions and requirements without recreating a new data set.

How could a modified suspension kinematics be evaluated regarding different development domain requirements?

For the road noise investigation, picking dedicated frequency ranges corresponding to road noise phenomena and creating prediction metamodels for them proved beneficial. Each metamodel predicts the correlations between kinematic hard point locations and a single frequency range of a single ear position. With 15 design variables for each metamodel, their intuitive interpretation proves difficult. Both numerical evaluation and graphical representation was considered. The graphical representations in particular required simplification for visualization, but were nevertheless able to provide suitable optimization potential. This evaluation provided the possibility to extract road noise design rules from the metamodels. The creation of metamodels for the direct connection between suspension parameters and road noise phenomena showed low correlations. These low correlations hint the possibility, to modify road noise phenomena by modifying kinematic hard point locations independently from changing suspension parameters.

Besides road noise phenomena, metamodels for basic suspension parameters were created as well. Normalization of the suspension parameters enabled the creation of a cost function, including suspension parameter boundary conditions into the kinematics evaluation. Weighting selected suspension parameters differently even opened the possibility to optimize dedicated road noise phenomena under consideration of dedicated suspension parameter deviation restrictions.

The investigation indicated separate metamodels for each frequency range and suspension parameter as promising. This way, the weighting can be changed in hindsight and the overall prediction quality is much higher when combined to a cost function afterwards. As there are frequency ranges correlating negatively, their effects could not be handled by one single metamodel when combining the values beforehand.

The metamodels for different frequency ranges and suspension parameters can be utilized in numeric suspension kinematics optimization or in qualitative design rule extraction. The latter enables a holistic suspension kinematics optimization, as the design rules can be shared with other suspension development domains. For that, the data set should contain as much information as possible, but ultimately the optimization has to be performed in close contact with all development domains. It would be difficult to include the boundary conditions and requirements for all development domains into a single optimization target, for a numerical suspension kinematics optimization.

Do suspension kinematics optima exist for road noise and how can such optima be integrated into the development process?

The small changes in suspension kinematics under investigation are small enough to ensure suitable FE prediction quality and large enough to cover kinematics modifications present in early suspension development phases between the early concept phase, when suspension topology and configuration are determined, and the phase when the suspension kinematics is completely fixed. In these phases in between, the different suspension development domains, for example ride, handling, durability, and safety determine the final suspension kinematics by applying small changes to the kinematics. With the presented methodology NVH optimization can be included in these development phases.

Optimization examples were presented, combining road noise optimization with suspension parameter requirements. For one specific example, a design rule based road noise optimization was performed changing only two kinematic hard points. The selected modifications were then discussed with different development domains like for example packaging, durability and handling. With small compensation measures, the optimized suspension kinematics

was suitable to be tested in hardware. The hardware validation confirmed a positive effect for wide speed ranges.

The example showed the suitability of extracting road noise design rules from metamodels. These design rules proved more valuable than finding a single numerically optimized suspension kinematics, as it never includes all the requirements from different development domains.

The requirement of compensating malicious effects introduced by the road noise optimization showed the necessary limitation to as few changed design variables as possible. Due to this requirement, suspension concepts using less kinematic hard points, for example a three link suspension, appear less suitable for the method, compared to a five link suspension. For simpler integration of the proposed changes, insensitive design variables should be used to minimize changes. For example, a length change of a suspension link requiring a modified component shape could be prevented by introducing additional length compensating kinematics changes.

In the real development process, the optimization should include not only a single, but all relevant ear positions and a combination of selected road noise phenomena. While committing to a modified suspension kinematics, a feasibility study by all affected development domains should be included in the process. This includes robustness analyses regarding road noise for all vehicle variations using the same suspension or at least the same suspension kinematics. The holistic optimization process was tested successfully using visual metamodel representations and multiple compensation iterations, increasing the product maturity in an early development phase. This enables the introduction of NVH optimization in an earlier development phase than previously possible.

9.2 Outlook

The optimization examples provided in this investigation confirmed the research hypothesis[a] and showed the potential in optimizing dedicated road noise phenomena by applying small changes to the suspension kinematics. The process should be included into a holistic suspension development process, increasing NVH maturity in an early development phase.

Especially the combination of classical NVH measures and suspension kinematics optimization could further increase the vehicle road noise comfort. Suspension kinematics modification offers an optimization opportunity, which is independent to ageing and changing temperatures. The suspension kinematics stays constant for the full vehicle life cycle, making the optimization approach lasting and sustainable.

Even though a proof of concept was provided and an optimization using the proposed methodology is possible, there is still potential for improvement. In hindsight, the data set should include more samples in order to create better performing metamodels. In a first investigation for a different suspension, increasing the sample number from 500 to 1500 proved effective. Adjusting the properties of the metamodels could also lead to better performing predictions. The investigation showed nevertheless that the combination of simple metamodels and verification simulations can create design rules and direct road noise optimization.

Increasing the morphing accuracy in combination with parallelization keeps the time investment constant, while improving the prediction quality. In general, the morphing process could benefit from further improvement in both accuracy and speed. The approach of providing as little input as possible should be retained, though.

In order to make the optimization process more holistic, metamodels for different development domains could be included as well. This enables a

[a] Small changes in suspension kinematics enable the optimization of specific road noise phenomena in an early development phase.

fast optimization process, where different development domains are able to interactively optimize the suspension kinematics. The same applies for the utilized road noise metamodels. Including additional frequency ranges, ear positions, and even body variants could make the optimization more holistic. Especially the consideration of different vehicles utilizing the same suspension or suspension kinematics is required for road noise optimized suspension kinematics without unrecognized malicious effects.

As the process is based on scalar inputs only, an advancement to other optimization design variables may be possible. This may include elastomer element properties or body parameters. Creating design rules for these additional parameters could improve NVH optimization or robustness investigations.

Using the kinematic hard point locations as statistical distributions, an investigation of manufacturing process influences on specific road noise phenomena could be performed. Using this approach, a robust road noise performance could form a new optimization target.

Applying the approach over a larger period of time creates a database of suspension components. Using this database could also enable the investigation of larger kinematics modifications and even include suspension configuration or suspension topology investigations. Adding different vehicle bodies could identify and increase the robustness for suspension kinematics optimizations in development phases, when not all vehicle variations are available yet.

Using systematic kinematics optimization with reduced road noise becoming part of the suspension kinematics development could increase the general acoustic vehicle comfort in the future. With an improved NVH base system in the early phase, an overall improvement is expected. Should a target conflict between driving dynamics and driving comfort occur, active systems could switch between different suspension kinematics, as today's switching component properties.

Bibliography

[2ge19] 2getthere: 2getthere's Self-driving people mover makes its maiden trip at brussels airport. 2019. URL: https://www.2getthere.eu/news/maiden-trip-at-brussels-airport/ (visited on 02/22/2021) (cit. on p. 5).

[2ge20] 2getthere: Vehicle Types Archives - 2getthere. 2020. URL: https://www.2getthere.eu/technology/vehicle-types/ (visited on 02/22/2021) (cit. on p. 5).

[Abe17] Abel, H.; Clauß, R.; Wagner, A. and Prokop, G.: "Analytical extension of the effective axle characteristics concept for the development of a structured chassis design process". In: *Vehicle System Dynamics* 55.9 (2017), pp. 1297–1320. DOI: 10.1080/00423114.2017.1309055 (cit. on p. 14).

[Ace21] Acerbi, M.; Malvermi, R.; Pezzoli, M.; Antonacci, F.; Sarti, A. and Corradi, R.: "Interpolation of Irregularly Sampled Frequency Response Functions Using Convolutional Neural Networks". In: *IEEE International Conference on Acoustics, Speech and Signal Processing (ICASSP)*. IEEE, 2021, pp. 950–954. DOI: 10.1109/ICASSP39728.2021.9413458 (cit. on p. 93).

[Ale02] Alexa, Marc: "Recent Advances in Mesh Morphing". In: *Computer Graphics Forum* 21.2 (2002), pp. 173–198. DOI: 10.1111/1467-8659.00575 (cit. on p. 63).

[Aly12] Alyaqout, S. F.; Papalambros, P. Y. and Ulsoy, A. Galip: "Combined design and robust control of a vehicle passive/active suspension". In: *International Journal of Vehicle Design* 59.4 (2012), p. 315. DOI: 10.1504/IJVD.2012.048975 (cit. on pp. 18, 19).

[Ans21] Ansys: Ansys optiSLang. 2021. URL: https://www.ansys.com/products/platform/ansys-optislang (visited on 03/11/2021) (cit. on pp. 93, 94).

[Ara15a] Arana, Carlos: "Active Variable Geometry Suspension for Cars". Dissertation. London, UK: Imperial College, 2015 (cit. on pp. 5, 18, 25).

[Ara15b] Arana, Carlos; Evangelou, Simos and Dini, Daniele: "Series Active Variable Geometry Suspension for Road Vehicles". In: *IEEE/ASME Transactions on Mechatronics* 20.1 (2015), pp. 361–372. DOI: 10.1109/TMECH.2014.2324013 (cit. on pp. 19, 25).

[Ara17] Arana, Carlos; Evangelou, Simos A. and Dini, Daniele: "Series Active Variable Geometry Suspension application to comfort enhancement". In: *Control Engineering Practice* 59 (2017), pp. 111–126. DOI: 10.1016/j.conengprac.2016.11.011. URL: https://www.sciencedirect.com/science/article/pii/S096706611630260X (cit. on p. 25).

[Auw07] Auweraer, H. van der; Langenhove, T. van; Brughmans, M.; Bosmans, I.; Masri, N. and Donders, Stijn: "Application of mesh morphing technology in the concept phase of vehicle development". In: *International Journal of Vehicle Design* 43.1-4 (2007), pp. 281–305. DOI: 10.1504/IJVD.2007.012308 (cit. on pp. 14, 60, 63–65, 74, 76, 78).

[Bac20] Backhaus, Richard: "Automatic Shuttle Buses - From the Test Track to Scheduled Services". In: *ATZ worldwide* 122.11 (2020), pp. 8–13. DOI: 10.1007/s38311-020-0321-y (cit. on p. 5).

[Bak87] Bakker, Egbert; Nyborg, Lars and Pacejka, Hans B.: "Tyre Modelling for Use in Vehicle Dynamics Studies". In: SAE International, 1987. DOI: 10.4271/870421 (cit. on p. 50).

[Bak89] Bakker, Egbert; Pacejka, Hans B. and Lidner, Lars: "A New Tire Model with an Application in Vehicle Dynamics Studies". In: SAE International, 1989. DOI: 10.4271/890087 (cit. on p. 50).

[Bal15] Balasubramanian, Murali and Shaik, Ahmed: "Optimizing Body Panels for NVH Performance". In: *SAE International Journal of Passenger Cars - Mechanical Systems* 8.3 (2015), pp. 948–955. doi: 10.4271/2015-01-2265 (cit. on p. 63).

[Ber14] Berger, Frank and Krimmel, Horst: "Active Rear Axle Kinematics for Cars". In: *ATZ worldwide* 116.6 (2014), pp. 4–7. doi: 10.1007/s38311-014-0186-z (cit. on p. 25).

[BET22a] BETA CAE Systems: ANSA version 22.1.x User Guide. Luzern, Switzerland, 2022 (cit. on p. 75).

[BET22b] BETA CAE Systems USA, Inc.: Morphing. 2022. url: https://www.ansa-usa.com/solutions/morphing/ (visited on 08/18/2022) (cit. on p. 64).

[Bin14] Bindauf, Axel; Angrick, Christian and Prokop, Günther: "Suspension Characterisation on a Highly Dynamic Axle Test Rig". In: *ATZ worldwide* 116.12 (2014), pp. 48–53. doi: 10.1007/s38311-014-0255-3 (cit. on pp. 14, 17, 52).

[Boh20] Bohrmann, Dominique; Koch, T.; Maier, C.; Just, W. and Bengler, K.: "Motion Comfort - Human Factors of Automated Driving". In: *Proceedings of the 29th Aachen Colloquium of Sustainable Mobility 2020.* 2020, pp. 1697–1708 (cit. on pp. 5, 6).

[Bot08] Botev, Stefan: "Digitale Gesamtfahrzeugabstimmung für Ride und Handling". Dissertation. Düsseldorf: TU Berlin, 2008 (cit. on pp. 6, 15, 18, 19).

[Bre11] Brembeck, Jonathan; Ho, Lok Man; Schaub, Alexander; Satzger, Clemens; Tobolar, Jakub; Bals, Johann and Hirzinger, Gerhard: "ROMO - The Robotic Electric Vehicle". In: *22nd IAVSD International Symposium on Dynamics of Vehicle on Roads and Tracks.* 2011. url: https://www.researchgate.net/publication/225022186 (visited on 10/21/2019) (cit. on p. 6).

[Bru18] Brune, Alexander; Weber Martins, Thiago and Anderl, Reiner: "Morphing boxes for the integration of shape optimization in the product design process". In: *Computer-Aided Design & Applications* 15.2 (2018), pp. 219–226. doi: 10.1080/16864360.2017.1375672 (cit. on p. 63).

[Bus21] Busch, Ingo; Lehmann, Ralf; Sickinger, Philipp; Herkenrath, Dirk and Kortenbruck, Julius: Suspension Kinematics Validation Project. 2021 (cit. on p. 123).

[Büt20] Büttner, Jana; Schwarz, Stefan and Schumacher, Axel: "Reduction of the Numerical Resource Requirements for Multidisciplinary Optimization". In: *ATZelectronics worldwide* 15.12 (2020), pp. 52–57. doi: 10.1007/s38314-020-0284-1 (cit. on pp. 60, 61, 64).

[Büt21] Büttner, Jana; Schwarz, Stefan; Schumacher, Axel and Bäck, Thomas: "Global Sensitivity Matrix for Vehicle Development". In: *ATZ worldwide* 123.3 (2021), pp. 26–31. doi: 10.1007/s38311-020-0630-1 (cit. on pp. 18, 35, 93).

[Cal18] Calì, M.; Oliveri, S. M.; Evangelos Biancolini, M. and Sequenzia, G.: "An Integrated Approach for Shape Optimization with Mesh-Morphing". In: *Advances on Mechanics, Design Engineering and Manufacturing II*. Ed. by Cavas-Martínez, Francisco; Eynard, Benoit; Fernández Cañavate, Francisco J.; Fernández-Pacheco, Daniel G.; Morer, Paz and Nigrelli, Vincenzo. Cham: Springer, 2018, pp. 311–322. doi: 10.1007/978-3-030-12346-8_31 (cit. on p. 63).

[Cao11] Cao, Dongpu; Song, Xubin and Ahmadian, Mehdi: "Editors' perspectives: road vehicle suspension design, dynamics, and control". In: *Vehicle System Dynamics* 49.1-2 (2011), pp. 3–28. doi: 10.1080/00423114.2010.532223 (cit. on pp. 7, 15, 19).

[Cha06] Chatillon, M. M.; Jezequel, L.; Coutant, P. and Baggio, P.: "Hierarchical optimisation of the design parameters of a vehicle suspension system". In: *Vehicle System Dynamics* 44.11 (2006), pp. 817–839. doi: 10.1080/00423110500497918 (cit. on pp. 16, 21).

[Cha19] Chahkar, Jason: "Automated construction of suspension axle part geometries for FE-simulations, focusing especially on the NVH-analysis". Master Thesis. Karlsruhe: Karlsruhe Institute of Technology, 2019 (cit. on p. 59).

[Che09] Chen, Michael Z.Q.; Papageorgiou, Christos; Scheibe, Frank; Wang, Fu-cheng and Smith, Malcolm C.: "The missing mechanical circuit element". In: *IEEE Circuits and Systems Magazine* 9.1 (2009), pp. 10–26. doi: 10.1109/MCAS.2008.931738 (cit. on p. 18).

[Chi18] Chilès, Jean-Paul and Desassis, Nicolas: "Fifty Years of Kriging". In: *Handbook of Mathematical Geosciences: Fifty Years of IAMG*. Ed. by Daya Sagar, B. S.; Cheng, Qiuming and Agterberg, Frits. Cham: Springer International Publishing, 2018, pp. 589–612. doi: 10.1007/978-3-319-78999-6_29 (cit. on p. 93).

[Cla22] Claus, Felix; Hamann, Bernd and Hagen, Hans: "A finite-element based mesh morphing approach for surface meshes". In: *Computer-Aided Design* 146 (2022). doi: 10.1016/j.cad.2022.103232 (cit. on p. 63).

[Con21] Conzade, Julian; Cornet, Andreas; Hertzke, Patrick; Hensley, Russell; Heuss, Ruth; Möller, Timo; Schaufuss, Patrick; Schenk, Stephanie; Tschiesner, Andreas and von Laufenberg, Karsten: Why the automotive future is electric. 2021. url: https://www.mckinsey.com/industries/automotive-and-assembly/our-insights/why-the-automotive-future-is-electric (visited on 05/09/2022) (cit. on p. 3).

[cos] cosin scientific software: FTire (Flexible Structure Tire Model). url: https://www.cosin.eu/ (visited on 04/28/2022) (cit. on p. 50).

[Cun22] Cunha, Barbara Zaparoli; DROZ, Christophe; Foulard, Stéphane; Ichchou, Mohamed and Zine, Abdelmalek: A Review of Machine Learning Methods Applied to Structural Dynamics and Vibroacoustic. 2022. doi: 10.13140/RG.2.2.14381.97760/1. url: https://hal.archives-ouvertes.fr/hal-03563614 (cit. on p. 93).

[Cyt18] Cytrynski, Stefan; Neerpasch, Uwe; Bellmann, Richard and Danner, Bernd: "The Active Suspension of the New Mercedes-Benz GLE". In: *ATZ worldwide* 120.12 (2018), pp. 42–45. doi: 10.1007/s38311-018-0172-y (cit. on p. 19).

[Dou06] Douville, H.; Masson, P. and Berry, A.: "On-resonance transmissibility methodology for quantifying the structure-borne road noise of an automotive suspension assembly". In: *Applied Acoustics* 67.4 (2006), pp. 358–382. url: https://sed.cir-mcs.e.corpintra.net/science/article/pii/S0003682X05001040 (visited on 10/15/2019) (cit. on p. 53).

[Dro15] Drotar, Timothy; Palandri, Jacopo; Wolf-Monheim, Friedrich; Zandbergen, Paul and Reff, Bjoern: "CAE-Based Driving Comfort Optimization of Passenger Cars". In: *SAE International Journal of Passenger Cars - Mechanical Systems* 8.2 (2015), pp. 703–710. doi: 10.4271/2015-01-1583 (cit. on pp. 2, 24).

[Dyn20] Dynardo GmbH: Methods for multi-disciplinary optimization and robustness analysis: optiSLang documentation. Weimar, 2020 (cit. on pp. 82, 83).

[Ede15] Eder, Torsten: "Frontloading in der Antriebsstrangentwicklung". In: *MTZ - Motortechnische Zeitschrift* 76.9 (2015), p. 82. doi: 10.1007/s35146-015-0097-6 (cit. on pp. 1, 19).

[Eis08] Eisele, Georg; Wolff, Klaus; Dohm, Marcus; Abtahi, Roozbeh and Hüser, Michael: "Chassis noise optimisation". In: *ATZ worldwide* 110.3 (2008), pp. 52–56. doi: 10.1007/BF03224995 (cit. on pp. 51, 53).

[Elb09] Elbers, Christoph; Bäumer, Benjamin; Siddiqui, Sami and Albers, Ingo: "Entwicklung und Optimierung einer innovativen Verbundlenkerachse". In: *18. Aachener Kolloquium für Fahrzeug- und Motorentechnik*. 2009, pp. 537–552 (cit. on pp. 10, 14–16, 18).

[Elb19] Elbers, Christoph; Zeitter, Markus; Meyer, Manfred and Bitzer, Thilo: "Predictive Chassis Concept for Passenger Cars". In: *ATZ worldwide* 121.11 (2019), pp. 38–43. doi: 10.1007/s38311-019-0120-5 (cit. on pp. 5, 19).

[Erb19] Erbes, Rainer and Dziegielewski, Andreas von: "Safeguarding of Complex Installation Spaces for Engine and Wheel Movements". In: *ATZ worldwide* 121.12 (2019), pp. 58–61. doi: 10.1007/s38311-019-0152-x (cit. on pp. 16, 34).

[Ers17] Ersoy, Metin and Gies, Stefan, eds.: Fahrwerkhandbuch: Grundlagen, Fahrdynamik, Komponenten, Systeme, Mechatronik, Perspektiven. 5th ed. ATZ / MTZ-Fachbuch. Wiesbaden: Springer Vieweg, 2017. doi: 10.1007/978-3-658-15468-4 (cit. on p. 29).

[Esk06] Eskandari, A.; Mirzadeh, O. and Azadi, Sh.: "Optimization of a McPherson Suspension System Using the Design of Experiments Method". In: SAE Technical Paper Series. SAE International, 2006. doi: 10.4271/2006-01-1953 (cit. on pp. 14, 15, 21).

[Fan15] Fang, Xiangfan and Tan, Kanlun: "Efficient Concept Design of Twist Beam Rear Axles". In: *ATZ worldwide* 117.1 (2015), pp. 24–29. doi: 10.1007/s38311-015-0149-z (cit. on p. 15).

[Fra] Fraunhofer ITWM: Reifenmodelle CDTire. url: https://www.itwm.fraunhofer.de/de/abteilungen/mf/reifenmodelle-cdtire.html (visited on 04/28/2022) (cit. on pp. 22, 50).

[Fro19] Frost & Sullivan: European Advanced Suspension Market 2018: Increasing Demand for Luxury Vehicles and Stringent Safety and Emission Norms to Drive Growth for Advanced Suspension Systems. 2019 (cit. on pp. 15, 19).

[Gäb18] Gäbel, Gunnar; Millitzer, Jonathan; Atzrodt, Heiko; Herold, Sven and Mohr, Andreas: "Development and Implementation of a Multi-Channel Active Control System for the Reduction of Road Induced Vehicle Interior Noise". In: *Actuators* 7.3 (2018), p. 52. doi: 10.3390/act7030052 (cit. on pp. 1, 4, 7, 9, 18, 19).

[Gae14] Gaetano, G. de; Mundo, D.; Vena, G.; Kroiss, M. and Cremers, L.: "A study on vehicle body concept modelling: beam to joint connection and size optimization of beam-like structures". In: *Proceedings of ISMA2014 including USD2014*. 2014, pp. 1653–1664. url: http://past.isma-isaac.be/downloads/isma2014/papers/isma2014_0670.pdf (cit. on pp. 14, 20, 48, 59).

[Gag10] Gagliardini, Laurent and Boudin, Michel: "Component analysis of random road-noise's multiple loads, using orders analysis during a run-up on rollers". In: *International Conference on Noise and Vibration Engineering*. 2010, pp. 4141–4148 (cit. on p. 17).

[Gen10] Genuit, Klaus, ed.: Sound-Engineering im Automobilbereich: Methoden zur Messung und Auswertung von Geräuschen und Schwingungen. Berlin, Heidelberg: Springer Berlin Heidelberg, 2010. doi: 10.1007/978-3-642-01415-4 (cit. on pp. 7–9, 14, 16–21, 33, 37, 52, 142).

[Ger19] Gerhards, Thomas; Zandbergen, Paul and Banks, Alan: "Lightweight Chassis Concept with Potential for Mass Production". In: *ATZ worldwide* 121.3 (2019), pp. 26–31. doi: 10.1007/s38311-018-0222-5 (cit. on pp. 11, 15).

[Gla17] Glandier, Christian and Grollius, Stefanie: "Improved Full Vehicle Finite Element Tire Road Noise Prediction". In: *SAE Technical Paper Series*. SAE Technical Paper Series. SAE International, 2017. doi: 10.4271/2017-01-1901 (cit. on pp. 7, 9, 50, 51).

[Gop20] Goppelt, Gernot: "Less Complexity Through Electrification?" In: *ATZ worldwide* 122.9 (2020), pp. 8–13. doi: 10.1007/s38311-020-0297-7 (cit. on pp. 4, 5).

[Gra14] Graening, Lars and Sendhoff, Bernhard: "Shape mining: A holistic data mining approach for engineering design". In: *Advanced Engineering Informatics* 28.2 (2014), pp. 166–185. doi: 10.1016/j.aei.2014.03.002 (cit. on pp. 15, 60, 61, 63, 83).

[Gro13] Grollius, Stefanie: "Analyse des gekoppelten Systems Reifen-Hohlraum-Rad-Radführung im Rollzustand und Entwicklung eines Rollgeräuschmodells". Dissertation. Karlsruhe: Karlsruhe Institute of Technology, 2013. doi: 10.5445/KSP/1000034776 (cit. on pp. 9, 50, 51).

[Gro74] Grotewohl, A.: "Lenkunruhe bei Federbeinachsen". Dissertation. Technische Universität Braunschweig, 1974 (cit. on p. 24).

[Gru03] Gruber, S.; Winner, H.; Haertel, V. and Holst, M.: "Beeinflussung des Fahrzeugverhaltens durch adaptive Fahrwerklager". In: *VDI-Berichte 1791*. Vol. 1791. VDI-Berichte. VDI-Verlag, 2003, pp. 171–183 (cit. on p. 18).

[Hab13] Haberzettl, Sebastian; Zschocke, Alexander K. and Gauterin, Frank: "Reduktion der niederfrequenten Lenkraddrehschwingungen bei wechselseitiger Fahrbahnanregung ohne Beeinflussung der fahrdynamischen Achskennwerte". In: *VDI-Berichte 2211*. VDI-Berichte. Düsseldorf: VDI-Verlag, 2013 (cit. on pp. 2, 19, 24).

[Hab14] Haberzettl, Sebastian; Stein, Wolfgang; Weijenberg, Niki and Gauterin, Frank: "Comparability of dynamic chassis measurements with full vehicle tests using the example of a sports car". In: *Proceedings of the 5th International Munich Chassis Symposium 2014*. Ed. by Pfeffer, Peter E. Wiesbaden: Springer Fachmedien Wiesbaden, 2014, pp. 259–280. doi: 10.1007/978-3-658-05978-1_21 (cit. on pp. 18, 24).

[Hah17] Hahn, Janna: "Eigenschaftsbasierte Fahrzeugkonzeption". Dissertation. Otto-von-Guericke-Universität Magdeburg, 2017. doi: 10.1007/978-3-658-20101-2 (cit. on pp. 14, 37).

[Har06] Harzheim, L. and Bohle, K.: "Vergleich verschiedener Strategien zur Optimierung der Road Noise Performance einer Mehrlenkerhinterachse". In: *VDI-Berichte 1967*. 2006, pp. 175–197 (cit. on pp. 2, 20, 22, 48, 50, 52, 56, 63, 93).

[Har10] Harzheim, Lothar and Warnecke, Ulrike: "Robustness optimization of the position of an anti-roll bar link to avoid the toggling of a rear axle stabilizer". In: *Structural and Multidisciplinary Optimization* 42.2 (2010), pp. 315–323. doi: 10.1007/s00158-010-0488-8 (cit. on pp. 27, 35, 63, 93).

[Har19] Harzheim, Lothar: Strukturoptimierung: Grundlagen und Anwendungen. 3rd ed. Edition Harri Deutsch. Haan-Gruiten: Verlag Europa Lehrmittel - Nourney Vollmer GmbH & Co. KG, 2019. url: https://www.europa-lehrmittel.de/t-1/strukturoptimierung-

4568/ (visited on 03/04/2021) (cit. on pp. 1, 18, 22, 27, 35, 37, 60, 61, 63, 64, 74, 82, 83, 92, 107, 108).

[Hei05] Heim, Rüdiger: FEM mit NASTRAN: Einstieg und Umsetzung mit Lernprogramm UNA. Munich: Hanser, 2005. DOI: 10.3139/9783446403611. URL: http://www.hanser-elibrary.com/action/showBook?doi=10.3139/9783446403611 (cit. on p. 16).

[Hei11] Heißing, Bernd and Ersoy, Metin: Chassis Handbook. Wiesbaden: Vieweg + Teubner, 2011. DOI: 10.1007/978-3-8348-9789-3 (cit. on pp. 7, 10–13, 17–20, 50, 54).

[Hei19] Heintzel, Alexander; Reichenbach, Michael; Ziegler, Marc; Unseld, Robert and Jung, Frank: "The Frankfurt Motor Show (IAA) 2019". In: *ATZ worldwide* 121.12 (2019), pp. 8–19. DOI: 10.1007/s38311-019-0164-6 (cit. on pp. 5, 6).

[Hel12] Helm, Detlef; Huf, Andreas; Zimmer, Hans and Kondziella, Rudolf: "Anforderungen in der frühen Phase der Gesamtfahrzeugauslegung". In: *VDI-Berichte 2169*. VDI-Berichte. Düsseldorf: VDI-Verlag, 2012, pp. 21–40. URL: https://www.tib.eu/de/suchen/id/BLCP%3ACN083482586/Anforderungen-in-der-fruhen-Phase-der-Gesamtfahrzeugauslegung/ (cit. on pp. 14, 16, 20, 59).

[Hem09] Hemsley, Ross: Interpolation on a magnetic field. 2009. URL: https://web.archive.org/web/20160114180318/http://interpolate3d.googlecode.com/files/Report.pdf (visited on 07/06/2020) (cit. on p. 93).

[Her21] Herrmann, Michael; Kralicek, Jan; Stein, Wolfgang and Gauterin, Frank: "Describing Road Booming Noise with a Hybrid Simulation Model Using a Time Segmentation of the Excitation Load Approach". In: *Vehicles* 3.3 (2021), pp. 469–479. DOI: 10.3390/vehicles3030028 (cit. on pp. 9, 20, 50).

[Hof15] Hofacker, Angelina: "Akustik für Fahrzeuge mit elektrifiziertem Antrieb". In: *Automobiltechnische Zeitschrift* 117.5 (2015), pp. 8–13. DOI: 10.1007/s35148-015-0061-2 (cit. on pp. 4, 16, 18).

[Hof16] Hofacker, Angelina: Stoßdämpfersystem von Audi ermöglicht Rekuperation von Energie im Fahrwerk. 2016. URL: https://www.springerprofessional.de/en/fahrwerk/bordnetze/stossdaempfersystem-von-audi-ermoeglicht-energierueckgewinnung/10570412 (visited on 11/04/2019) (cit. on p. 15).

[Hu17] Hu, Yinlong; Chen, Michael Z.Q. and Sun, Yonghui: "Comfort-oriented vehicle suspension design with skyhook inerter configuration". In: *Journal of Sound and Vibration* 405 (2017), pp. 34–47. DOI: 10.1016/j.jsv.2017.05.036 (cit. on p. 18).

[Hua20] Huang, Hai B.; Wu, Jiu H.; Huang, Xiao R.; Ding, Wei P. and Yang, Ming L.: "A novel interval analysis method to identify and reduce pure electric vehicle structure-borne noise". In: *Journal of Sound and Vibration* 475 (2020), p. 115258. DOI: 10.1016/j.jsv.2020.115258 (cit. on pp. 4, 7, 9, 16, 17).

[Hua21] Hua, Xia; Thomas, Alan and Shultis, Kurt: "Recent progress in battery electric vehicle noise, vibration, and harshness". In: *Science progress* 104.1 (2021), p. 368504211005224. DOI: 10.1177/00368504211005224 (cit. on p. 4).

[Jeo22] Jeon, Jaemin; Kim, Jaeyong; Lee, Jong Jun; Shin, Dongil and Kim, Yoon Young: "Development of deep learning-based joint elements for thin-walled beam structures". In: *Computers & Structures* 260 (2022), p. 106714. DOI: 10.1016/j.compstruc.2021.106714. URL: https://www.sciencedirect.com/science/article/pii/S0045794921002364 (cit. on p. 59).

[Jun20a] Jung, Frank: "Enhanced Noise Quality in Hybrid Cars". In: *ATZ worldwide* 122.7-8 (2020), pp. 14–15. DOI: 10.1007/s38311-020-0275-0 (cit. on p. 4).

[Jun20b] Jung, Frank: "From a technical perspective, we're ready to go". In: *ATZ worldwide* 122.9 (2020), pp. 22–25. DOI: 10.1007/s38311-020-0290-1 (cit. on p. 5).

[Jun20c] Jung, Frank: "It has been essential to keep noise levels low in the Kuga". In: *ATZ worldwide* 122.7-8 (2020), pp. 22–25. doi: 10.1007/s38311-020-0274-1 (cit. on pp. 16, 19).

[Jun21] Jung, Frank: "The triple constraints of efficiency, performance and ride comfort". In: *ATZ worldwide* 123.5-6 (2021), pp. 22–25. doi: 10.1007/s38311-021-0678-6 (cit. on pp. 15, 16, 18).

[Kal21] Kalabis, Marcus; Hoffmann, Uwe and Coerman, Cyril: "Maschinelles Lernen bei der Fahrwerksentwicklung". In: *ATZextra* 26.6 (2021), pp. 32–36. doi: 10.1007/s35778-021-0492-1 (cit. on p. 18).

[Kar84] Karnopp, Dean and Margolis, Donald: "Adaptive Suspension Concepts for Road Vehicles". In: *Vehicle System Dynamics* 13.3 (1984), pp. 145–160. doi: 10.1080/00423118408968772 (cit. on p. 18).

[Kei19] Keilhoff, Dan et al.: "UNICARagil - New Architectures for Disruptive Vehicle Concepts". In: *19th Stuttgart International Symposium - Automotive and Engine Technology*. Ed. by Bargende, Michael; Reuss, Hans-Christian and Wiedemann, Jochen. Vol. 19. Springer Fachmedien Wiesbaden, 2019 (cit. on pp. 5, 6).

[Kha19] Khan, Sikandar; Horoub, Mamon M.; Shafiq, Saifullah; Ali, Sajid and Bhatti, Umar Nawaz: "Optimization of Vehicle Suspension System Using Genetic Algorithm". In: *2019 IEEE 10th International Conference on Mechanical and Aerospace Engineering (ICMAE)*. 2019, pp. 203–207. doi: 10.1109/ICMAE.2019.8880941 (cit. on pp. 14, 19).

[Kid11] Kido, Ichiro; Ueyama, Sagiri; Hashioka, Masato; Yamamoto, Seigo; Tsuchiyama, Minoru and Yamaoka, Hiroo: "Tire and road input modeling for low-frequency road noise prediction". In: *SAE International Journal of Passenger Cars-Mechanical Systems* 4.2011-01-1690 (2011), pp. 1277–1282. doi: 10.4271/2011-01-1690 (cit. on p. 51).

[Kid99] Kido, Ichiro; Nakamura, Akeru; Hayashi, Takeshi and Asai, Makoto: "Suspension Vibration Analysis for Road Noise Using Finite Element Model". In: SAE Technical Paper Series. SAE International, 1999. doi: 10.4271/1999-01-1788 (cit. on p. 18).

[Kim11] Kim, Myung-Gyu: "Transfer Function Analysis of Rear Multi-Link Suspension to Improve Ride Vibration and Road Noise". In: SAE Technical Paper Series. SAE International, 2011. doi: 10.4271/2011-01-1571 (cit. on pp. 18, 22).

[Kim16] Kim, S. K.; Kim, S. S.; Cho, Y. G. and Jung, H. K.: "Accumulated tolerance analysis of suspension by geometric tolerances based on multibody elasto-kinematic analysis". In: *International Journal of Automotive Technology* 17.2 (2016), pp. 255–263. doi: 10.1007/s12239-016-0025-x (cit. on pp. 21, 22).

[Kim18] Kim, Joong-Kwan; Lee, Jinmo; Kim, Hyoung-Gun; Cho, Munhwan; Ih, Kang-Duck; Ko, Han-Young and Shim, Jeong-Soo: "The Effects of Suspension Component Stiffness on the Road Noise: A Sensitivity Study and Optimization". In: *10th International Styrian Noise, Vibration & Harshness Congress 2018*. SAE Technical Paper Series. SAE International, 2018, pp. 1–7. doi: 10.4271/2018-01-1510 (cit. on pp. 17, 53).

[Kle15] Klein, Bernd: FEM. Wiesbaden: Springer Fachmedien Wiesbaden, 2015. doi: 10.1007/978-3-658-06054-1 (cit. on p. 74).

[Kle18] Klein, Holger: "Post-CES, every car will still have a chassis". In: *ATZ worldwide* 120.6 (2018), pp. 26–29. doi: 10.1007/s38311-018-0069-9 (cit. on p. 10).

[Köl19] Köllner, Christiane: Autofahrer erwarten vor allem Komfort von ihrem Neuwagen. 2019. url: https://www.springerprofessional.de/fahrzeugtechnik/ergonomie---hmi/autofahrer-erwarten-vor-allem-komfort-von-ihrem-neuwagen/17376416 (visited on 12/02/2019) (cit. on p. 1).

[Köl20] Köllner, Christiane: Wie das Interieur zum neuen Exterieur wird. 2020. URL: https://www.springerprofessional.de/interieur/ergonomie---hmi/wie-das-interieur-zum-neuen-exterieur-wird/18183776 (visited on 05/01/2023) (cit. on p. 1).

[Köl23] Köllner, Christiane: Was Verkehrsteilnehmer 2023 wissen müssen. 2023. URL: https://www.springerprofessional.de/en/verkehrspolitik/mobilitaetskonzepte/was-verkehrsteilnehmer-2023-wissen-muessen/23789528 (visited on 01/04/2023) (cit. on p. 4).

[Kos14] Kosaka, Fumihiko; Mizuno, Hiroaki; Inoue, Tsuyoshi and Takagi, Kentaro: "Road noise sensitivity analysis with respect to suspension geometry". In: *INTER-NOISE and NOISE-CON congress and conference proceedings*. Vol. 249. 2014, pp. 2127–2136 (cit. on pp. 1, 2, 7, 15, 18, 23, 50, 51).

[Kra00] Krautstrunk, A.; Uhler, R.; Zimmer, M. and Mutschler, P.: "Elektrisch lenken: Handkraftaktor für steer-by-wire". In: *Therna FORSCHUNG* (2000), pp. 104–113 (cit. on pp. 5, 6, 12).

[Kra19] Krauss, Oliver: "Experimentelle Untersuchungen zum Innengeräusch von Fahrzeugluftreifen". Dissertation. Karlsruhe: Karlsruhe Institute of Technology, 2019. DOI: 10.5445/KSP/1000087790 (cit. on pp. 4, 7, 9, 16).

[Lam20] Lambert, Fred: Amazon's Zoox unveils its autonomous electric vehicle with massive battery pack. 2020. URL: https://electrek.co/2020/12/14/amazons-zoox-unveils-autonomous-electric-vehicle-battery-pack/ (visited on 12/16/2020) (cit. on p. 5).

[Lan22] Lang, Patrick; Stegmaier, Gerd; Baumann, Uli and Harloff, Thomas: Verbrenner-Aus bei Autoherstellern. 2022. URL: https://www.auto-motor-und-sport.de/tech-zukunft/alternative-antriebe/verbrenner-ausstieg-auto-hersteller-elektro-zukunft/ (visited on 05/09/2022) (cit. on p. 3).

[Lei19] Leistner, Bastian: Fahrwerkentwicklung und produktionstechnische Integration ab der frühen Produktentstehungsphase. Wiesbaden: Springer Fachmedien Wiesbaden, 2019. doi: 10.1007/978-3-658-26867-1 (cit. on pp. 1, 10–15, 19).

[Lei20] Leidenfrost, David and Moarefi, Bahman: "Generative Engineering Approach for a B-pillar Car Body Node". In: *ATZ worldwide* 122.11 (2020), pp. 68–71. doi: 10.1007/s38311-020-0306-x (cit. on p. 16).

[Let19] Lethbridge, Alfred: "Improved Comfort for the Future Vehicle Interior". In: *ATZ worldwide* 121.11 (2019), pp. 28–33. doi: 10.1007/s38311-019-0123-2 (cit. on pp. 1, 6).

[Leu20] Leupolz, Michael: "Automatisierte Gestaltoptimierung von Bauteilen bezüglich ihres NVH-Verhaltens durch Geometriemorphing". Master Thesis. Karlsruhe: Karlsruhe Institute of Technology, 2020. doi: 10.5445/IR/1000142474 (cit. on p. 64).

[Li07] Li, Lei; Xia, Changgao and Qin, Wei: "Analysis of Kinetic Characteristic and Structural Parameter Optimization of Multi-Link Suspension". In: SAE Technical Paper Series. SAE International, 2007. doi: 10.4271/2007-01-3558 (cit. on pp. 21, 22).

[Llo18] Lloret, Maria Gavila; Duvigneau, Fabian; Müller, Gregor and Rottengruber, Hermann: "Computer-aided Prediction of Airborne Sound Transmission through the Front Car End". In: *ATZ worldwide* 120.7 (2018), pp. 76–79. doi: 10.1007/s38311-018-0078-8 (cit. on pp. 14, 53).

[Lv21] Lv, Tianqi; Zhang, Yunqing; Duan, Yupeng and Yang, James: "Kinematics & compliance analysis of double wishbone air suspension with frictions and joint clearances". In: *Mechanism and Machine Theory* 156 (2021), p. 104127. doi: 10.1016/j.mechmachtheory.2020.104127. url: https://www.sciencedirect.com/science/article/pii/S0094114X20303426 (cit. on p. 15).

[Lyo20] Lyon, Peter: "World's Biggest-Ever Self-Driving Experiment To Coincide With Tokyo Olympics". In: *Forbes* (Jan. 29, 2020). URL: https://www.forbes.com/sites/peterlyon/2020/01/28/tokyo-olympics-to-coincide-with-biggest-self-driving-demonstration-in-history/ (visited on 08/03/2021) (cit. on p. 5).

[Lyo21] Lyon, Peter: "Covid Won't Stop The Olympics Nor Toyota's Autonomous EV Transportation For Athletes". In: *Forbes* (June 30, 2021). URL: https://www.forbes.com/sites/peterlyon/2021/06/30/covid-wont-stop-the-olympics-nor-toyotas-autonomous-ev-transportation-for-athletes (visited on 08/03/2021) (cit. on pp. 4, 5).

[Mac21] Mackenrodt, Johannes; Koo, Taeyun; Müller, Jens and Bhae, Harrison: "Technical Approaches and the Feeling of Safety with Steer-by-Wire". In: *ATZ worldwide* 123.2 (2021), pp. 50–55. DOI: 10.1007/s38311-020-0611-4 (cit. on p. 5).

[Man18] Mantovani, Maurizio: "Rolling noise does not evoke an emotional response". In: *ATZ worldwide* 120.7-8 (2018), pp. 18–21. DOI: 10.1007/s38311-018-0099-3. URL: https://link.springer.com/content/pdf/10.1007/s38311-018-0099-3.pdf (cit. on pp. 1, 4, 7).

[Mar11] Maressa, Antonio; Pluymers, Bert; Desmet, Wim and Donders, Stijn: "Optimization methodologies based on structural modification analysis in automotive NVH design". In: *Proceedings of ICSV 18*. Ed. by Crocker, M. Vol. 2. International Institute of Acoustics & Vibration, 2011, pp. 1780–1787. URL: https://limo.libis.be/primo-explore/fulldisplay?docid=LIRIAS1572415&context=L&vid=Lirias&search_scope=Lirias&tab=default_tab&lang=en_US (visited on 04/15/2020) (cit. on pp. 1, 14, 19, 63).

[Mar15] Marinescu, D. G.; Popescu, C. L.; Tabacu, I.; Nicolae, V.; Serban, F.; Tabacu, S.; Vieru, I. and Adrian, I.: "A full electric vehicle 4WD type". In: *28th International Electric Vehicle Symposium and Exposition (EVS 28)*. Seoul: Korean Society of Automotive Engineers, 2015 (cit. on p. 15).

[Mat07] Matschinsky, Wolfgang: Radführungen der Straßenfahrzeuge: Kinematik, Elasto-Kinematik und Konstruktion. 3., aktualisierte und erweiterte Auflage. Berlin, Heidelberg: Springer Berlin Heidelberg, 2007. doi: 10.1007/978-3-540-71197-1. url: http://site.ebrary.com/lib/alltitles/docDetail.action?docID=10181047 (cit. on pp. 14, 54).

[Mat14] Matej, Glavac and Schmidt, Edmund: "Erlebbare Digitale NVH Auslegung der neuen Mercedes-Benz C-Klasse". In: *VDI-Berichte 2224*. VDI-Berichte. Düsseldorf: VDI-Verlag, 2014, pp. 249–259 (cit. on pp. 20, 50, 140).

[Mei15] Meier, Christoph: "2 Fragen an Christoph Meier". In: *Automobiltechnische Zeitschrift* 117.5 (2015), p. 11. doi: 10.1007/s35148-015-0061-2 (cit. on pp. 1, 7).

[Mer16] Mercedes-Benz Group Media: Mercedes-AMG E 63, Suspension. 2016. url: https://group-media.mercedes-benz.com/marsMediaSite/pic/en/14826860 (cit. on p. 28).

[Mer18] Mercedes-Benz Group Media: Vision URBANETIC: On demand, efficient and sustainable: Vision URBANETIC answers the questions of future urban mobility. 2018. url: https://group-media.mercedes-benz.com/marsMediaSite/ko/en/41169541 (visited on 11/07/2022) (cit. on p. 5).

[Mer19] Mercedes-Benz Group Media: Test and Technology Center Immendingen: Systematic torture: the test and assessment stretches. 2019. url: https://group-media.mercedes-benz.com/marsMediaSite/ko/en/44801275 (visited on 11/07/2022) (cit. on p. 128).

[Mer20a] Mercedes-Benz Group Media: designo patagonia red bright, Leather Nappa exclusive Maybach: designo crystal white/silver grey pearl. 2020. url: https://group-media.mercedes-benz.com/marsMediaSite/pic/en/48141329 (visited on 07/28/2022) (cit. on p. 28).

[Mer20b] Mercedes-Benz Group Media: More manoeuvrable and dynamic thanks to steerable rear wheels. 2020. URL: https://group-media.mercedes-benz.com/marsMediaSite/ko/en/47872380 (cit. on p. 5).

[Mer21a] Mercedes-Benz Group Media: Agile innovator 20 years ago: Mercedes-Benz F 400 Carving research vehicle. 2021. URL: https://group-media.mercedes-benz.com/marsMediaSite/ko/en/51666948 (cit. on p. 25).

[Mer21b] Mercedes-Benz Group Media: The new Mercedes-Maybach S-Class up close: active road noise compensation. 2021. URL: https://group-media.mercedes-benz.com/marsMediaSite/ko/en/50185532 (visited on 05/26/2022) (cit. on p. 19).

[Mer22a] Mercedes-Benz Group: The front runner in automated driving and safety technologies. 2022. URL: https://group.mercedes-benz.com/innovation/case/autonomous/drive-pilot-2.html (visited on 05/09/2022) (cit. on p. 4).

[Mer22b] Mercedes-Benz Group Media: Conditionally automated driving: Mercedes-Benz announces sales launch of Drive Pilot. 2022. URL: https://group-media.mercedes-benz.com/marsMediaSite/ko/en/53213668 (visited on 05/09/2022) (cit. on p. 4).

[Mer22c] Mercedes-Benz Group Media: Der EQS SUV mit Platz für bis zu sieben Personen und verschiedenen Sitzverstellungen. 2022. URL: https://group-media.mercedes-benz.com/marsMediaSite/pic/de/54106231 (visited on 11/07/2022) (cit. on p. 47).

[Mer22d] Mercedes-Benz Group Media: Magical Garage by Mercedes-Benz Showcasing Innovations II. 2022. URL: https://group-media.mercedes-benz.com/marsMediaSite/pic/en/54119631 (visited on 11/07/2022) (cit. on pp. 44, 47).

[Meß07] Meß, Michael and Pelz, Peter: "Luftfederung und Luftdämpfung im Spannungsfeld Komfort, Dynamik und Sicherheit". In: *Automobiltechnische Zeitschrift* 109.3 (2007), pp. 230–237. DOI: 10.1007/BF03221874 (cit. on pp. 12, 18).

[Mor12] Moroncini, A.; Cremers, L. and Baldanzini, N.: "Car body concept modeling for NVH optimization in the early design phase at BMW: a critical review and new advanced solutions". In: *Proc. Int. Conf. Noise and Vibration Engineering ISMA*. 2012, pp. 3809–3824. URL: http://past.isma-isaac.be/downloads/isma2012/papers/isma2012_0278.pdf (visited on 09/07/2020) (cit. on pp. 20, 48, 59, 63, 64).

[Mos08] Most, Thomas and Will, Johannes: "Metamodel of Optimal Prognosis - An automatic approach for variable reduction and optimal meta-model selection". In: *Weimar Optimization and Stochastic Days 5*. Weimar, Germany: Dynardo GmbH, 2008. DOI: 10.13140/2.1.2194.4007 (cit. on pp. 35, 89, 92–94).

[Mos11] Most, Thomas and Will, Johannes: "Sensitivity analysis using the Metamodel of Optimal Prognosis". In: *Weimar Optimization and Stochastic Days 8*. Weimar, Germany: Dynardo GmbH, 2011, pp. 24–40. URL: https://www.dynardo.de/fileadmin/Material_Dynardo/bibliothek/WOST_8.0/Paper_Most.pdf (visited on 05/07/2020) (cit. on pp. 83, 94, 96).

[Nee19] Neemann, Andreas: Smarte Transporter gegen den Verkehrskollaps. 2019. URL: https://www.zf.com/site/magazine/de/articles_15168.html (visited on 10/21/2019) (cit. on p. 5).

[Nem11] Nemeth, Balazs and Gaspar, Peter: "Integration of control design and variable geometry suspension construction for vehicle stability enhancement". In: *2011 50th IEEE Conference on Decision and Control and European Control Conference*. Piscataway, NJ: IEEE, 2011, pp. 7452–7457. DOI: 10.1109/CDC.2011.6160441 (cit. on p. 25).

[Nie12] Niersmann, Alexandra: "Modellbasierte Fahrwerkauslegung und -optimierung". Dissertation. Braunschweig: Technische Universität Braunschweig, 2012 (cit. on pp. 12, 14, 16, 18, 20, 21, 50).

[Nol21] Nolting, Michael: Künstliche Intelligenz in der Automobilindustrie: Mit KI und Daten vom Blechbieger zum Techgiganten. Technik im Fokus. Wiesbaden: Springer Fachmedien Wiesbaden, 2021. doi: 10.1007/978-3-658-31567-2 (cit. on pp. 35, 93).

[Nun09] Nunes, Ronaldo F.; Will, Johannes; Bayer, Veit and Karthik, Chittepu: "Robustness Evaluation of brake systems concerned to squeal noise problem". In: *Weimar Optimization and Stochastic Days 6*. Weimar, Germany: Dynardo GmbH, 2009. url: https://www.dynardo.de/fileadmin/Material_Dynardo/bibliothek/WOST_6.0/WOST_6_Paper_Nunes.pdf (visited on 05/19/2020) (cit. on p. 63).

[Nun13] Nunes, Ronaldo F. and Büttner, Christian: "Sensitivity of brake squealing concerning scattered component, joint and bearing properties". In: *Weimar Optimization and Stochastic Days 10*. Weimar, Germany: Dynardo GmbH, 2013. url: https://www.dynardo.de/fileadmin/Material_Dynardo/bibliothek/WOST10/17_WOST2013_RDO3_nunes_buettner.pdf (visited on 05/19/2020) (cit. on p. 63).

[Nun15] Nunes, Ronaldo F.; Stump, Oliver and Wolff, Sebastian: "Use of Random Fields to Characterize Brake Pad Surface Uncertainties". In: *Weimar Optimization and Stochastic Days 12*. Weimar, Germany: Dynardo GmbH, 2015. url: https://www.dynardo.de/fileadmin/Material_Dynardo/bibliothek/WOST12/03_WOST2015_Session1_Nunes.pdf (visited on 05/19/2020) (cit. on pp. 63, 74).

[Oer01] Oertel, Christian and Fandre, Andreas: "RMOD-K tyre model system". In: *ATZ worldwide* 103.11 (2001), pp. 23–25. doi: 10.1007/BF03224524 (cit. on p. 50).

[Ope22a] Open Source Initiative: The 3-Clause BSD License. 2022. url: https://opensource.org/licenses/BSD-3-Clause (visited on 08/25/2022) (cit. on pp. 68, 70).

[Ope22b] Open Source Initiative: The MIT License. 2022. url: https://opensource.org/licenses/MIT (visited on 08/25/2022) (cit. on pp. 68, 69).

[Par06] Park, Sung W.; Linsen, Lars; Kreylos, Oliver; Owens, John D. and Hamann, Bernd: "Discrete Sibson interpolation". In: *IEEE transactions on visualization and computer graphics* 12.2 (2006), pp. 243–253. doi: 10.1109/TVCG.2006.27 (cit. on pp. 68, 69).

[Par21] Paravan GmbH: Driving a car without a steering wheel or pedals. 2021. url: https://www.paravan.com/technology/paravan-drive-by-wire (visited on 05/31/2022) (cit. on pp. 5, 6).

[Pfe18] Pfeffer, Peter E.: "„Die Komplexität kann man nicht reduzieren"". In: *ATZextra* 23.S9 (2018), pp. 6–9. doi: 10.1007/s35778-017-0095-z (cit. on p. 5).

[Pro19] Protean Electric: "360-degree Steering". In: *ATZ worldwide* 121.9 (2019), p. 37. doi: 10.1007/s38311-019-0119-y (cit. on pp. 5, 6).

[pyp18] pypy.org: naturalneighbor 0.2.1. 2018. url: https://pypi.org/project/naturalneighbor/0.2.1/ (visited on 01/02/2023) (cit. on pp. 68, 69).

[Rad21] Rade, Jaydeep; Balu, Aditya; Herron, Ethan; Pathak, Jay; Ranade, Rishikesh; Sarkar, Soumik and Krishnamurthy, Adarsh: "Algorithmically-consistent deep learning frameworks for structural topology optimization". In: *Engineering Applications of Artificial Intelligence* 106 (2021), p. 104483. doi: 10.1016/j.engappai.2021.104483. url: https://www.sciencedirect.com/science/article/pii/S0952197621003316 (cit. on p. 93).

[Rah14] Rahman, M. Shafiqur and Kibria, Khan Muhammad Golam: "Investigation of Vibration and Ride Characteristics of a Five Degrees of Freedom Vehicle Suspension System". In: *Procedia Engineering* 90 (2014), pp. 96–102. doi: 10.1016/j.proeng.2014.11.820 (cit. on p. 18).

[Ram17] Rambacher, Christoph; Ehrt, Tobias and Sell, Hendrik: "Vibration optimisation of entire axles". In: *ATZ worldwide* 119.6 (2017), pp. 50–55. doi: 10.1007/s38311-017-0038-8 (cit. on pp. 1, 4, 15–18, 37, 52, 53).

[Ran13] Ranjbar, Mostafa and Marburg, Steffen: "Fast Vibroacoustic Optimization of Mechanical Structures Using Artificial Neural Networks". In: *International Journal of Mechanical Engineering and Applications* 1.3 (2013), p. 64. doi: 10.11648/j.ijmea.20130103.11 (cit. on p. 94).

[Rau20] Raulf, Christian; Pethe, Chris; Vietor, Thomas and Henze, Roman: "Dynamically Configurable Vehicle Concepts for Autonomous Driving". In: *ATZ worldwide* 122.12 (2020), pp. 46–51. doi: 10.1007/s38311-020-0329-3 (cit. on p. 5).

[REE20] REE: REE hits the track with 3 modular EV platforms. 2020. url: https://ree.auto/press-release/5768/ (visited on 02/22/2021) (cit. on p. 5).

[REE21] REE: REE Automotive Opens New Engineering Center of Excellence. 2021. url: https://ree.auto/press-release/ree-automotive-opens-new-engineering-center-of-excellence/ (visited on 02/22/2021) (cit. on pp. 5, 6).

[Ref15] Reff, Bjoern; Palandri, Jacopo; Rambacher, Christoph and Sell, Hendrik: "Chassis system NVH: advanced analysis methods - full vehicle correlation". In: *Automotive Acoustics Conference*. Zürich, 2015 (cit. on pp. 13, 17, 20, 37, 89).

[Rei19] Reichenbach, Michael: "10th Munich Chassis Symposium chassis.tech plus 2019". In: *ATZ worldwide* 121.9 (2019), pp. 80–81. doi: 10.1007/s38311-019-0113-4 (cit. on pp. 5, 16).

[Röm22] Römer, Jürgen: "Steuerung und Regelung des Lenkradmoments durch Nutzung radselektiver Frontantriebe". Dissertation. Karlsruhe: Karlsruhe Institute of Technology, 2022. doi: 10.5445/KSP/1000132577 (cit. on p. 15).

[Rös12] Röski, Karsten: "Eine Methode zur simulationsbasierten Grundauslegung von PKW-Fahrwerken mit Vertiefung der Betrachtungen zum Fahrkomfort". Dissertation. Munich: Technical University of Munich, 2012. url: https://mediatum.ub.tum.de/doc/1109076/file.pdf (visited on 07/31/2018) (cit. on p. 18).

[San02] Sandberg, Ulf and Ejsmont, Jerzy A.: Tyre/road noise: Reference book. 1st ed. Kisa, Sweden: INFORMEX Ejsmont & Sandberg Handelsbolag, 2002 (cit. on p. 142).

[San10] Sancibrian, Ramon; Garcia, Pablo; Viadero, Fernando; Fernandez, Alfonso and De-Juan, Ana: "Kinematic design of double-wishbone suspension systems using a multiobjective optimisation approach". In: *Vehicle System Dynamics* 48.7 (2010), pp. 793–813. doi: 10.1080/00423110903156574 (cit. on pp. 10, 12, 100).

[Sch09] Schlecht, Albert; Heißing, Bernd and Krome, Helmut: "Entwicklung einer schwingungsunempfindlichen Vorderachskinematik mit Hilfe von Optimierungsmethoden". In: *VDI-Berichte 2086*. Ed. by VDI Wissensforum GmbH. Düsseldorf: VDI-Verlag, 2009, pp. 99–116 (cit. on p. 24).

[Sch10] Schlecht, Albert; Heißing, Bernd; Krome, Helmut and Hackenberg, Günter: "Entwicklung einer schwingungsunempfindlichen Vorderachskinematik". In: *ATZextra* 15.2 (2010), pp. 32–37. doi: 10.1365/s35778-010-0363-7 (cit. on pp. 23, 24).

[Sch12] Schlecht, Albert: "Minimierung der Schwingungsempfindlichkeit von Kraftfahrzeugvorderachsen". Dissertation. Munich: Technical University of Munich, 2012. url: https://mediatum.ub.tum.de/doc/1086602/1086602.pdf (visited on 02/05/2021) (cit. on pp. 1, 2, 11, 14, 17, 19, 20, 23, 24, 33, 37, 50, 51).

[Sch17] Schilp, Andreas and Bathelt, Hartmut: "NVH development strategies for suspensions - challenges and chances by autonomous driving." In: *Proceedings of the Automotive Acoustics Conference*. Ed. by Siebenpfeiffer, W. Wiesbaden: Springer Vieweg, 2017. doi: 10.1007/978-3-658-20251-4_18 (cit. on pp. 5, 9, 17).

[Sch18] Schlott, Stefan: "Endless conflicts". In: *ATZ worldwide* 120.5 (2018), pp. 6–7. doi: 10.1007/s38311-018-0063-2 (cit. on pp. 1, 18).

[Sch19a] Schäfer, Patrick: "Projekt erforscht Radmodul-Konzepte für autonome Fahrzeuge". In: *springerprofessional.de* (Dec. 16, 2019). URL: https://www.springerprofessional.de/fahrwerk/automatisiertes-fahren/projekt-erforscht-radmodul-konzepte-fuer-autonome-fahrzeuge/17499788 (visited on 05/01/2023) (cit. on p. 5).

[Sch19b] Schirle, Thomas: "Systementwurf eines elektromechanischen Fahrwerks für Megacitymobilität". Dissertation. Karlsruhe: Karlsruhe Institute of Technology, 2019. DOI: 10.5445/IR/1000098303. URL: http://doi.org/10.5445/IR/1000098303 (visited on 11/11/2019) (cit. on pp. 5, 6, 15, 19).

[Sch20a] Schäfer, Patrick: "Autonome Shuttles werden im realen Straßenverkehr getestet". In: *springerprofessional.de* (Nov. 24, 2020). URL: https://www.springerprofessional.de/automatisiertes-fahren/multimodale-mobilitaet/autonome-shuttles-werden-im-realen-strassenverkehr-getestet/18601426 (visited on 02/08/2021) (cit. on p. 4).

[Sch20b] Schäfer, Patrick: "Rolls-Royce verbessert seine Selbstfahrer-Limousine Ghost". In: *springerprofessional.de* (Sept. 15, 2020). URL: https://www.springerprofessional.de/limousinen/fahrzeugakustik---nvh/rolls-royce-verbessert-seine-selbstfahrer-limousine-ghost/18376234 (visited on 05/05/2021) (cit. on p. 16).

[Sch21a] Schaeffler Paravan Technologie GmbH & Co.KG: Mit Steer-by-Wire durch die grüne Hölle. Pfronstetten, 2021. URL: https://www.schaeffler-paravan.com/unternehmen/veroeffentlichte-pressemitteilungen/mit-steer-wire-durch-die-gruene-hoelle-am (visited on 05/06/2023) (cit. on p. 5).

[Sch21b] Schäfer, Johannes and Leidhold, Roberto: "Steer-by-Wire: Eine analytische Beurteilung von unterschiedlichen Zahnstangenkraftschätzungen im Fahrzeug". In: *at - Automatisierungstechnik* 69.1 (2021), pp. 65–72. DOI: 10.1515/auto-2020-0100 (cit. on p. 5).

[Sch21c] Schäfer, Patrick: "Corona hält den Wandel der Automobilbranche nicht auf". In: *springerprofessional.de* (June 1, 2021). URL: https://www.springerprofessional.de/elektrofahrzeuge/automatisiertes-fahren/corona-haelt-den-wandel-der-automobilbranche-nicht-auf/19212012 (visited on 06/01/2021) (cit. on p. 3).

[Sch21d] Schäfer, Patrick: "Volkswagen präsentiert autonome Robotaxi-Studie OnePod". In: *springerprofessional.de* (Oct. 19, 2021). URL: https://www.springerprofessional.de/automatisiertes-fahren/elektrofahrzeuge/volkswagen-praesentiert-autonome-robotaxi-studie-onepod/19766136 (visited on 05/01/2023) (cit. on p. 5).

[Sch21e] Schütte, Jan and Sextro, Walter: "Tire Wear Reduction Based on an Extended Multibody Rear Axle Model". In: *Vehicles* 3.2 (2021), pp. 233–256. DOI: 10.3390/vehicles3020015 (cit. on pp. 21, 50, 59).

[Sch22] Schäfer, Patrick: "Optimierte Achssysteme können den Reifenabrieb reduzieren". In: *springerprofessional.de* (Jan. 12, 2022). URL: https://www.springerprofessional.de/fahrwerk/schadstoffe/optimierte-achssysteme-koennen-den-reifenabrieb-reduzieren/20018666 (visited on 05/01/2023) (cit. on p. 21).

[Sci22a] SciPy. 2022. URL: https://scipy.org/ (visited on 08/25/2022) (cit. on pp. 68, 70).

[Sci22b] SciPy: License. 2022. URL: https://github.com/scipy/scipy/blob/main/LICENSE.txt (cit. on pp. 68, 70).

[Sci22c] SciPy: scipy.interpolate.RegularGridInterpolator. 2022. URL: https://docs.scipy.org/doc/scipy/reference/generated/scipy.interpolate.RegularGridInterpolator.html (visited on 08/25/2022) (cit. on p. 70).

[Sed06] Sedlan, K.: "Simulation unwuchterregter und bremsinduzierter Lenkunruhe bei Pkw mit Federbeinachse". In: *15. Aachener Kolloquium Fahrzeug- und Motorentechnik*. 2006 (cit. on p. 24).

[Sei16] Seifi, Abolfazl; Hassannejad, Reza and Hamed, Mohammad A.: "Optimum design for passive suspension system of a vehicle to prevent rollover and improve ride comfort under random road excitations". In: *Proceedings of the Institution of Mechanical Engineers, Part K: Journal of Multi-body Dynamics* 230.4 (2016), pp. 426–441. doi: 10.1177/1464419315618034 (cit. on pp. 14, 18).

[Sei21] Seijs, Maarten van der; Harvie, Julie and Song, David: "Road Noise NVH: Embedding Suspension Test Benches in NVH Design using Virtual Points and the TPA Framework". In: *IMAC XXXIX*. 2021 (cit. on pp. 1, 4, 8, 9, 16, 17).

[Sel01] Sell, Hendrik: "Geräuschpfadanalyse für hochfrequenten Körperschall". In: *Fortschritte der Akustik – DAGA 2001*. Deutsche Gesellschaft für Akustik, 2001 (cit. on p. 18).

[Sel08] Sell, Hendrik; Ehrt, Tobias and Meß, Michael: "Vibration-optimized components for chassis systems". In: *ATZ worldwide* 110.2 (2008), pp. 26–31. doi: 10.1007/BF03224984 (cit. on pp. 12, 14, 15, 17, 18, 52).

[Sel22] Sell, Hendrik; Löcken, Florian; Kruse, Enrico and Reinauer, Andreas: "Holistic Approach to Axle NVH Assessment and Optimization". In: *Proceedings of the 12th International Munich Chassis Symposium 2021*. Ed. by Pfeffer, Peter. Berlin, Heidelberg: Springer Berlin Heidelberg, 2022, pp. 624–642. doi: 10.1007/978-3-662-64550-5_35 (cit. on pp. 13–15, 17–19, 52).

[Sib80] Sibson, Robin: "A vector identity for the Dirichlet tessellation". In: *Mathematical Proceedings of the Cambridge Philosophical Society* 87.1 (1980), pp. 151–155. doi: 10.1017/S0305004100056589. url: https://www.cambridge.org/core/article/vector-identity-for-the-dirichlet-tessellation/98F37D6EC7435F5110F6CC526B06DDC9 (cit. on p. 68).

[Sie17] Siebertz, Karl; Bebber, David van and Hochkirchen, Thomas: Statistische Versuchsplanung. Berlin, Heidelberg: Springer Berlin

Heidelberg, 2017. DOI: 10.1007/978-3-662-55743-3 (cit. on pp. 83, 92).

[Spi12] Spickenreuther, Michael; Bersiner, Frank and Fricke, Ernst: "Virtuelle Auslegung und Absicherung im Schwingungskomfort". In: *VDI-Berichte 2169*. VDI-Berichte. Düsseldorf: VDI-Verlag, 2012 (cit. on pp. 10, 14).

[Sta12] Staten, Matthew L.; Owen, Steven J.; Shontz, Suzanne M.; Salinger, Andrew G. and Coffey, Todd S.: "A Comparison of Mesh Morphing Methods for 3D Shape Optimization". In: *Proceedings of the 20th International Meshing Roundtable*. Ed. by Quadros, William Roshan. Berlin, Heidelberg: Springer Berlin Heidelberg, 2012, pp. 293–311. DOI: 10.1007/978-3-642-24734-7_16 (cit. on pp. 60, 62, 63, 74, 78).

[Sti10] Stigliano, Giambattista; Mundo, Domenico; Donders, Stijn and Tamarozzi, Tommaso: "Advanced Vehicle Body Concept Modeling Approach Using Reduced Models of Beams and Joints". In: *Proceedings of ISMA 2010*. Katholieke Univ Leuven, Dept Werktuigkunde, 2010, pp. 4179–4190. URL: https://lirias.kuleuven.be/558772?limo=0 (visited on 04/15/2020) (cit. on pp. 14, 20, 48, 59).

[Tan18] Tan, Kanlun and Fang, Xiangfan: "Automatic concept design and optimization of twist beam axles". In: *Automotive and Engine Technology* (2018), pp. 1–18. DOI: 10.1007/s41104-018-0033-0 (cit. on p. 59).

[Tem20] Templeton, Brad: Robocars 2020 In Review: Winter To Spring. 2020. URL: https://www.forbes.com/sites/bradtempleton/2021/12/28/robocars-2020-in-review--winter-to-spring/?sh=79bb44c59dd5 (visited on 01/11/2021) (cit. on p. 5).

[Tho21] Thomas, S. S.; Palandri, J.; Lakehal-Ayat, M.; Chakravarty, P.; Wolf-Monheim, F. and Blaschko, M. B.: "Kinematics Design of a MacPherson Suspension Architecture Based on Bayesian Optimization". In: *IEEE Transactions on Cybernetics* (2021), pp. 1–14. DOI: 10.1109/TCYB.2021.3114403 (cit. on p. 24).

[Tre15] TrelleborgVibracoustic: Schwingungstechnik im Automobil: Grundlagen, Werkstoffe, Konstruktion, Berechnung und Anwendungen. 1st ed. Würzburg: Vogel Business Media, 2015. URL: http://site.ebrary.com/lib/tubraunschweig/docDetail.action?docID=11158629 (cit. on p. 13).

[Tre20] Treichel, Volker; Schaller, Enrico and Soost, Friedrich: "Neue Mobilitätskonzepte am Beispiel einer universellen Fahrzeugplattform". In: *ATZextra* 25.S3 (2020), pp. 30–33. DOI: 10.1007/s35778-020-0129-9 (cit. on pp. 5, 15).

[Tro02] Troulis, Markos: "Übertragungsverhalten von Radaufhängungen für Personenwagen im komfortrelevanten Frequenzbereich". Dissertation. Karlsruhe: Universität Karlsruhe, 2002 (cit. on p. 14).

[Tro04] Troulis, Markos; Gnadler, Rolf and Unrau, Hans-Joachim: "The transfer characteristics of wheel suspensions for passenger cars in the comfort-relevant frequency range". In: *ATZ worldwide* 106.4 (2004), pp. 13–17. DOI: 10.1007/BF03224661 (cit. on pp. 17, 18).

[Tso19] Tsokaktsidis, Dimitrios Ernst; Wysocki, Timo von; Gauterin, Frank and Marburg, Steffen: "Artificial Neural Network predicts noise transfer as a function of excitation and geometry". In: *Proceedings of the 23rd International Congress on Acoustics*. Ed. by Ochmann, Martin; Vorländer Michael and Fels, Janina. Berlin, 2019, pp. 4378–4382. DOI: 10.18154/RWTH-CONV-239340 (cit. on pp. 25, 93).

[Tso21] Tsokaktsidis, Dimitrios Ernst; Nau, Clemens; Maeder, Marcus and Marburg, Steffen: "Using rectified linear unit and swish based artificial neural networks to describe noise transfer in a full vehicle context". In: *The Journal of the Acoustical Society of America* 150.3 (2021), p. 2088. DOI: 10.1121/10.0005535 (cit. on p. 93).

[Uhl20a] Uhlar, Stefan: "Reduction of Body Boom by Optimizing the Dynamic Axle Forces". In: *ATZ worldwide* 122.4 (2020), pp. 36–39.

DOI: 10.1007/s38311-020-0204-2 (cit. on pp. 2, 14, 17, 18, 22, 23, 52, 85).

[Uhl20b] UHLAR, Stefan: "Reduktion des Dröhnens durch Optimierung der dynamischen Achskräfte". In: *Automobiltechnische Zeitschrift* 122.4 (2020), pp. 36–41. DOI: 10.1007/s35148-020-0220-y (cit. on p. 23).

[Uhl21a] UHLAR, Stefan: "Hybrid Simulation of Structure-borne Road Noise". In: *ATZ worldwide* 123.1 (2021), pp. 50–55. DOI: 10.1007/s38311-020-0606-1 (cit. on pp. 1, 8, 9, 18, 23, 50, 52).

[Uhl21b] UHLAR, Stefan: "Simulating and optimizing the dynamic chassis forces of the Audi e-tron". In: *Proceedings of the 11th International Munich Chassis Symposium 2020*. Ed. by PFEFFER, Peter. Morgan Kaufmann, 2021, pp. 253–262. DOI: 10.1007/978-3-662-63193-5_18 (cit. on pp. 2, 4, 17, 18, 23, 50, 52, 85, 117).

[Uhl21c] UHLAR, Stefan; HEYDER, Florian and KÖNIG, Thomas: "Assessment of two physical tyre models in relation to their NVH performance up to 300 Hz". In: *Vehicle System Dynamics* 59.3 (2021), pp. 331–351. DOI: 10.1080/00423114.2019.1681475 (cit. on p. 50).

[Vem15] VEMIREDDY, Karthik; DITTMAR, Torben; ECKSTEIN, Lutz; HESSE, Lars and RETTWEILER, Peter: "Development of a driving dynamics-oriented suspension design during the early concept phase". In: *Proceedings of the 6th International Munich Chassis Symposium 2015*. Ed. by PFEFFER, Peter E. Wiesbaden: Springer Fachmedien Wiesbaden, 2015, pp. 233–255. DOI: 10.1007/978-3-658-09711-0_18 (cit. on pp. 14, 15, 21, 35).

[Vir20] VIRTANEN, Pauli et al.: "SciPy 1.0: Fundamental Algorithms for Scientific Computing in Python". In: *Nature Methods* 17 (2020), pp. 261–272. DOI: 10.1038/s41592-019-0686-2 (cit. on pp. 68, 70).

[Vos08] VOSTEEN, Klaus: "Ein Realtool zur Fahrwerkentwicklung". In: *17. Aachener Kolloquium für Fahrzeug- und Motorentechnik*. 2008, pp. 1573–1591. URL: https://www.tib.eu/de/suchen/id/tema%3ATEMA20090305219/Ein-Realtool-zur-Fahrwerkentwicklung/ (cit. on pp. 2, 24).

[Wat12] Wattenberg, Klaus; Mahler, Kornel; Wiehe, Ludwig; Breitling, Thomas; Dragon, Ludger and Bauer, Walter: "Ohne Prototypen schneller zum Ziel". In: *ATZextra* 17.4 (2012), pp. 92–96. doi: 10.1365/s35778-012-0744-1 (cit. on p. 14).

[Wil04] Will, Johannes; Möller, Jörg-Stefan and Bauer, Eric: "Robustheitsbewertungen des Fahrkomfortverhaltens an Gesamtfahrzeugmodellen mittels stochastischer Analyse". In: *VDI-Berichte* 1846 (2004), pp. 505–525. url: https://www.dynardo.de/fileadmin/Material_Dynardo/bibliothek/Robustheit_Zuverlaessigkeit/paper_VDI2004_DC_Dynardo_Robustheit.pdf (visited on 07/31/2018) (cit. on pp. 14, 83, 92, 93).

[Wol14] Wolf-Monheim, Friedrich; Palandri, Jacopo; Zandbergen, Paul and Drotar, Tim: "CAE-based driving comfort optimization for passenger cars". In: *Proceedings of the 5th International Munich Chassis Symposium 2014*. Ed. by Pfeffer, Peter E. Wiesbaden: Springer Fachmedien Wiesbaden, 2014, pp. 133–149. doi: 10.1007/978-3-658-05978-1_11 (cit. on pp. 2, 6, 13, 14, 18, 24, 50).

[Woo20] Woopen, Timo; Kempen, Raphael van; Böddeker, Torben and Eckstein, Lutz: "UNICARagil - Where We Are and Where We Are Going". In: *Proceedings of the 29th Aachen Colloquium of Sustainable Mobility 2020*. 2020, pp. 285–308. doi: 10.18154/RWTH-2020-10407. url: https://publications.rwth-aachen.de/record/804601 (visited on 01/11/2021) (cit. on pp. 5, 6).

[Wys20a] Wysocki, Timo von; Chahkar, Jason and Gauterin, Frank: "Small Changes in Vehicle Suspension Layouts Could Reduce Interior Road Noise". In: *Vehicles* 2.1 (2020), pp. 18–34. doi: 10.3390/vehicles2010002 (cit. on pp. 25, 30, 38, 46, 50, 53, 59, 134, 135, 137, 144).

[Wys20b] Wysocki, Timo von; Leupolz, Michael and Gauterin, Frank: "Metamodels Resulting from Two Different Geometry Morphing Approaches Are Suitable to Direct the Modification of Structure-Born Noise Transfer in the Digital Design Phase". In: *Applied*

System Innovation 2.4 (2020). DOI: 10.3390/asi3040047 (cit. on pp. 25, 38, 46, 63–65, 93).

[Wys21] Wysocki, Timo von; Rieger, Frank; Tsokaktsidis, Dimitrios Ernst and Gauterin, Frank: "Generating Component Designs for an Improved NVH Performance by Using an Artificial Neural Network as an Optimization Metamodel". In: *Designs* 5.2 (2021). DOI: 10.3390/designs5020036 (cit. on pp. 25, 38, 46, 72, 84, 93).

[Wys22] Wysocki, Timo von and Gauterin, Frank: "Ein neuer Ansatz zur Optimierung des Rollgeräuschs im Pkw". In: *Fortschritte der Akustik - DAGA 2022*. Ed. by Leistner, Philip. Berlin, 2022. DOI: 10.5445/IR/1000145288 (cit. on pp. 25, 36, 38, 46, 52, 82, 129).

[Xue11] Xue, X. D.; Cheng, K. W. E.; Zhang, Z.; Lin, J. K.; Wang, D. H.; Bao, Y. J.; Wong, M. K. and Cheung, N.: "Study of art of automotive active suspensions". In: *Conference Proceedings*. 2011, pp. 360–366. DOI: 10.1109/PESA.2011.5982958 (cit. on pp. 11, 18, 19).

[You19] YouGov: Komfort und Bequemlichkeit gehören für die deutschen, US-amerikanischen und chinesichen Autofahrer zu den wichtigsten Kaufkriterien bei der Wahl eines neuen Autos. Ed. by Vibracoustic. 2019. URL: https://www.vibracoustic.com/de/media/pressemeldungen/2019/komfort-und-bequemlichkeit-gehoeren-fuer-die-deutschen-autofahrer-zu-den (visited on 12/02/2019) (cit. on p. 1).

[Yu19] Yu, Min; Cheng, Cheng; Evangelou, Simos and Dini, Daniele: "Robust Control for a Full-Car Prototype of Series Active Variable Geometry Suspension". In: *2019 IEEE 58th Conference on Decision and Control (CDC)*. IEEE, 2019, pp. 7615–7622. DOI: 10.1109/CDC40024.2019.9029344 (cit. on p. 25).

[Yu21a] Yu, Min; Cheng, Cheng; Evangelou, Simos and Dini, Daniele: "Series Active Variable Geometry Suspension: Full-Car Prototyping and Road Testing". In: *IEEE/ASME Transactions on Mechatronics* (2021). DOI: 10.1109/TMECH.2021.3097153 (cit. on p. 25).

[Yu21b] Yu, Min; Evangelou, Simos and Dini, Daniele: "Parallel Active Link Suspension: Full Car Application with Frequency-Dependent Multi-Objective Control Strategies". In: *Control Systems Technology, IEEE Transactions on* (2021) (cit. on pp. 19, 25).

[Zaf18] Zafeiropoulos, Nikos; Zollner, Jürgen and Kandade Rajan, Vasudev: "Active Road Noise Cancellation for the Improvement of Sound Quality in the Vehicle". In: *ATZ worldwide* 120.3 (2018), pp. 38–43. doi: 10.1007/s38311-018-0003-1 (cit. on pp. 7, 16, 18, 19).

[Zan13] Zandbergen, Paul and Girelli Consolaro, Alberto: "Ford Motor Company's New Rear Suspension Architecture for the Global CD Platform". In: *Proceedings of the FISITA 2012 World Automotive Congress*. Vol. 198. Lecture Notes in Electrical Engineering. Berlin and Heidelberg: Springer, 2013, pp. 9–20. doi: 10.1007/978-3-642-33795-6_2 (cit. on p. 18).

[Zel18] Zeller, Peter: Handbuch Fahrzeugakustik: Grundlagen, Auslegung, Berechnung, Versuch. 3rd ed. ATZ / MTZ-Fachbuch. Wiesbaden: Vieweg +Teubner Verlag, 2018. doi: 10.1007/978-3-658-18520-6 (cit. on pp. 4, 7, 9, 17, 18, 53).

[Zhu12] Zhu, Jian Jun; Khajepour, Amir; Esmailzadeh, Ebrahim and Kasaiezadeh, Alireza: "Ride quality evaluation of a vehicle with a planar suspension system". In: *Vehicle System Dynamics* 50.3 (2012), pp. 395–413. doi: 10.1080/00423114.2011.592591 (cit. on p. 18).

[Zim13] Zimmer, Hans: "Parametrischer Bauraum - synchronisierter Fahrzeugentwurf". In: *FAT-Schriftenreihe 251*. Ed. by Verband der Automobilindustrie. FAT-Schriftenreihe. 2013. url: https://www.vda.de/de/services/Publikationen/fat-schriftenreihe-251-synchronisierter-fahrzeugentwurf.html (visited on 08/14/2018) (cit. on p. 16).

[Zom70] Zomotor, Adam: "Untersuchung über den Einfluß der Vorderachskinematik auf die Lenkungsunruhe". Dissertation. Stuttgart,

1970. URL: http://swb.bsz-bw.de/DB=2.1/PPN?PPN=055677622 (visited on 08/20/2018) (cit. on pp. 14, 24).

[Zom71] Zomotor, Adam: "Einfluß der Vorderachskinematik auf die Lenkungsunruhe". In: *Automobiltechnische Zeitschrift* 73.8 (1971), pp. 275–280 (cit. on p. 24).

[Zop20] Zoppke, Hartmut; Scherer, Matthias; Braband, Matthias and Dietz, Alexander: "Lightweight Passenger Car with Natural Fiber Reinforced Monocoque". In: *ATZ worldwide* 122.7-8 (2020), pp. 70–74. DOI: 10.1007/s38311-020-0255-4 (cit. on pp. 6, 15).

Norms and Standards

DIN EN 61672-1:2014-07: Elektroakustik – Schallpegelmesser – Teil 1: Anforderungen (cit. on p. 51).

DIN ISO 8855:2013-11: Straßenfahrzeuge – Fahrzeugdynamik und Fahrverhalten – Begriffe. Nov. 1, 2013 (cit. on pp. 8, 13, 54).

SAE J3016_202104: Taxonomy and Definitions for Terms Related to Driving Automation Systems for On-Road Motor Vehicles. DOI: 10.4271/J3016_202104 (cit. on p. 4).

SAE J670_200801: Vehicle Dynamics Terminology. DOI: 10.4271/J670_200801 (cit. on p. 13).

VDI/VDE 2206:2021-11: Development of mechatronic and cyber-physical systems (cit. on pp. 13, 37).

Own Publications

This section presents a complete list of the author's publications. The publications [3], [4], [5], [6], and [7] address the research presented in the present work, whereas [1] and [2] originate different research projects.

[1] Albers, Albert; Schille, Fabian; Behrendt, Matthias; Wysocki, Timo von; Cortès, Sven and Birkhold, Joerg-Michael: "Methode zur Kalibrierung des Kupplungssystems und Objektivierung des Wiederstartkomforts hybrider Antriebsstränge auf dem Akustikrollenprüfstand". In: *VDI-Berichte 2309*. 2017, pp. 399–416. DOI: 10.51202/9783181023099-399.

[2] Tsokaktsidis, Dimitrios Ernst; Wysocki, Timo von; Gauterin, Frank and Marburg, Steffen: "Artificial Neural Network predicts noise transfer as a function of excitation and geometry". In: *Proceedings of the 23rd International Congress on Acoustics*. Ed. by Ochmann, Martin; Vorländer Michael and Fels, Janina. Berlin, 2019, pp. 4378–4382. DOI: 10.18154/RWTH-CONV-239340.

[3] Wysocki, Timo von; Chahkar, Jason and Gauterin, Frank: "Small Changes in Vehicle Suspension Layouts Could Reduce Interior Road Noise". In: *Vehicles* 2.1 (2020), pp. 18–34. DOI: 10.3390/vehicles2010002.

[4] Wysocki, Timo von; Leupolz, Michael and Gauterin, Frank: Cover Story: Applied System Innovation, Volume 3, Issue 4. 2020. URL: https://www.mdpi.com/2571-5577/3/4 (visited on 08/09/2022).

[5] Wysocki, Timo von; Leupolz, Michael and Gauterin, Frank: "Metamodels Resulting from Two Different Geometry Morphing Approaches Are Suitable to Direct the Modification of Structure-Born

Noise Transfer in the Digital Design Phase". In: *Applied System Innovation* 2.4 (2020). DOI: 10.3390/asi3040047.

[6] Wysocki, Timo von; Rieger, Frank; Tsokaktsidis, Dimitrios Ernst and Gauterin, Frank: "Generating Component Designs for an Improved NVH Performance by Using an Artificial Neural Network as an Optimization Metamodel". In: *Designs* 5.2 (2021). DOI: 10.3390/designs5020036.

[7] Wysocki, Timo von and Gauterin, Frank: "Ein neuer Ansatz zur Optimierung des Rollgeräuschs im Pkw". In: *Fortschritte der Akustik - DAGA 2022*. Ed. by Leistner, Philip. Berlin, 2022. DOI: 10.5445/IR/1000145288.

Supervised Student Theses

[1] Chahkar, Jason: "Automated Construction of Suspension Axle Part Geometries for FE-Simulations, Focusing Especially on the NVH-Analysis". Master Thesis. Karlsruhe: Karlsruhe Institute of Technology, 2019.

[2] Behling, Hendrik: "Erarbeitung und Anwendung einer Methodik zur Kompetenzanalyse mit Fokus auf die Powertrain-Entwicklung und -Produktion im Kontext der Transformation der Automobilindustrie". Bachelor Thesis. Karlsruhe: Karlsruhe Institute of Technology, 2020.

[3] Betzholz, David: "Methodische Entwicklung eines optimalen Scheibenkleberkonzeptes zur Torsionssteifigkeitserhöhung eines Gesamtfahrzeugs". Master Thesis. Karlsruhe: Karlsruhe Institute of Technology, 2020.

[4] Boddaert, Maxence: "Erarbeitung einer Empfehlung zur sicheren Erreichung des ASEP 2024". Master Thesis. Karlsruhe: Karlsruhe Institute of Technology, 2020.

[5] Eckert, Lukas. Working Student. 2020.

[6] Leupolz, Michael: "Automatisierte Gestaltoptimierung von Bauteilen bezüglich ihres NVH-Verhaltens durch Geometriemorphing". Master Thesis. Karlsruhe: Karlsruhe Institute of Technology, 2020. doi: 10.5445/IR/1000142474.

[7] Rieger, Frank: "Entwicklung eines Algorithmus zur automatischen Veränderung von Übertragungsfunktionen im Frequenzbereich durch Geometrieänderungen im Fahrwerk mittels Regression und Optimierung in Python". Master Thesis. Karlsruhe: Karlsruhe Institute of Technology, 2020.

[8] Tok Si Yi, Iris: “Evaluation of Future Challenges in the Development of Suspension Concepts”. Bachelor Thesis. Karlsruhe: Karlsruhe Institute of Technology, 2020.

[9] Eberle, Lukas: “Objektivierung & Klassifizierung von BSR-Störgeräuschen im PKW-Interieur”. Master Thesis. Karlsruhe: Karlsruhe Institute of Technology, 2021.

[10] Scheffold, Michael. Working Student. 2023.

[11] Shi, Ning. Internship. 2023.

[12] Shi, Ning: “Untersuchung des Einflusses von Schraubenfederparametern auf das Abrollgeräusch im Fahrzeuginneren”. Master Thesis. Stuttgart: University of Stuttgart, 2024.

[13] Zehren, Aaron. Internship and Working Student. 2024.

List of Figures

List of Tables

Notation

This chapter introduces the notation and symbols used in this thesis.

General Notation

Scalars	italic Roman and Greek lowercase letters	x, α
Vectors	italic Roman letters with an arrow on top	$\vec{x}$
Lists	bold Roman letters	$\mathbf{x}$

Symbols

a	Element aspect ratio
α	Rotation angle for a suspension link
c	Spring stiffness
f	Frequency
F	Force
$F_{\mathrm{m,i}}$	Coordinate direction i for a fixed node boundary condition of $\mathbf{x}_{\mathrm{f}}$
h_{i}	Height of individual elements
I	Cartesian coordinate system positioned in the center of the suspension
$k_{\mathrm{i,abs}}$	Absolute value for suspension parameter i

$k_{\mathrm{i,abs,orig}}$	Original absolute value for suspension parameter i
$k_{\mathrm{i,rel}}$	Standardized changes for suspension parameter i
k_{res}	Weighted relative suspension parameter changes
l	Length
l_{i}	Length of individual element edges
l_{n}	Length of suspension link n
Δl	Length change
L_{p}	Sound Pressure Level
$\bar{L}_{\mathrm{p}}$	Average Sound Pressure Level in a frequency range
$\bar{L}_{\mathrm{p_{i,j}}}$	Average Sound Pressure Level for frequency range i and ear position j
$\bar{L}_{\mathrm{p,res}}$	Weighted Average Sound Pressure Level for multiple frequency ranges and ear positions
λ	Spacing of regular grid $\mathbf{x}_{\mathrm{g}}$
n_{f}	Number of fixed nodes
n_{c}	Number of control nodes
n_{k}	Number of suspension parameters used in the optimization function
n_{l}	Number of levels in a full factorial DoE
n_{m}	Number of morphable FE nodes
n_{p}	Number of road noise phenomena used in the optimization function
n_{r}	Number of samples in a DoE
n_{v}	Number of design variables
p	Sound Pressure
p_0	Reference sound pressure 2×10^5 Pa
$\vec{P}_{\mathrm{n}}$	Body-side kinematic hard point coordinate
$P_{\mathrm{n,i}}$	Coordinate direction i for the body-side kinematic hard point coordinate $\vec{P}_n$

$P_{\mathrm{n,i,new}}$	Coordinate direction i for the body-side kinematic hard point coordinate $\vec{P}_n$ after modification
$P_{\mathrm{n,i,old}}$	Coordinate direction i for the body-side kinematic hard point coordinate $\vec{P}_n$ before modification
$\Delta\vec{P}_{\mathrm{n}}$	Body-side kinematic hard point modification
$\Delta P_{\mathrm{n,i}}$	Coordinate direction i for the body-side kinematic hard point change $\Delta\vec{P}_n$
ψ	Element skewness angle
$\vec{R}_n$	Wheel-side kinematic hard point
$R_{\mathrm{n,i}}$	Coordinate direction i for the wheel-side kinematic hard point coordinate $\vec{R}_n$
$R_{\mathrm{n,i,new}}$	Coordinate direction i for the wheel-side kinematic hard point coordinate $\vec{R}_n$ after modification
$R_{\mathrm{n,i,old}}$	Coordinate direction i for the wheel-side kinematic hard point coordinate $\vec{R}_n$ before modification
$\Delta\vec{R}_{\mathrm{nachfolgend}}$	Wheel-side kinematic hard point modification
$\Delta R_{\mathrm{n,i}}$	Coordinate direction i for the wheel-side kinematic hard point coordinate change $\Delta\vec{R}_n$
s	Element skewness
$S_{\mathrm{E}}^{\mathrm{Prediction}}$	Squared prediction errors
S_{E}	Total variation
$\mathbf{v}_{\mathrm{c}}$	List of imposed displacements at control nodes
$\Delta v_{\mathrm{c,rel,i}}$	Relative morphing deviation at control nodes for coordinate direction i
$\mathbf{v}_{\mathrm{d}}$	List of imposed displacements at boundary condition nodes
$\mathbf{v}_{\mathrm{f}}$	List of zero displacements at fixed nodes
$\mathbf{v}_{\mathrm{FE}}$	List of displacements at morphable FE nodes
$w_{\mathrm{k_i}}$	Weighting factor for suspension parameter i
$w_{\mathrm{L_{i,j}}}$	Weighting factor for Sound Pressure Level at ear position j and frequency range i

x	Translational DOF
$\mathbf{x}_\mathrm{c}$	List of control nodes
$\mathbf{x}_\mathrm{d}$	List of displacement boundary condition nodes
$\mathbf{x}_\mathrm{f}$	List of fixed nodes
$\mathbf{x}_\mathrm{g}$	List of regular grid nodes
$\mathbf{x}_\mathrm{FE}$	List of morphable FE nodes
φ	Rotational DOF

Acronyms

ANC	Active Noise Canceling
ANN	Artificial Neural Network
ARNC	Active Road Noise Cancellation
ATG	Automotive Testing Papenburg GmbH
BEM	Boundary Element Method
BEV	Battery Electric Vehicle
CAD	Computer Aided Design
CAE	Computer Aided Engineering
CoP	Coefficient of Prognosis
DoE	Design of Experiments
DOF	Degree of Freedom
DPT	Digital Prototype
FE	Finite Element
FEM	Finite Element Method

FRF	Frequency Response Function
GPU	Graphics Processing Unit
HEV	Hybrid Electric Vehicle
ICE	Internal Combustion Engine
ICR	Instant Center of Rotation
MAC	Modal Assurance Criterion
MBS	Multi Body Simulation
MLS	Moving Least Squares
MPC	Multi Point Constraint
NTF	Noise Transfer Function
NVH	Noise, Vibration, and Harshness
OEM	Original Equipment Manufacturer
PALS	Parallel Active Link Suspension
PHEV	Plugin Hybrid Electric Vehicle
PSD	Power Spectral Density
RBE	Rigid Body Element
RMS	Root Mean Square
SAE	Society of Automotive Engineers

SAVGS	Series Active Variable Geometry Suspension
SEA	Statistical Energy Analysis
SOL	Solution
SPL	Sound Pressure Level
SUV	Sport Utility Vehicle
UNIKAT	Universeller Komponenten- und Aggregateträger

A Road Noise Transfer Path

The road noise transfer path from contact patch between tire and road and passenger ears was introduced in section 2.2.3 and illustrated in fig. 2.1 on page 8. The detailed transfer path suspension was introduced in section 4.1 and illustrated in fig. 4.2 on page 43. Figure A.1 combines both presentations into the full road noise transfer path.

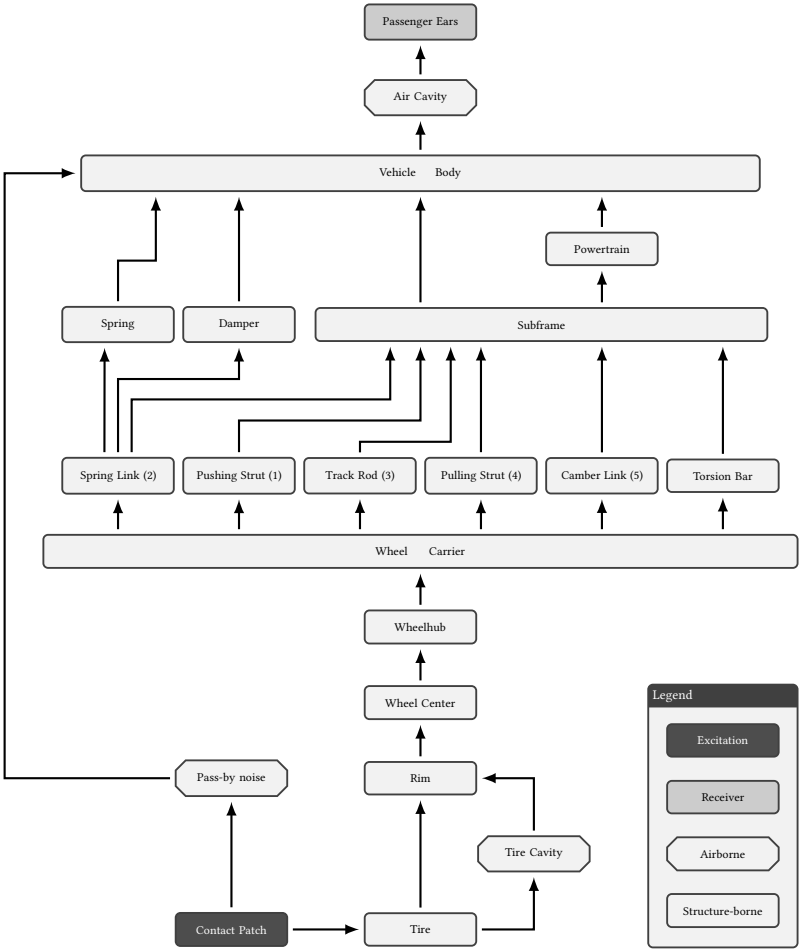

Figure A.1: Full road noise transfer path. Combination of figs. 2.1 and 4.2.

B Derivations

This chapter details formula and calculations previously used and presents their derivations.

B.1 Frequency Band Averaging

Section 5.2.2 identified relevant frequency ranges for the evaluation of specific road noise phenomena. For the reduction from an SPL function $L_\mathrm{p}(f)$ to a phenomenon specific scalar value $\bar{L}_\mathrm{p}$, eq. (5.3) on page 89 was used. The equation results from dividing an integral approximation by the interval length.

The trapezoidal rule

$$\int_{f_1}^{f_2} L_\mathrm{p}(f)\,\mathrm{d}f = h\left(\frac{1}{2}L_\mathrm{p}(f_1) + \frac{1}{2}L_\mathrm{p}(f_2) + \sum_{i=1}^{n-1} L_\mathrm{p}(f_1 + ih)\right) \tag{B.1}$$

approximates the integral of a function in the domain between f_1 and f_2. The factor

$$h = \frac{f_2 - f_1}{n} = \Delta f \tag{B.2}$$

divides the length of the interval by the number of equidistant segments n. In the NVH application this value h is equivalent to the frequency bin width Δf. This simplifies the equation to

$$\int_{f_1}^{f_2} L_\mathrm{p}(f)\,\mathrm{d}f = \Delta f\left(\frac{1}{2}L_\mathrm{p}(f_1) + \frac{1}{2}L_\mathrm{p}(f_2) + \sum_{i=1}^{n-1} L_\mathrm{p}(f_1 + i\Delta f)\right) \tag{B.3}$$

for the evaluation of the integral.

In order to receive the averaged function value in the domain, the integral value is divided by the length of the domain

$$l = f_2 - f_1 \quad . \tag{B.4}$$

Combined, this leads to the averaged SPL

$$\bar{L}_\mathrm{p} = \frac{\Delta f}{f_2 - f_1}\left(\frac{1}{2}L_\mathrm{p}(f_1) + \frac{1}{2}L_\mathrm{p}(f_2) + \sum_{i=1}^{n-1} L_\mathrm{p}(f_1 + i\Delta f)\right) \tag{B.5}$$

$$= \frac{1}{n}\left(\frac{1}{2}L_\mathrm{p}(f_1) + \frac{1}{2}L_\mathrm{p}(f_2) + \sum_{i=1}^{n-1} L_\mathrm{p}(f_1 + i\Delta f)\right) \quad , \tag{B.6}$$

which is equivalent to eq. (5.3) on page 89.

B.2 Morphing Compensation

In section 4.5.4, the compensation calculation for the morphing deviation compensation was introduced. Considering the interpolation as linear, fig. B.1 illustrates the compensation problem.

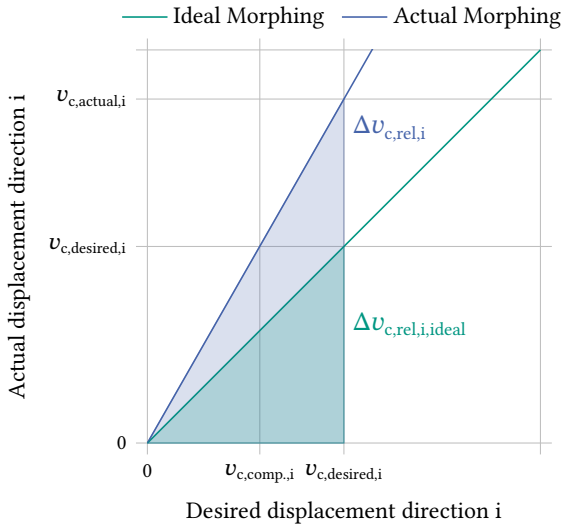

Figure B.1: Illustration of the morphing compensation for the coordinate direction i. Colored triangles indicate the slope of the two functions.

In an ideal morphing, the desired displacement $\vec{v}_{c,desired}$ exactly matches the actual displacement $\vec{v}_{c,actual}$. The slope of this function is

$$\Delta v_{c,rel,i,ideal} = \frac{v_{c,desired,i}}{v_{c,desired,i}} = 1 \quad . \tag{B.7}$$

The second function in fig. B.1 illustrates the actual morphing behavior. The actual displacement $\vec{v}_{c,actual}$ does not match the desired displacement $\vec{v}_{c,desired}$. The slope of this function is

$$\Delta v_{c,rel,i} = \frac{v_{c,actual,i}}{v_{c,desired,i}} \neq 1 \quad . \tag{B.8}$$

If $\Delta v_{c,rel,i} > 1$, the morphing displacement is too high, if $\Delta v_{c,rel,i} < 1$, the morphing displacement is too little.

To compensate the morphing deviation the condition

$$\Delta v_{\mathrm{c,rel,i}} v_{\mathrm{c,compensated,i}} \overset{!}{=} v_{\mathrm{c,desired,i}} \tag{B.9}$$

needs to be true. Solving for $v_{\mathrm{c,compensated,i}}$ and inserting eq. (B.8) results in

$$v_{\mathrm{c,compensated,i}} = \frac{v_{\mathrm{c,desired,i}}}{\Delta v_{\mathrm{c,rel,i}}} \tag{B.10}$$

$$= \frac{v_{\mathrm{c,desired,i}}^2}{v_{\mathrm{c,actual,i}}} \quad . \tag{B.11}$$

This is eq. (4.20) on page 72.

C Metamodels

In this appendix chapter, details for the metamodeling approach are presented.

C.1 Full Methodology Scheme

Figure 3.3 on page 36 presented the workflow for the creation of optimized suspension kinematics regarding road noise reduction. Figure 4.14 on page 68 detailed the creation of FE components for modified suspension kinematics using a morphing approach. Figure C.1 combines both figures into one flowchart, visualizing the full methodology.

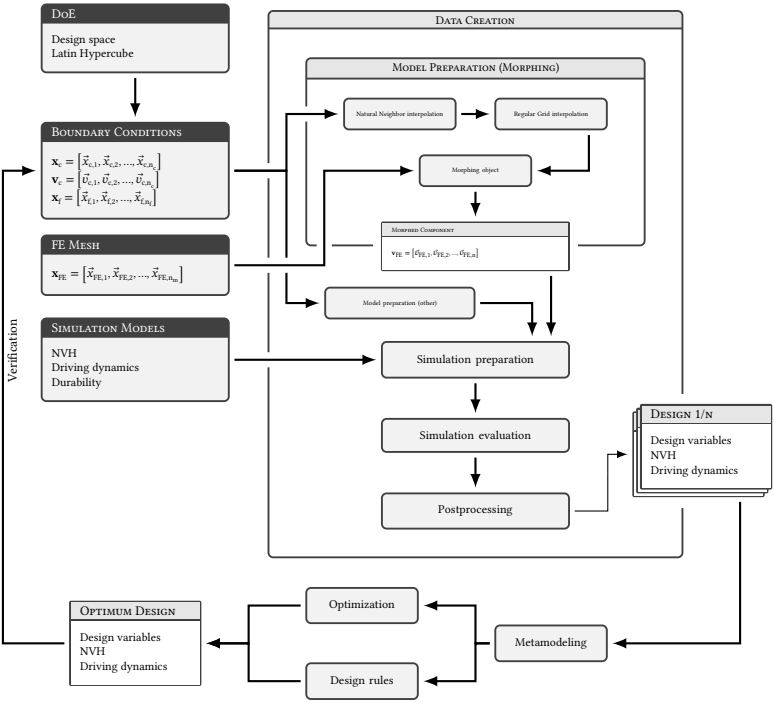

Figure C.1: Detailed Procedure of the investigation for the creation of design rules or Numeric optimization. Combination of figs. 3.3 and 4.14

C.2 Metamodel Configuration

Except for the testing against Polynomial metamodels of order 2 and Isotropic Kriging metamodels, ANN metamodels were used for the investigation. For the configuration of the ANNs, the *Ansys optiSLang* parameter optimization was used, as finding the best performing metamodel was out of scope in this research. The number of hidden layers was limited to 5 with altogether not more than 100 neurons. As an activation function, tanh was used. Due to the optimization approach, there is not a single ANN configuration, applicable to all created metamodels. Overall, the approach with unoptimized metamodels shows the possibility to generate suspension kinematics optimization approaches with relatively unoptimized metamodels and small numbers of samples.

C.3 Example Metamodels for Frequency Ranges

This section presents with fig. C.2 additional selected acoustic metamodels and provides short insights into their messages. All metamodels presented in this section are based on ANNs. The metamodels for the cavity noise frequency range are presented in figs. 5.9b and 6.16.

Figures C.2a and C.2c indicate a target conflict for the design variables $R_{3,x}$ and $R_{5,x}$ in the frequency ranges 58 to 68 Hz and 105 to 125 Hz. Figure 5.5 supports this assumption, indicating a negative correlation between the two frequency ranges. Figures C.2c and C.2d indicate an optimization potential for the design variables $R_{2,x}$ and $R_{3,x}$ in the frequency ranges 80 to 90 Hz and 210 to 220 Hz.

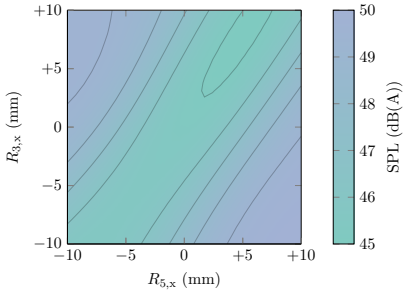

(a) Metamodel for frequency range 58 to 68 Hz depending on design variables $R_{3,x}$ and $R_{5,x}$.

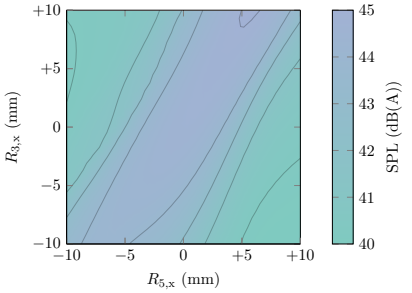

(b) Metamodel for frequency range 105 to 125 Hz depending on design variables $R_{3,x}$ and $R_{5,x}$.

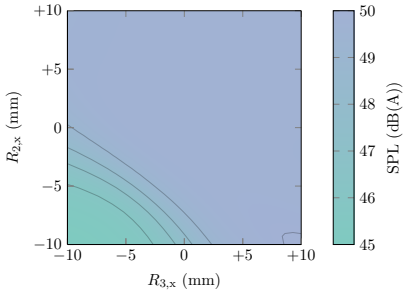

(c) Metamodel for frequency range 80 to 90 Hz depending on design variables $R_{2,x}$ and $R_{3,x}$.

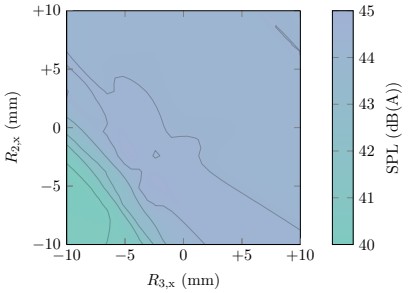

(d) Metamodel for frequency range 210 to 220 Hz depending on design variables $R_{2,x}$ and $R_{3,x}$.

Figure C.2: Example metamodels for selected frequency ranges as a function of their two respective dominating design variables.

D Translations

Table D.1 presents the German translations for selected English terms used in the present work.

Table D.1: Suspension terms in English and German. Words in parenthesis are left out for better readability.

English	German
Anti-Dive	Bremsnickausgleich
Anti-Squat	Anfahrnickausgleich
Camber angle	Sturzwinkel
Camber angle gradient	Sturzwinkelgradient
Camber arm	Sturzstrebe
Camber change	Sturzänderung
Caster angle	Nachlaufwinkel
(Caster) Trail	Nachlaufstrecke
Damper ratio	Dämpferübersetzung
Diagonal spring angle	Schrägfederungswinkel
Instant Center of Rotation (ICR)	Momentanzentrum
ICR height	Momentanzentrumshöhe
ICR gradient	Momentanzentrumsgradient
Kingpin inclination (angle)	Spreizungswinkel
Kingpin offset	Stoßradius
Kingpin offset at wheel center	Spreizungsversatz
Lateral acceleration gain	Querbeschleunigungsverstärkung
Normal steering axis offset	Störkrafthebelarm

continued on the next page

English	German
(Overall) Steering ratio	Gesamtlenkübersetzung
Pulling strut	Zugstrebe
Pushing strut	Schubstrebe
Roll center	Wankzentrum
Scrub radius	Lenkrollradius
Side slip angle	Schwimmwinkel
Sound Pressure Level (SPL)	Schalldruckpegel
Spring link	Federlenker
Spring ratio	Federübersetzung
Steering arm	Lenkspurhebel
Steering wheel angle	Lenkradwinkel
Subframe	Fahrschemel
Toe angle	Vorspurwinkel
Toe angle gradient	Spurgradient
Toe change	Vorspuränderung
Torsion bar	Drehstab
Torsion bar link	Drehstabgestänge
Track rod	Spurstange
Track width	Spurweite
Wheel carrier	Radträger
Wheel load lever arm	Radlasthebelarm
Yaw rate gain	Gierverstärkung

Index

S